The Effect of Film Thickness on the Behavior of Polystyrene-Coated Steel Disks Under Fretting Conditions

by

Romolo Raciti

Thesis submitted to the Faculty of the

Virginia Polytechnic Institute and State University

in partial fulfillment of the requirements for the degree of

Master of Science

in

Mechanical Engineering

APPROVED:

N. S. Eiss, Jr.

M. J. Furey

H. H. Mabie

January 1987

Blacksburg, Virginia

The Effect of Film Thickness on the Behavior of Polystyrene-Coated Steel Disks Under Fretting Conditions

by

Romolo Raciti

N. S. Eiss, Jr.

Mechanical Engineering

(ABSTRACT)

The purpose of this study was to evaluate the effect of film thickness on a polystyrene coating used to prevent fretting corrosion in a steel-on-steel system. The polystyrene coating was applied to a 1045 steel disk and fretted against a 52100 steel ball. Two sets of experiments were employed. The first set evaluated film life by using seven different film thicknesses ranging from 7.9 to 52 μm. The results from this set of experiments indicated that a drastic increase in film life occurred for coatings thicker than 40 μm. The other set of experiments was used to study how fretting damage progressed with time and how it was affected by film thickness. For this purpose two film thicknesses, 38 and 52 μm, were used. The results from these experiments led to the speculation that stress and temperature conditions were different in the 38 and 52 μm films. These differences resulted in a milder fretting regime, and therefore longer life, in the thicker film. Optical and scanning electron microscopy and computer graphics were used to study in detail the fretting interface. The fretting mechanisms were explained in terms of mechanical, chemical, tribochemical, and tribophysical effects.

Acknowledgements

I would like to express my gratitude and appreciation to my major professor Dr. Norman S. Eiss, Jr., for his guidance and advice throughout the duration of this research. I would also like to thank Dr. M. J. Furey and Dr. H. H. Mabie for serving on my advisory committe and for their valuable advice and assistance, Dr. G. L. Wilkes for his advice in understanding the chemical aspect, Prof. C. Kajdas for his advice on the tribochemical and tribophysical aspects, Mr. J. Sankar for his help with the three-dimensional mapping, and the Army Research Office for sponsoring this study.

Special thanks are due to my family and my parents in particular. It is from their support, encouragement, and faith in my abilities that I have drawn the strength and confidence to succed in my endeavors.

Table of Contents

List of Illustrations

List of Tables

1.0 Introduction.

Fretting is a type of wear occurring when two surfaces undergo small relative motion and in which both mechanical and chemical factors are significant. It is a very complex phenomenon and far from being completely understood. Fretting can cause severe damage to the surface of a part which may result in loss of fit and/or tolerances, or initiate fatigue cracks. This can lead to noise, vibrations, and eventually to failure. Severe failures have been reported as having been caused by fretting damage.

Research on fretting at VPI&SU started in 1981 [1][1] . The aim of this research is to try to gain a better understanding of the fretting process as well as explore methods by which fretting could be either prevented or somewhat mitigated. Since 1983 [2], under the sponsorship of the Army Research Office, research at VPI&SU has been aimed at trying to use thin polymeric films as a method to prevent fretting. Sweitzer [3] investigated four different polymers, polyvinyl chloride (PVC), low-density polyethylene (LDPE), polytetrafluorethylene (PTFE), and polysulfone (PSO), and found that three of them fretted the steel counterface: LDPE, PTFE, and PSO. Puzio [4] investigated the

[1] The numbers in the square parenthesis refer to the List of References

chemical processes occurring when fretting steel coated with chlorinated polymers (polyvinyl chloride and polyvinylidene chloride). He looked at polymer degradation as a possible cause for film failure. Rorrer [5] studied the effect of five different parameters (load, slip amplitude, frequency, relative humidity, and film thickness) on the fretting behavior of a PVC coated steel disk. His most interesting finding was the effect of relative humidity on film life. He found that film life was 15 times longer at low humidity than at high humidity. The other important finding of his work is the importance of film thickness. Film thickness had significant effects, at a 95 percent confidence level, on film life, wear, and friction. Its effect was mainly seen in interaction with other variables such as load and frequency. However, film thickness was the single most important variable in affecting the coefficient of friction. The average coefficient of friction for the thick film was found to be 1.6 times greater than the one for the thin film probably because of the larger contact area. Day [6] investigated the effect of normal load on ten different polymer films: polymethylmethacrylate (PMMA), polytetrafluoroethylene (PTFE), polyimide (PI), polyvinylidene fluoride (PVDF), polyvinylidene chloride (PVDC), low-density polyethylene (LDPE), high-density polyethylene (HDPE), polyvinyl chloride (PVC), polysulfone (PSO), and polystyrene (PS). The polymer that stood out the most was polystyrene because of its long life and because it did not cause any fretting of the steel counterface. The ability of polystyrene, or any other polymer used, to resist wear decreased as the normal load increased. At high load the film life was drastically reduced, on the average, from over an hour to about 230 sec.. The mode of failure at the higher load was described as one of "...gross brittle fracture." The other interesting point of Day's work was the fact that all the polymers which showed resistance to fretting wear had a relatively high compressive strength (about 80 MPa or higher). The only polymers not following this rule were PMMA and HDPE. PMMA had a very short life (13 sec) even though it had physical properties which were very similar to those of

polystyrene. The only difference was that the PMMA coating was much thinner than the one of PS (7.1 μm for PMMA and 86 μm for PS). HDPE had a very long life (over 3600 sec) even though it had a compressive strength of only about 20 MPa; but the coating thickness was 111.8 μm, about 23 percent thicker than PS. These observations tend to indicate that the thickness of the polymeric films greatly affects the fretting behavior.

In this thesis polystyrene is studied in more detail. Preliminary experiments done by the author confirmed that polystyrene films are very sensitive to thickness. Therefore this work searched for reasons of this behavior by applying films of seven different thicknesses on a steel flat and fretting them against a steel sphere. The wear progression with respect to time was also studied by stopping the test at different time intervals and observing the changes in the wear scar. In this phase two different film thicknesses were used. Both optical and scanning electron microscopy were used to obtain evidence for the failure mechanism. A new technique which uses surface profile traces combined with computer graphics was employed to obtain three- dimensional maps of the fretted area. The maps were an accurate visual representation of the worn surface. The three-dimensional maps were also used to estimate the wear and debris volumes. This study was conducted at one load, one frequency, one slip amplitude, and one atmospheric condition so that the only variable was film thickness.

2.0 Literature Review.

In this section a review of the extensive literature available on fretting corrosion is presented. Fretting is a very complex phenomenon and far from being completely understood. Previous studies [7] have determined that in fretting there are more than fifty variables involved and that mechanical and chemical factors are equally important. In this review there will be an attempt to briefly expose the present theories in the field. It is followed by a discussion of what has been done to either prevent or mitigate fretting. Also, in this review, the chemical and physical characteristics of polystyrene, the polymer used in this study, are presented and discussed.

2.1 Fretting.

Fretting is defined [8] as the type of "...wear phenomenon occurring between two surfaces having oscillatory relative motion of small amplitude." Sometimes it is referred to as fretting corrosion when the chemical reaction predominates. Collins [7] describes

fretting as the combined mechanical and chemical action in which the contacting surfaces of two solid bodies are loaded and caused a small oscillatory motion between them. The loading force is large enough and the motion small enough to restrict the flow of debris away from the originating site. This type of wear can eventually lead to failure. Its importance as a major mode of failure is evident both in terms of frequency of occurrence as well as in the seriousness of the failure. Typical areas where failures occur as a direct consequence of fretting are: riveted or bolted static joints subjected to vibrations [9,10], wheel seat of automobile hub-on-axle assemblies, flexible couplings of toothed or splined variety, keys and keyways, reactors and heat exchangers [11,12], and the classical example of the auto roller bearings in transport from Detroit to the West coast [13].

2.1.1 Mechanism of Fretting.

Even though fretting was observed as early as 1911 when the formation of red rust in the grips of a fatigue testing machine was noticed [14], the first paper on the subject was written in 1927 by Tomlinson [15] who also coined the term "fretting corrosion." In this first paper, and in a following one written in 1939 [16], Tomlinson explains the phenomenon as being one of molecular adhesion and subsequent breaking of the bond. Another mechanism was proposed by Feng and Rightmire [17]. They explained the mechanism of fretting as being one of simple wear where loose particles are formed by the plastic contact and shear of asperities. In a second stage the loose particles will cause abrasion of the mating surfaces making the wear process more severe. Both theories presented above explain fretting as being purely a mechanical phenomenon. It was not until 1950 that the importance of the chemical factor was made evident by Uhlig

[18]. According to his theory as the contacting surfaces slide over one other, clean metallic surface is exposed by the plowing effect of the asperities. The clean metal will then easily react with the surrounding atmosphere producing metallic oxide. Today it is recognized that both mechanical and chemical factors are important. However, there is great controversy about the role and the importance of each factor. Another point of discussion concerns the role of oxidation during fretting and its effect on subsequent damage.

It has been proposed [19,20,21] that fretting goes through three different stages: initial stage, oxide debris generation stage, and steady state stage. These stages are not well divided in time and might very well occur simultaneously within the fretted region.

Initial Stage. During the initial stage loose particles are produced. The mechanism by which the particles are formed is subject of great discussion. However it is agreed that this is a stage where the mechanical factor is the predominant one. The old models (Tomlinson [15], Uhlig [18], Hurricks [20]) proposed cold welding and/or adhesion as the mechanism by which the loose particles are formed. More recently [22,23] however, the delamination mechanism is thought to be the most suitable model for the metal removal process. The delamination theory was introduced in 1973 by Suh [24]. According to this theory as the two surfaces come into contact, and are loaded one against the other, the subsurface voids tend to pile up and form a crack parallel to the surface. Eventually this crack will emerge to the surface and a plate-like wear particle is formed. It is therefore argued [7,22] that during the early stages of the fretting process the surface is heavily cold worked to the point where the ductility of the surface is exhausted and subsurface cracks start to form. Eventually a crack comes to the surface and a metal flake is formed. As sliding continues the flake rolls or breaks into smaller particles. This process then continues repeatedly as new surfaces are exposed.

Oxidation Stage. During this stage the metal particles will oxidize. Some argue that as the metal debri is formed it will spontaneously react with the environment [20,22]. Others [18] argue that the mechanical energy developed during sliding provides the activation energy required to produce the oxide. In the absence of such activation energy the oxidation process will be too slow. However no matter what the actual mechanism is, the removed metal particles do oxidize and form a layer that eventually reduces contact between the fretted surfaces. The oxide formed is generally hematite (α- Fe_2O_3). It is interesting to note that not all the loose particles formed in the first stage oxidize [7,13,19]. This fact seems to confirm the need for some type of activation energy or high temperature [18,25] in order to trigger the oxidation. On the other hand Campbell [25] argues that oxygen concentrates in the irregularities of the surface because of the high local pressures. Fretting, then, proceeds by the removal and reformation of the oxide film. In this case the oxidation stage will be the first stage.

Steady-State Stage. This stage is characterized by a general disintegration and dispersal of the zones affected by the two initial stages. It is recognized by a mixture of oxide debris and metal (not oxidized) particles in the wear contours. During this stage fatigue is the major cause of damage since the fatigue strength of the fretted parts is greatly affected. Fatigue cracks start to form and the fatigue life of the part is greatly reduced [7,13,19,22].

2.1.2 Variables in Fretting.

There are as many as fifty variables which affect fretting in one way or the other. Most of these variables are interdependent and cannot be treated separately. However, eight of these variables are considered the most important and some general trends have in-

deed been observed [7,13]. The following is a brief review of the most important findings.

Slip Amplitude - the magnitude of relative motion between the surfaces being fretted. There is not a well defined boundary between the region of fretting wear and unidirectional wear. Some [23,26,27] say that this limit is 70 μm but they do not make any attempt to relate this limit to experimental conditions such as geometry, load, or area of contact. Others [13], give 100 μm as the upper limit. It is generally agreed that fretting wear increases with increasing amplitude [13,23,26,27]. Rorrer [5], for PVC coated steel disk against a steel ball, found slip amplitude to be a significant factor for film life. He found the film life to decrease with increasing slip amplitude.

Load - the magnitude and the distribution of pressure between the surfaces at the fretting interface. It is well agreed [7,13,18,19,20] that an increase in load will cause an increase in fretting wear except in the case where the load increase prevents motion [7,13]. Rorrer [5] found load to have a large effect on film life (reduced) and friction (increased).

Stress - the magnitude, direction, and variation of stress with respect to time in the region of the fretting surfaces. During fretting a compressive mean stress either static or cyclic is produced resulting in a drastic reduction of the material fatigue strength and life. Local compressive stresses are found to be beneficial in minimizing fretting fatigue damage. Residual compressive stresses can be produced by shot-peening and cold rolling [7].

Frequency - the cyclic frequency of relative motion between the surfaces being fretted. Toth [27] and Feng and Uhlig [28] find fretting wear to be inversely proportional to frequency. Rorrer [5] found frequency to affect film life. At low frequency the a verage life was 2.3 times longer than at high frequency.

Materials - the material from which each of the fretting member is fabricated including surface conditions. Reading through the literature, it is very much evident that each material combination has its own characteristics and particularities of behavior [4,5,6]. The proper selection of material pairs can greatly reduce fretting damage [7].

Temperature - the temperature in the region of the two surfaces being fretted. Feng and Uhlig [28] found that wear increased with decreasing temperature. Also at a temperature above 200 ^{0} C the iron oxide acts as a solid lubricant [29,30]. The decrease in wear with increasing temperature is evident up to the point where the temperature is high enough to degrade the mechanical properties of the materials involved. After this point wear starts to increase quite drastically. There is great difference of opinions and of evidence in the literature about the temperature in the contact region. Some use the fact that FeO was detected in the oxide debris formed as an evidence for temperatures as high as 400 ^{0}C [25,31,32]. Mason and White [33] fretted nylon against nickel silver. The appearance of the wear marks on the nylon suggest that the surface is melted rather than abraded off. Such a process requires a temperature of 260 ^{0}C. Duquette [22,34,35] however, actually tried to measure the temperature at the interface by using a thermocouple. He found that for martensitic 4130 steel fretted against copper-constantan the average temperature rise is only of 18-20 ^{0}K. Because of the complexity of the fretting process, it would seem most likely that each particular situation would lead to different temperature behavior.

Atmosphere - the atmospheric environment surrounding the surfaces being fretted. Atmosphere affects fretting mainly because of its role in the oxidation stage. A non-oxidizing environment, such as nitrogen, produces less fretting than an oxidizing one such as air [4,36,37]. Another important factor is humidity. Rorrer [5] found that, for PVC coated steel disk fretted against a steel ball, wear was less at lower humidity. The film life at 16.6 percent R.H. was found to be, on the average, fifteen times longer than

at 58.4 percent R.H.. He argues that two different degradation processes exist at the two different humidity levels.

2.1.3 Methods to Prevent or Mitigate Fretting.

Collins [7] rightly points out that prevention of fretting damage must be carefully considered as a separate problem in each individual design application. Sometimes it is possible to eliminate fretting by changing the design to either separate the contacting surfaces, or to prevent their relative motion by isolating the driving force or by increasing the clamping pressure. These are the only cases for which fretting will be completely eliminated. Several methods have been found to reduce fretting. Providing the fretted surfaces with compressive residual stresses or by properly selecting the mating materials has resulted in reduced fretting damage [7]. Other methods include lubrication by oils or greases [38] and the creation of debris escape routes by surface grooving or roughening [7]. Nowadays there is a tendency to use solid adherent coatings which will function both as a lubricant as well as a mean of preventing contact between the two surfaces. The applied coating can be either metallic or non-metallic. Metallic coatings generally consist of electrochemical plating of cadmium, chromium, nickel, and other metals. These coatings were found to be effective in reducing fretting corrosion. However a reduction in the fatigue strength of the part will result as a consequence of the hydrogen embrittlement occurring during the film deposition [39]. Different deposition techniques were tried. Ohmae, Nakai, and Tsukizoe [40] found ion-plated films to be more effective in preventing fretting than the sputtered or the vacuum evaporated ones. The major problem of these films is adhesion to the base metal [41].

Polymer coatings seem to be the most promising of the non- metallic ones. Furey [42], in 1973, proposed the formation of polymeric films directly on rubbing surfaces to reduce wear. Bill [43] reduced fretting wear by interposing polymers between the contacting surfaces. The fretting fatigue strength of a titanium alloy is only 20 percent of its normal value. In 1957 Liu, Corten, and Sinclair [44] were able to raise the alloy fretting fatigue strength to about 60 percent of its normal value by using a polytetrafluoroethylene coating. Highman, Stott, and Bethune [45] found that no wear occurred for polychlorotrifluoroethylene (PCTFE) and polymethylmethacrylate (PMMA) when fretted against a metal pin. They also found that polytetrafluoroethylene (PTFE), polyethylene (PE), polyvinylidene fluoride (PVDF), polysulfone (PSO), polyvinylchloride (PVC), polycarbonate (PC), and nylon 66 all caused wear of the metal pin. It is clear that some polymers are actually capable of preventing fretting while others may simply mitigate or retard the effects of fretting. More importantly some polymers cause fretting.

Sweitzer [3] found that steel protected with a thin layer of PVC could be fretted for a longer time than one protected with PTFE, PSO, or low-density polyethylene (LDPE) before fretting debris was observed. It is speculated that when fretted PVC degrades and it is transferred as chlorine atoms rather than bulk polymer. Therefore, at the interface, a low shear strength chloride is present rather than an abrasive oxide. Puzio [4] investigated the chemical process involved. He found evidence of chlorine at the interface as a result of the polymer degradation. He concluded that iron would act as a catalyst for the dehydrochlorination of the polymer. In another study, Rorrer [5] found the PVC coating to be very sensitive to the surrounding environment, particularly humidity. This would seem to confirm Puzio observation that the catalytic effect of iron is greatly influenced by the environment.

Day [6] studied the behavior of ten different polymer coatings: PMMA, PTFE, PVDF, PVDC, LDPE, PVC, PSO, polyimide (PI), high-density polyethylene (HDPE), and polystyrene (PS). He found that LDPE, PTFE, PVDF, PI, and PS prevented fretting corrosion while PVC, PSO, and HDPE damaged the steel countersurface. PMMA and PVDC did not last long enough to make any conclusions. He observed a wide variety of physical behavior among the polymer films ranging from plastic flow to brittle fracture. Overall, Day concluded that a strong rigid film would be desirable as long as it does not fret the countersurface.

2.2 Polystyrene.

Polystyrene is a thermoplastic with a clear, glass-like appearance. It is atactic and therefore, completely amorphous. However, crystalline, isotactic polystyrene has been produced. Its clarity is due to the irregular arrangements of the bulky phenol side groups [46]. It is easily colored and easily fabricated and it has exceptionally good dimensional stability. It has reasonably good mechanical and thermal properties, but it is brittle and softens above 100 °C. Polystyrene has been produced since 1937 but it did not reach relevant production until World War II as a result of the synthetic rubber program. After the war large quantities of the monomer were available and the polymerization techniques were well established. Today, one third of the polystyrene produced is used for packaging [47]. Another important application is high voltage insulation and its usage in dielectric materials [47]. Other applications include disposables, toys, refrigerator door liners and insulation, and construction application such as window moldings and frames, doors and door frames, and footing profiles [48]. Polystyrene

products can be made by any commercial technique used for thermoplastics such as injection molding, and extrusion.

2.2.1 Polymerization.

Styrene is prepared from ethyl benzene in the presence of heat and a catalyst. It is then polymerized by either bulk, suspension, emulsion, or solution polymerization in the presence of heat and/or an initiator. Only suspension polymerization and polymerization in bulk are commercially important. The monomer will homopolymerize in the presence of solvents, fillers, pigments, plasticizers, rubbers, and resins. It is used with a wide variety of other monomers to form copolymers [47,48,49]. If the bulk process is used, polymerization is carried out in a stepwise conversion. Heat is generally the sole catalyst. The process has three distinct phases: initiation, propagation, and termination. In the first phase, styrene of 99.5 percent purity is heated to 80-85 °C. The polymer starts to form and after forty or sixty hours, 30 to 40 percent of the monomer has polymerized. In the second phase, the viscous solution is passed through a series of reactors at temperatures ranging from 120 to 200 °C. In the third phase, the molten polymer is cooled and granulated. Bulk polymerization requires careful temperature control [47,49]. In the suspension process temperature control is not as critical. Styrene globules are dispersed in water and polymerized into a bead shaped structure through exposure to two or three stepwise increases in temperature, from 50 to 120 °C, and subsequent separation and washing [49].

2.2.2 Properties.

Polystyrene has a glass transition temperature, T_g, of about 100 °C. It becomes a viscous liquid at 185 °C and at temperatures between 360 and 420 °C degrades to 40 percent styrene, 24 percent toluene and other low molecular weight products [50]. It is a transparent material with good optical properties. It has a refrective index around 1.6 and bends light. It is not very resistant to ultraviolet. Prolonged exposure causes yellowing and premature failure [47,49].

Polystyrene is relatively inert chemically. It resist alkalis, halide acids, and oxidizing and reducing agents. However, it is readily attacked by a large variety of solvents. Exposure to fats and oils may cause stress-crack failure [49]. It is water resistant even though films are permeable to water vapor.

Polystyrene is a good electrical insulator with a low dielectric loss factor. Volume and surface resistivity are very high and power factor is almost zero. A summary of the most important properties of polystyrene is shown in Table 1.

2.2.2.1 Mechanical Properties.

Polystyrene has reasonably good mechanical properties. It is generally unmodified since a wide variety of properties ranges can be obtained through modification of the polymerization reaction to produce resins with varying molecular weights.

Polystyrene is one of the most rigid thermoplastics. Its tensile strength can be as high as 82.7 MPa, while its flexural modulus can be 3.3 GPa. Polystyrene is highly creep re-

Table 1. Properties Of Polystyrene [46,47,48,49].

Repeat Unit:	$-CH_2CH(C_6H_5)-$
Cohesive Energy Density (J/cm^3):	310
Characteristic Ratio (r_0^2/l^2x):	10
Specific Gravity:	1.04-1.09
Specific Volume (m^3/Kg):	939.58-925.12
Glass Transition Temperature, T_g (°C):	100-105
Melting Temperature (°C):	180-190
Degradation Temperature (°C):	360-420
Poisson Ratio:	0.33
Tensile Strength (MPa):	34.5-82.7
Elongation (%):	1.0-2.5
Shear Strength (MPa):	20.7-29.7
Flexural Yield Strength (MPa):	55.2-96.5
Compressive Yield Strength (MPa):	82.7-89.6
Impact Strength (N-m/cm of notch): Standard Izod Test, 63.5 mm bar	0.136-0.218
Flexural Elastic Modulus (GPa):	2.8-3.3
Thermal Conductivity (°C/cm):	2.4-3.3
Specific Heat (cal/°C/gm):	0.32
Thermal Expansion (μm/μm/°C):	60-80
Resistivity (ohm-cm):	$> 10^{16}$
Dielectric Constant:	2.4-3.1
Dissipation (power) Factor:	0.0001-0.0006
Refractive Index:	1.59-1.6
Transmittance (%):	87-92

sistant. It is a very brittle material with a tensile elongation of, at the most, 2.5 percent [47]. Because of its brittle nature polystyrene has very low impact resistance. Another area where polystyrene falls short is its low heat-deflection temperature, 82-88 °C, which prevents polystyrene articles from being sterilized [48].

Many of the polymer faults can be diminished by copolymerization and blending. Toughness can be greatly improved by incorporating rubber, usually 5-10 percent, polybutadiene, or copolymer rubber [47,48]. Heat and impact resistance can be enhanced by using a minor amount of acrylonitrile as a comonomer [48].

2.2.2.2 Tribological Properties.

The exceptionally good performance of some plastics in friction and wear applications has resulted in an increasing number of plastic bearings, bushings, seals, wear plates, and sliding parts [51]. Plastics can produce low friction, low wear sliding contacts. Because of its brittle nature, polystyrene is not used for tribological applications. Therefore very little is known about polystyrene frictional and wear behavior.

Shooter and Thomas [52] suggest that friction is dependent on chemical structure. A polymer with a strong interchain bonding will shield the positive charge of the carbon atom and therefore molecular cohesion and interchain bonding forces are minimzed yielding low friction. According to the authors this is the reason why polytetrafluoroethylene has the lowest friction followed by polyethylene, polystyrene, and polymethylmethacrylate. The cohesion energy of these polymers also increases in the same order. A more recent theory which has received wide acceptance proposes the smooth molecular profile of PTFE which provides for easy shear as the reason for its low

friction [53]. On the same line is the finding of Higham, Stott, and Bethune [45]. They found that there is a close correlation between the fretting damage done by a polymer on a metal and the property of the polymer that indicates its adhesive properties or surface energetics. An amorphous polymer, such as polystyrene, has a frictional behavior very similar to that of metals when below the glass transition temperature (T_g). But above T_g the frictional behavior may become quite complicated. The picture is further complicated by the fact that the Amonton's and Couloumb's laws of friction are not followed. Friction of plastics depends on sliding speed and is not linearly dependent on load [51]. The coefficient of friction of polystyrene, or any other plastic, cannot be regarded as a material constant but it will vary according to sliding speed, normal load, and environmental conditions. Polystyrene is a polymer which exhibits true interfacial sliding. When polystyrene slides over a smooth clean surface, at a temperature below T_g, no coherent material transfer is detected on the counterface. Transfer of chemically degraded or lower molecular weight products is however, possible [54].

Polystyrene, and any plastic, can be affected by different types of wear: adhesive, thermal, abrasive, fatigue, and corrosion. Thermoplastics, such as polystyrene, are not very resistant to abrasive wear, but are less affected by thermal wear [51]. The simple wear laws, Archard's law [55], and Lewis' wear factor (K) [56,57], apply only over limited ranges of load and/or sliding velocities. Clinton, Ku, and Schumacker [58] showed that the IBM wear model, developed by Bayer, Clinton, Nelson, and Schumacker [59] for metals, is also applicable to plastics. According to this model wear is zero or negligible as long as the maximum shear stress in the contact region is below a certain value. The experimental work done by Clinton et al. showed that under unlubricated conditions higher stresses are possible with plastics than with metals for the same wear.

Day [6] successfully used a 86.0 μm thick polystyrene film to prevent fretting corrosion in a ball on disk system. Under the same test conditions polystyrene outperformed polymers, such as polyvinyl chloride and low density polyethylene, which should have been better. Day observed that the polystyrene underwent a "wearing-in" process which may explain the film long life. In the initial stage large particles are formed. As fretting proceeds the contact area becomes larger and more conforming. The stresses within the coating will be reduced and possibly the wear rate will decrease. The particulary extraordinary behavior of polystyrene in this situation is just another indication that the tribological behavior of plastics cannot be explained by simple laws.

3.0 Experimental Work.

This work had two objectives. The first objective was to study how polystyrene coatings of different thickness behaved under fretting conditions. The second objective was to try to obtain information on how fretting damage of the polystyrene coating progressed with time.

In order to achieve the first objective tests were run until the coating was broken and there was complete metal-to-metal contact. The testing time was recorded. The coefficients of friction, at the beginning of the test and at the end of the test, right before breakthrough, were also recorded. Optical and scanning electron microscopy were used to determine the presence of cracks and/or plastically deformed regions in the wear scar as well as the scar size and shape.

The other objective required the test to terminate at precise time intervals. Again optical and scanning electron microscopy were used. In addition profile traces of the wear scar were taken and combined with computer graphics. The result was three-dimensional

maps of the wear scar surface. The three-dimensional maps were also used to estimate the wear and debris volumes at the different time intervals.

In this section the preparation of the specimen before testing is presented and explained. The apparatus used in this study is called the MARK III. It was developed by Frantz [1] to study fretting of a bearing and its cartridge. A detailed explanation of this machine is also included. The chapter is concluded by a description of the experiments and measurements made.

3.1 Preparation of Test Specimens.

In order to achieve the objectives of this study several specimen had to be used. In total twenty-eight coated steel disks and forty-nine steel balls were used. The disks were made of 1045 steel and were 2.541 cm in diameter and 0.79 cm in thickness. The balls were made of AISC 52100 steel and were 1.588 cm in diameter. Both the disk and the ball were thoroughly cleaned in order to have a surface free of any contaminant before they were used in the tests. In addition the steel disks required some preparation prior to being coated.

3.1.1 Surface Preparation and Cleaning.

The 1045 steel disks were cut from a stock bar and one side was ground to approximately 1.0 μm R_a. When the disks were needed they were first sandblasted to about 1.5 μm R_a.

The sandblasting assured better adhesion of the polymer to the steel substrate by enhancing mechanical interlocking. Following the sand blasting the disks were placed in a methanol bath in an ultrasonic cleaner in order to remove all the loose debris and any oil or grease which was on the surface. Next they were put through two twenty-minute vapor baths, one in methanol and one in hexane, in order to clean the surface of any organic or inorganic contaminant. The same cleaning procedures, that is the ultrasonic cleaning and the vapor baths, were also used for the steel balls. The step-by-step procedures are shown in Appendices B.1 and B.2.

3.1.2 Polymer Used.

The polymer used in this study was polystyrene. Polystyrene is a linear amorphous polymer. Because of its brittle nature it is generally not used in tribological applications. The particular one used in this study had a molecular weight (M_w) of 3.2×10^5 . The complete molecular weight distribution as obtained from Gel Permeation Chromatography (GPC), is shown in Figure 1. The analysis was conducted in the Chemistry Department of VPI & SU. The polymer was dissolved in methyl ethyl ketone (MEK) at room temperature.

3.1.3 Disk Coating.

The method used for coating the disks was one of solvent deposition. The disks were dipped in a polymer solution and the polymer was allowed to dry on the disks. After the amount of polymer necessary to obtain the desired thickness had been deposited, the

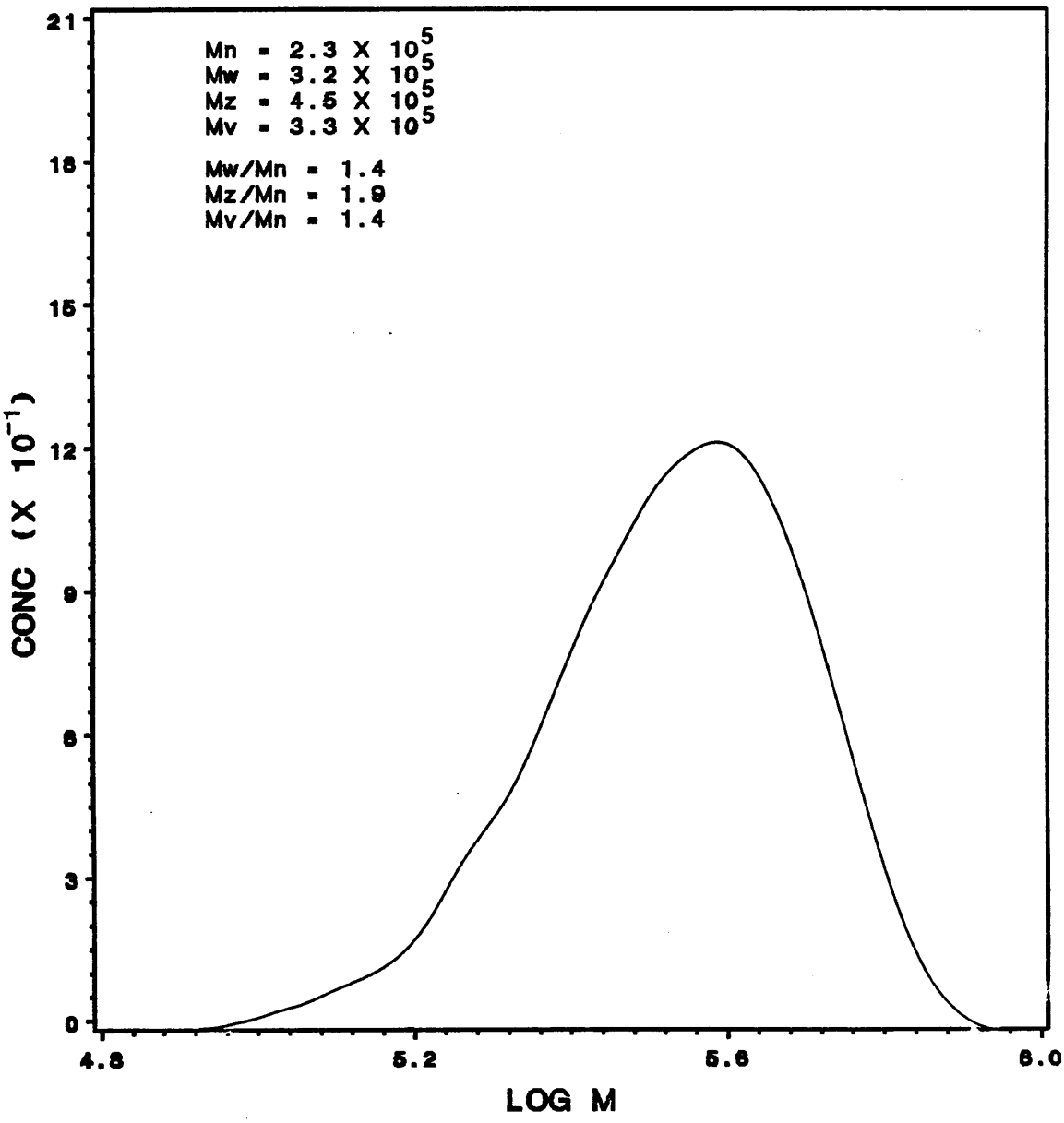

Figure 1. Polystyrene Molecular Weight Distribution.

coated disks were placed in an oven for twenty- four hours at a temperature of 75 °C to assure complete evaporation of the solvent. The final curing was done by placing the disks in a vacuum at a temperature of 120 °C for two hours. The vacuum was then released and the disks were allowed to slowly cool to room temperature. The amount of polymer deposited, and therefore the coating thickness, was controlled by varying the number of dips and/or the solution concentrations. Seven different film thicknesses, ranging from 8 μm to 52 μm, were used. To obtain the seven different thicknesses, three different concentrations were used: 100, 150, and 200 grams of polymer per liter of total solution. Different number of dips, ranging from one to four, at different concentrations, were required for each thickness. Appendix B.3 shows the detailed procedure as well as the required concentrations and number of dips for each of the seven thicknesses.

3.1.4 Film Thickness Measurement.

After the film was deposited on the disk its thickness was determined by using a thickness gage which operated on the basis of eddy currents. The measurements were made by placing a 1 mm diameter probe on the film. The film thickness was then read in thousandth of an inch on a metering device. Prior to measurement, the device had to be calibrated (see device manual). For each disk, four measurements were made across the area in which the tests were to be done.

3.2 The MARK III Machine.

As already mentioned the MARK III was originally developed for studying fretting of a bearing and its cartridge. Later it was modified to allow for a ball-on-plate type of contact geometry. To accomplish this, a plate holder (1)[2], and yoke (2) were added to the existing machine. Also several other modifications were made in an attempt to better simulate such a complex phenomenon as fretting. In Figure 2 the modified MARK III machine as it was used in this study is shown. The needed horizontal movement was obtained by changing the vertical motion of a shaker table (3) into a horizontal motion by means of a simple linkage (4). The vertical motion was provided by a vibration fatigue testing machine. Built into this device were means of controlling the frequency (0-100 Hz), and the magnitude of vertical motion (0-200 μm). By adjusting the vertical motion, the slip amplitude could be set at the desired level. The slip amplitude was statically measured by the dial displacement gage (5) and set by locking the eccentricity at the appropriate position. The value of the slip amplitude was then dynamically monitored by means of a linear variable distance transducer (LVDT) (6). The frequency of motion could be set to the desired level by moving the manual control (7) until the desired frequency was read on the meter (8).

3.2.1 Specimen Assembly and Loading.

The disk was placed in the disk holder and secured by tightening the set screw (9). The disk holder was then moved along the angled iron bracket (10) to the desired position

[2] The number in parenthesis refers to the numbers in Figure 2 on page 25

Legend:

1. Plate Holder
2. Ball Strain Arm
3. Shaker Table
4. Linkage
5. Displacement Gage
6. LVDT
7. Frequency Manual Control
8. Frequency Meter
9. Plate Set Screws
10. Iron Bracket
11. Plate Holder Set Screws
12. Ball Insert
13. Ball Holder
14. Weight Hanging Points
15. Environmental Chamber
16. Gas Inlet
17. Hygrometer
18. Strain Ring
19. Force Calibration Pulley System
20. Variable Speed Motor
21. Cycle Counter
22. Motor On/Off Switch

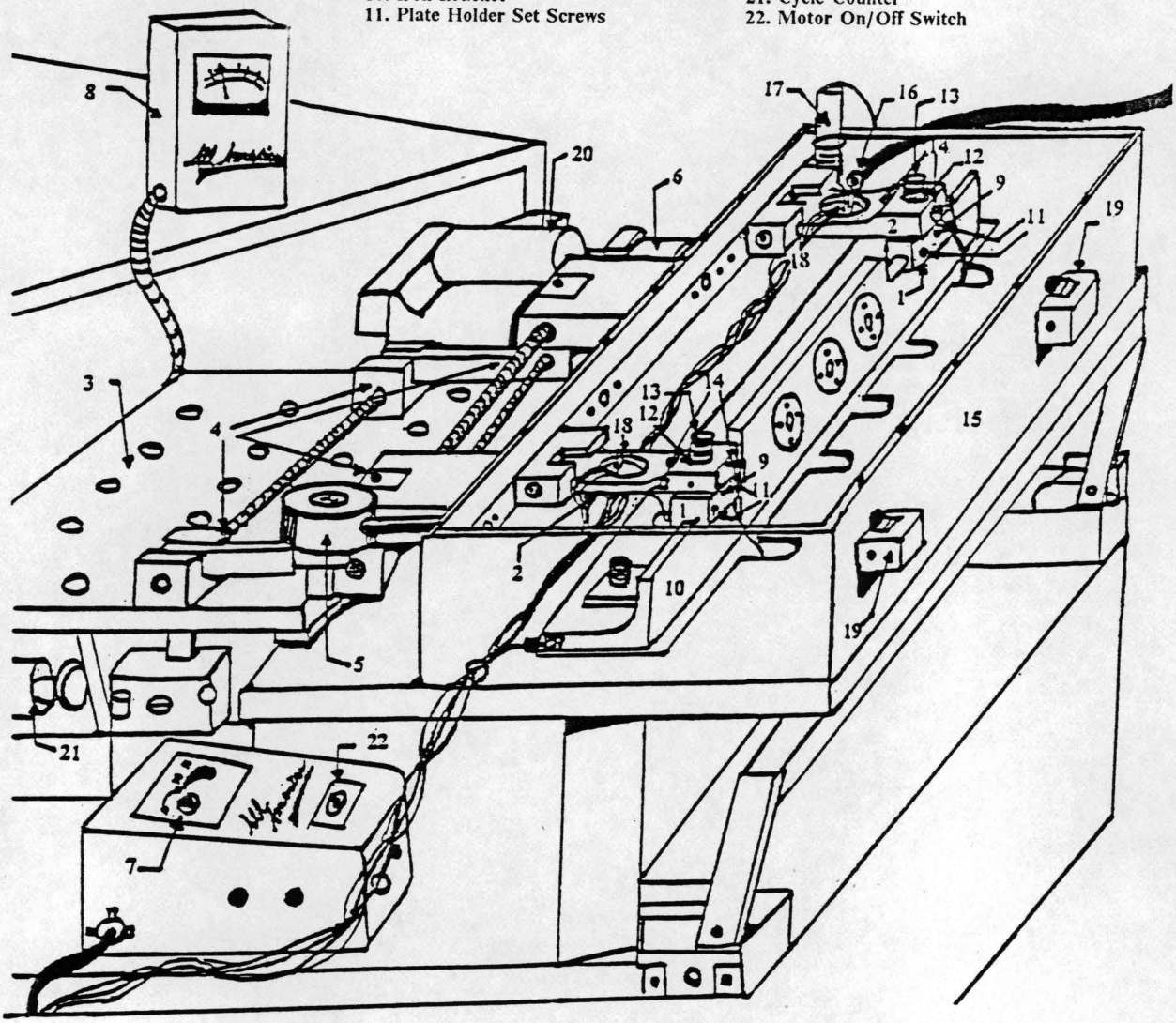

Figure 2. The MARK III Fretting Machine.

and secured by tightening two set screws (11). An insert was provided (12) on the head of the yoke to allow the mounting of the steel ball specimen. The insert was designed so that the ball would protrude 5.1 mm below the head assuring contact with the steel plate as well as proper alignment of the yoke. The ball was held in place by a threaded ball holder (13). Figure 3 shows in more detail the way in which the specimens are assembled and placed in contact with each other.

The specimens were loaded normally by means of weights. The weights were attached to a pulley running on a cable connected to the yoke at two connection points (14) which were equidistant from the center of the area of contact.

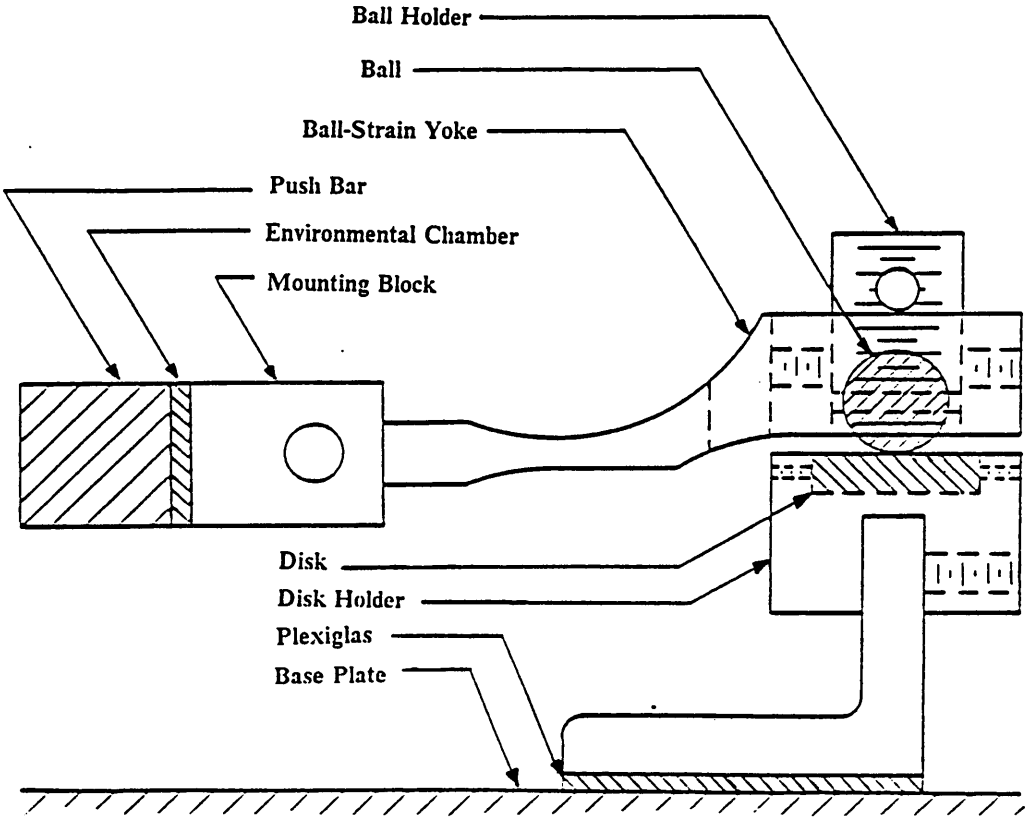

Figure 3. Ball and Flat Specimen Holders in the MARK III Fretting Machine.

3.2.2 Contact Geometry.

The MARK III, in the configuration just described, employed a ball-on-flat type of contact geometry. A ball was loaded against a disk and forced into a small amplitude motion as shown in Figure 4. This type of contact geometry had the advantage of creating high stresses in a concentrated area. Hence fretting damage was accelerated and the specimen were subjected to the worst possible conditions.

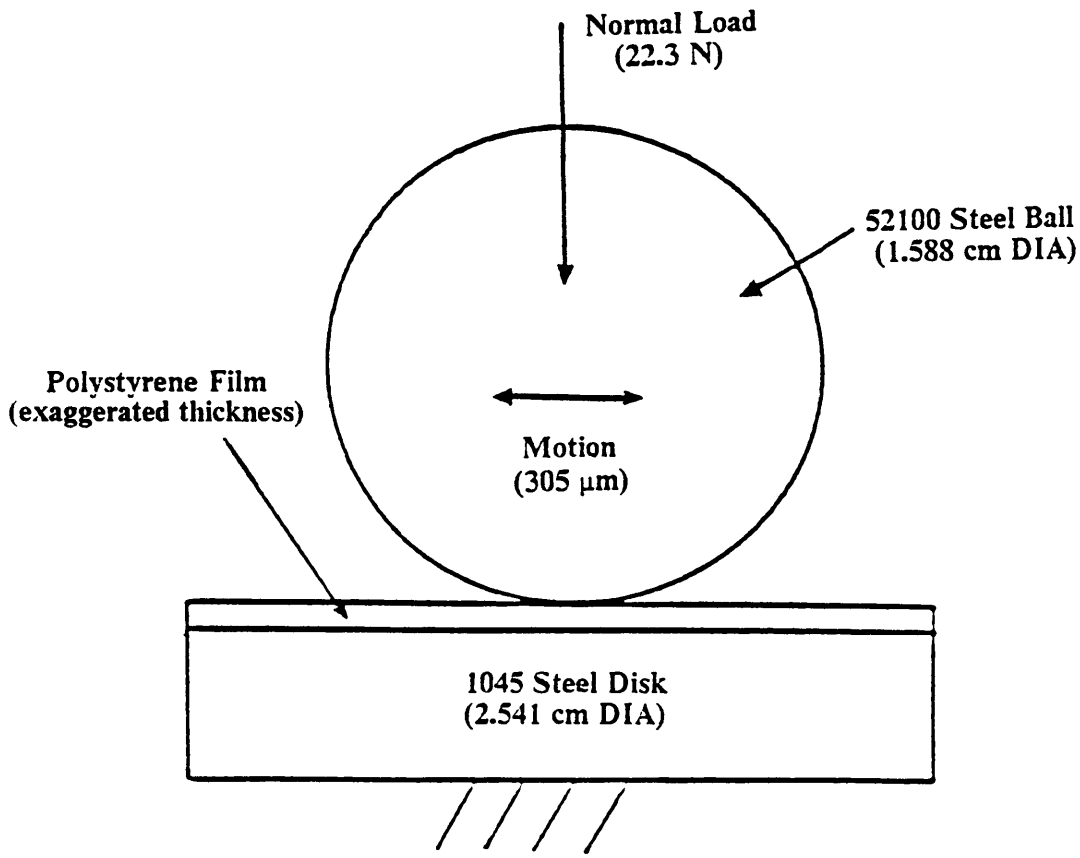

Figure 4. Geometry of Contact.

3.2.3 Environmental Chamber.

One of the fundamental variables in fretting is the surrounding environment. The MARK III was therefore equipped with an environment chamber (15). It was possible to fill the chamber with any desired gas or atmosphere. A small orifice (16) was provided in the otherwise sealed enclosure so that a continuous flow of the desired gas was established and a positive pressure maintained. The flow was measured by means of a flow meter. The temperature and the humidity of the gas were measured with a digital hygrometer (17) placed in front of the flow to obtain the best possible reading as well as act like a baffle.

3.2.4 Instrumentation.

Built in the MARK III fretting machine was the capability of measuring the friction force at the interface of the fretted elements. For this purpose a strain ring (18) was built into the yoke and strain gages were mounted to measure the strain in the yoke. The strain gages were then connected to a bridge amplifier. The signal was sent to a chart recorder for display. Prior to running a test the strain gauge circuitry had to be calibrated. To do this, weights were hung on a cable which ran over a pulley (19) and attached to the ball strain yoke. The resulting tension placed on the yoke caused a strain in the strain ring. The strain magnitude was indicated by the deflection of the pen in the chart recorder. The recorder pen deflection could be adjusted by changing the sensitivity of the recorder itself. By properly adjusting the chart recorder and using different known weights a calibration chart was developed. Appendix B.4 shows the procedure used for the calibration.

The MARK III was used to measure the life of the polymer film (or any non-conductive type of film). For this purpose a voltage divider circuit was used to place a 15 mV potential across across the ball and the disk which measured the resistance of the interface [60]. When the polymer was present between the ball and the disk the interface resistance was infinite. When contact occurred the electrical resistance and voltage dropped to zero. The voltage change deflected the pen in a chart recorder. The time between the start of the test and when the contact occurred determined the film life. Appendix B.5 gives the detailed procedure for calibration of the contact resistance circuit.

3.2.5 Operation.

After the vibration fatigue testing machine was set at the right slip amplitude by locking the eccentric at the appropriate position, the instruments were calibrated and the specimens were mounted and loaded as described before, the variable speed motor (20) was turned on and after thirty seconds the machine was ready for testing. The test was started by engaging the shaker table and setting the desired frequency by turning the manual control (21). During the first few minutes of operation it was necessary to adjust the frequency to the desired level. When it was time to stop the test, the shaker table was disengaged by turning the frequency control down to zero. Next the variable speed motor was turned off, the specimens removed, and the instruments turned off. When the instruments were turned off and on a change in the calibration occurred. Hence, if more tests had to be run, the instruments and the variable speed motor were left on while the specimens were changed.

3.3 Experimental Procedure.

The experimental work was divided into two phases. During the first phase the change in life as a function of thickness was measured. In the second phase the wear of films of two different thicknesses was studied as a function of time. In the first phase the fretting process was studied by optical and scanning electron microscopy. In the second phase, in order to estimate the fretting wear, computer graphics was used to create a computer representation of the wear scar. Wear and debris volumes, as well as depth of penetration, were then calculated from this computer representation.

3.3.1 Life-Thickness Experiments.

In the life-thickness experiments, tests were run until the films failed. Film life was determined from electrical contact measurements, that is the time between the start of the test and the moment complete metal-to-metal contact occurred determined the film life. The test conditions are shown in Table 2. Seven different film thicknesses were used. For each thickness twelve tests were run, four tests per disk. Therefore three disks for each thickness were needed for a total of twenty-one disks. The seven thickness values were chosen because they were easily obtained by the technique described before. For each test the measured friction force was used to calculate the coefficient of friction. The experimental data are shown in Appendix D.1.

Table 2. Experimental Conditions.

Normal Load (N):	22.3
Amplitude of Vibration (μm):	305
Frequency of Vibration (Hz):	20.0
Temperature (°C):	18-24
Environment:	Room Air, 50-60 % R.H.
Film Thickness (μm):	7.9 13 23 30 38 46 52

3.3.2 Wear-Time Experiments.

In the wear-time experiments the tests were stopped at different time intervals before metallic contact occurred. The time intervals were chosen to cover the life span, as determined by the thickness-life experiments. Two different coating thicknesses 38 μm and 52 μm were used, one with a short life and one with a long life. Twelve time intervals (from 30 sec to 360 sec) were chosen for the 38 μm film . Sixteen time intervals (from 30 sec to 5400 sec) were chosen for the 52 μm film. Table 3 shows the time intervals for each thickness. Four tests were run on a disk. Therefore three disks and twelve balls were used for the short life film, while four disks and sixteen balls were used for the long

Table 3. Time Intervals for the Wear-Time Experiments.

Film Thickness (μm)	Time Intervals (sec)
38	30 60 90 120 150 180 210 240 270 300 330 360
52	30 60 90 120 150 300 600 900 1200 1800 2400 3000 3600 4200 4800 5400

life film. The test conditions shown in Table 2 were also used for these experiments. Appendix D.2 contains all the experimental data.

3.3.3 Characterization of the Fretting Process.

From the thickness-life experiments some representative tests were chosen to be photographed. The tests chosen were those which lasted close to the average life of each film thickness. Both the ball and the disk scar from these tests were photographed with an optical microscope and with a scanning electron microscope. The optical microscope was provided with an automatic exposure meter and shutter piece connected to a 35 mm film carrier loaded with Kodak Ektachrome 160 Tungsten film. The macroscope was

also provided with a quarter-wave plate which allowed for changes of contrast. Two types of illumination were used. One was built into the microscope and consisted of a quartz halogen coaxial lamp and was normal to the object being photographed. The other source of illumination consisted of an external light source which could be positioned at any angle with the object being photographed. For each of the ball and the disk scar two standard magnifications were used: 20X, and 64X. Other magnifications were used as needed. Great care was taken so that the loose polymer debris present on the disk and the ball were neither removed nor moved from their original position.

After the optical microscopy was completed, the specimens were sputter-coated with Au-Pd and photographed in a scanning electron microscope (SEM). The SEM had an accelerating voltage of 15 KV and was set in the "y-mode." In this mode the surface of the object being photographed is scanned as in the standard operational mode but the signal is also proportional to changes in slope. A change in slope resulted in a peak. The sensitivity, therefore the height of the peaks, of the instrument could be controlled so to limit the distortion of the real surface. For this study the sensitivity was set to a minimum value so that the surface itself would still be visible and identifiable, and at the same time regions of changing slopes were readily seen. All specimens were photographed at a magnification of 43X. The 43X magnification produced photographs with approximately the same scale as the optical ones. This allowed for direct comparison between the two. SEM photographs provide clearer details. Deformed areas are more visible and not disturbed by optical effects. The combination of optical and SEM photographs of the wear scar gives information on the degree and the type of deformation and the changes in optical properties of the coating. Other higher magnifications were used to photograph particular regions of the wear scar.

For the wear-time experiments, in addition to the optical and SEM photographs, a three-dimensional map of the wear scar surface was generated. The main reason for creating such a map was to be able to estimate wear and debris volumes and depth of penetration. Additional information on the debris distribution and the position of the identation with respect to the debris was also obtained. The map was generated by a system which combines surface roughness profiles with computer graphics and it was displayed on a graphic terminal using MOVIE.BYU. The system was developed by Sankar [61] and is available in the tribology lab at VPI&SU.

The system combined a series of parallel traverses of the profilometer stylus to generate a surface. The specimen was placed on a x-y table so that the stylus ran in the direction of sliding. A 2.5 μm steel tape was positioned on the edge of the specimen so that the stylus skid was resting on it while the stylus itself was on the specimen surface away from the wear scar. The steel tape had the double purpose of properly aligning the traces and triggering the sampling. The vertical position of the gear box was set and left untouched for all the traces within one wear scar. This was done to assure that the same voltage level was used for all traces, hence the same vertical alignment. The sampling rate was set so that the signal was sampled 300 times during each traverse with the distance travelled between two samples being 2.0 μm. The distance between traces was 0.127 mm. The sampling intervals were limited by the fact that a total maximum of 5000 points could be handled by MOVIE.BYU. A minimum of six traverses were taken for each wear scar. Large wear scars required as many as twelve profiles. The signal was digitized using an analog to digital I/O card interface. An interactive computer program was used to control the sampling rate, total number of samples, and other parameters. Other programs were used to set up and generate the surface map of the region of interest. For further details and other computer program listings see reference 61.

A computer program was written to estimate the wear and debris volumes from the three-dimensional maps of the fretted region. The program is called WEAR, is written in FORTRAN, and is shown in appendix E.3. It uses the same data files used for generating the three-dimensional maps. The specimen surface is simulated as a flat plane with its equation given by:

$$aX + bY + cXY + d = Z,$$

where X is in the direction of sliding, Z is vertical, and Y is normal to both X and Z. This mean plane was found by using data from profiles outside of the wear scar. Next, all the data from each profile were compared to the fitted plane. If a data point was above the plane it was considered either as debris or as plastically deformed material. If, on the other hand, the data point was below the plane it was considered as wear. Because the mean plane is positioned so that the initial surface irregularities were averaged out, they did not influence the calculations of wear and debris volumes. After the data points had been separated the wear area and the debris area for each profile were estimated by using Simpson's rule. The wear and the debris volumes were finally calculated by multiplying the respective areas by the number of traces times the distance between the traces.

The computer programs needed to set up and generate the three-dimensional maps of the wear scar, as well as the one required to estimate the wear and debris volumes, were assembled together in a single program called AUTOMAP2. It is an interactive program and is written in EXEC2. Since a few improvements and the addition of the WEAR program have considerably modified the original one, its listing is shown in Appendix E.1.

4.0 Results.

Wear phenomena are largely random and influenced by a great variety of factors. For this reason data collected from wear experiments are generally spread over a range. To overcome this difficulty the same test is run several times. The collected data are then statistically analyzed and averages are determined. In this study, this procedure was followed for the life-thickness experiments. Such a procedure was not feasible for the wear-time experiments. Only one test was run for each time interval. This resulted in scattered data from which it was difficult to determine the progression in time of the phenomenon being observed. However, by plotting the data with appropriate interpolation routines, it was still possible to determine average tendencies.

All the graphs shown in this work were plotted using a SAS spline interpolation routine. The particular routine used is designed for fitting experimental data. It fits a cubic spline that minimizes a linear combination of the sum of the squares of the residuals of fit and the integral of the squares of the second derivative. The relative importance of the two terms could be varied by changing an index number (between 0 and 99). A high index

number gave more importance to the second derivative of the cubic spline resulting in a smoother fit. For this study a value of 75, for the index number, was used in all plots.

In this chapter, the experimental results are divided into two separate sections corresponding to the two types of experiments conducted. All the pertinent experimental data and measurements, as well as the macroscope and SEM work done, for each section are presented.

4.1 Results of the Life-Thickness Experiments.

In this set of experiments the film life as a function of its thickness was evaluated. Preliminary tests were conducted to determine the seven thicknesses to be used. The thinnest film was chosen so that metallic contact would not occur upon static loading. The reason for a minimum thickness can be found from elastic theory. Hertzian theory yields a value of 5.8 μm for the deflection of polystyrene under a load of 22.3 N. Therefore films of at least 6 μm must be used to prevent contact between the ball and the disk. The thickest film was chosen because it had a film life in excess of one hour. The five intermediate thicknesses were chosen to cover this range as uniformly as possible. The thickness values given represent the average of twelve measurements done for each thickness (see Appendix C.1).

Surface roughness can be used to qualitatively estimate the extent of the effect of the substrate. A certain part of the polymer coating goes into covering the substrate irreg-

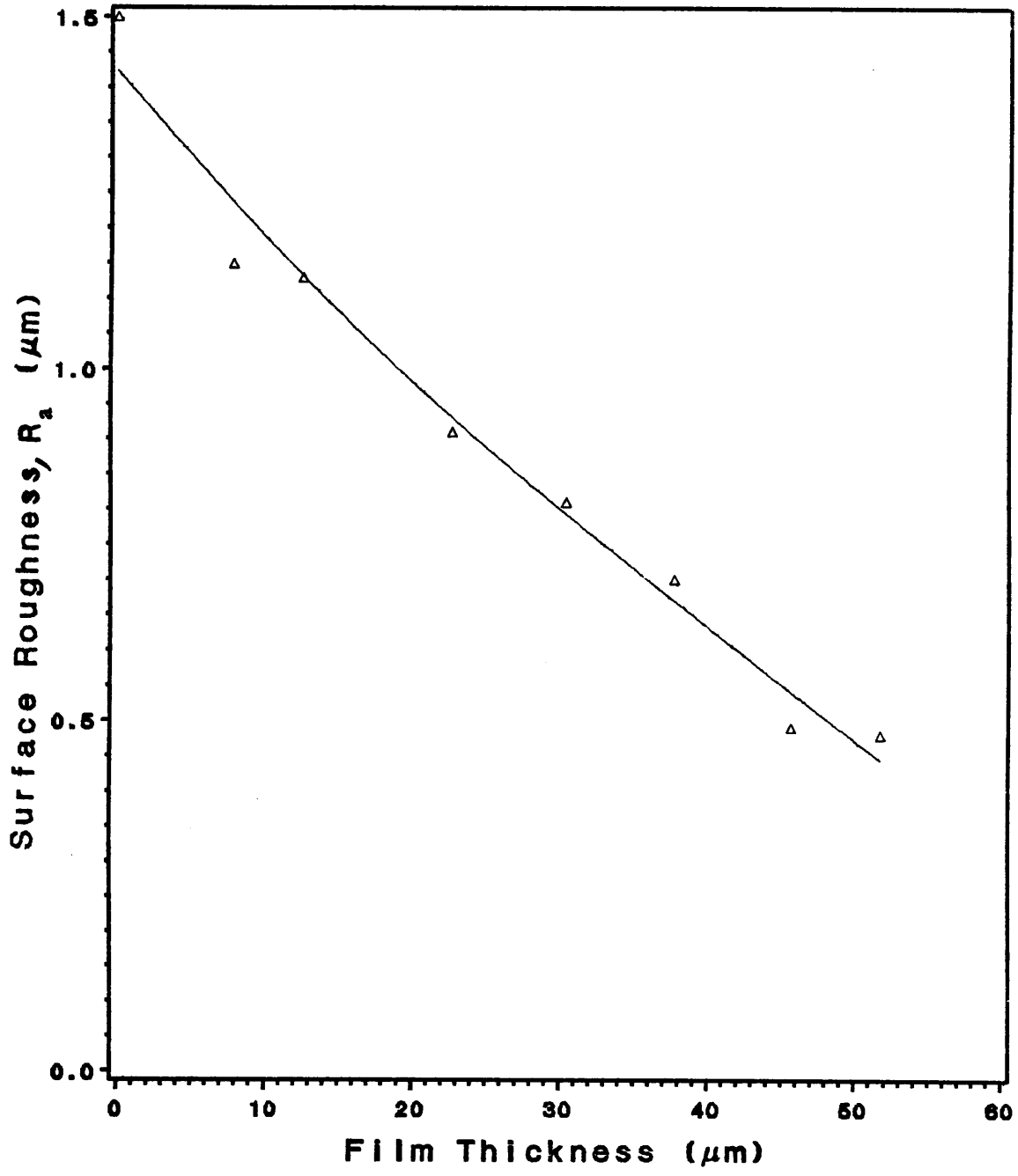

Figure 5. Film Surface Roughness.

ularities. Because of the effect of gravity the surface valleys must be filled up with polymer solution before the peaks can also be covered. However, a small amount of polymer still goes into covering the surface peaks because of the viscosity of the solution. As a result thin films will be rougher than thick films. This is shown in Figure 5. The figure shows film roughness to be inversely proportional to film thickness. As a consequence, for thin films, the effect of the substrate is higher than for thick films.

4.1.1 Life-Thickness Behavior.

To evaluate film life, twelve tests were run for each thickness until contact between the metals occurred. The contact detection circuit of the MARK III is capable of registering partial or intermediate contact as well as full contact. These two types of contacts are shown in Figure 6. By intermediate contact is meant a contact point which occurs occasionally in the course of one cycle and does not extend through the full amplitude of slide. Also this type of contact is intermittant in nature and does not occur for every cycle. Full contact, on the other hand, occurs over a greater portion of the sliding distance and is repeated with every cycle. Polystyrene films showed that some intermediate contact can occur before full contact. During intermediate contact no evidence of red-brown oxide debris was noted. However, if full contact occurred only a few more cycles were necessary to form a considerable amount of the oxide. Therefore the tests were terminated when full metal-to-metal contact occurred. Appendix D.1.1 contains all of the films life data. The results are summarized in Table 4. It is apparent that for each thickness there is a range of lives.

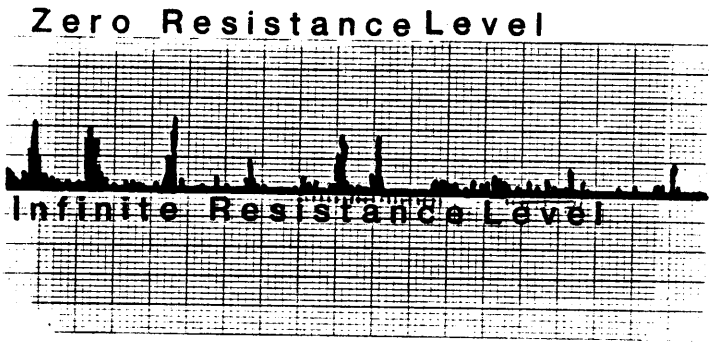

(a) Intermediate Contact

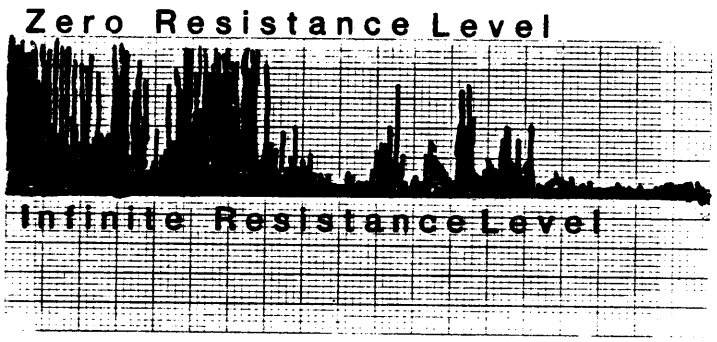

(b) Full Contact

Figure 6. Intermediate and Full Metal-To-Metal Contact.

Table 4. Summary of the Life Results.

Thickness (μm)	Life (sec)	Range (sec)	95 % Conf. Interval (sec)
7.9	37	0 - 100	12 - 60
13	76	12 - 190	33 - 114
23	214	130 - 283	182 - 246
31	382	239 - 540	318 - 447
38	592	310 - 1000	426 - 718
46	1795	700 - 3600	1174 - 2416
52	8156	4788 - 10920	6802 - 9509

Figure 7 shows the relationship between film thickness and film life. The nature of the curve suggests that two different fretting conditions occur as the polymer coating gets thicker. For films less than 40 μm severe fretting conditions exist that greatly limit the film life and are only partially affected by film thickness. This is reflected in the almost flat slope of the curve. After 40 μm the fretting conditions change enough to cause longer film life and the effect of film thickness is more evident resulting in a much steeper curve.

4.1.2 Friction-Thickness Behavior.

The frictional behavior of the system followed the same pattern for all of the seven thicknesses used. At the beginning of the test, during the very first few cycles, the fric-

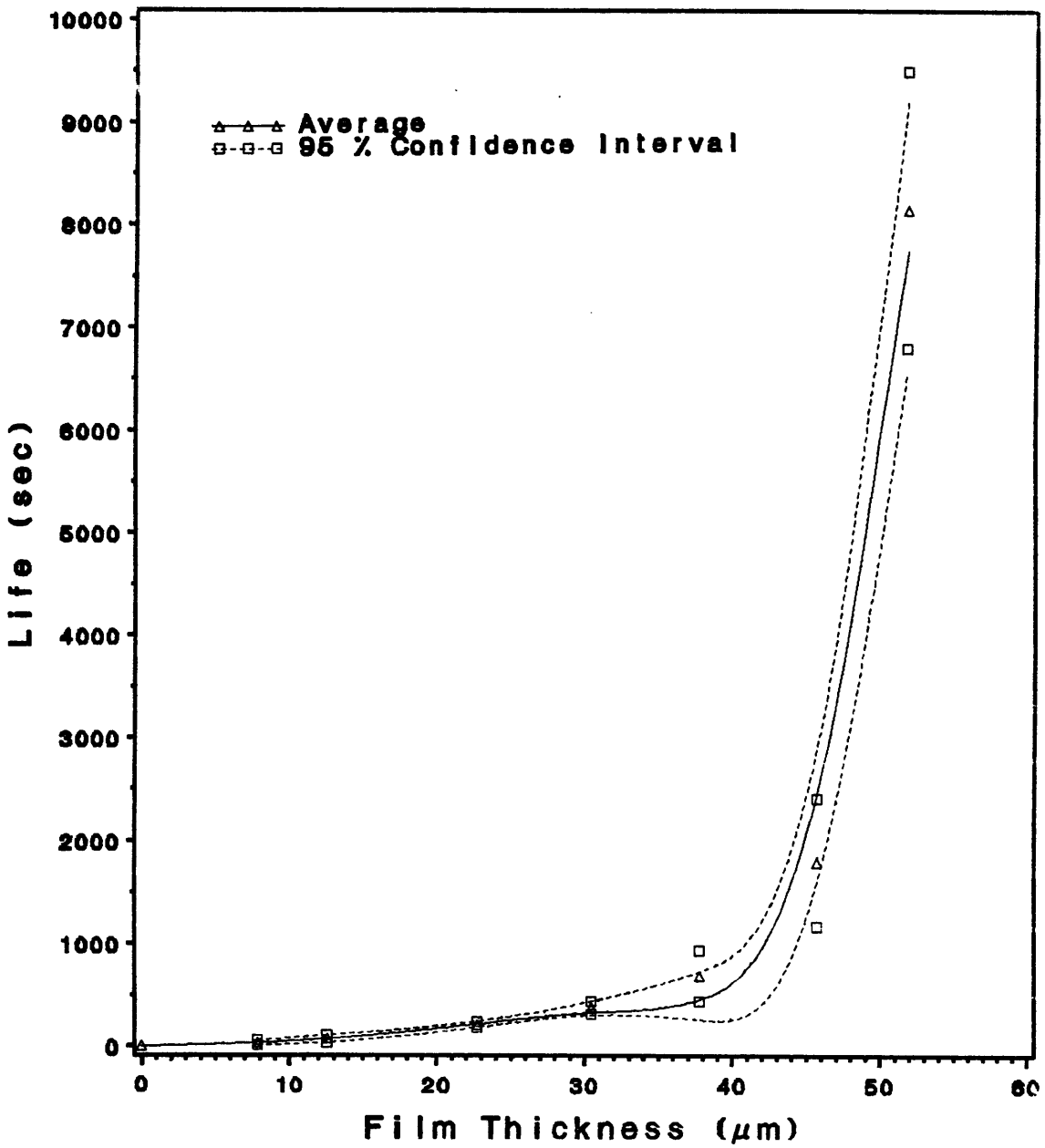

Figure 7. Average Film Life.

tion force rapidly increased to some steady-state. For this reason an initial, and a final, or steady-state, friction are reported. Occasionally some variation in the friction force was observed during a test. However, this variation did not seem to affect the film performance. All the frictional data are shown in appendix D.1.2. Friction data had very little variation for a given thickness even though film lives varied much more. This is an indication that in fretting the effect of friction is of minor importance. Figure 8 shows the relationship between friction and film thickness. Both the initial and final friction increase with increasing film thickness.

4.1.3 Fretting Behavior.

The fretting behavior was characterized by using optical and SEM photography. Figures 9 through 15 show optical and SEM photographs of the wear scars for each film thickness after breakthrough. The photographed wear scars were chosen from tests which lasted for a time very close to the average life of each of the seven thicknesses. All of the photographs are shown so that the direction of motion is horizontal. The shape of the wear scar varies from an oval, almost rectangular, shape for the 7.9 and the 13 μm films to an almost perfect circle for the 52 μm film. Deformation for the two thinnest films (Figure 9 and Figure 10) appears to be more evident on the edges of the wear scar while the center seems to be relatively untouched. The central region, approximately equal in length to the sliding amplitude seems to be a characteristic of all wear scars. However, for films thicker than 13 μm, plastic deformation and cracking have occurred in this central region. This can also be seen in Figure 16 where the photographs of the 7.9 and the 52 μm films are compared. The photographs were taken

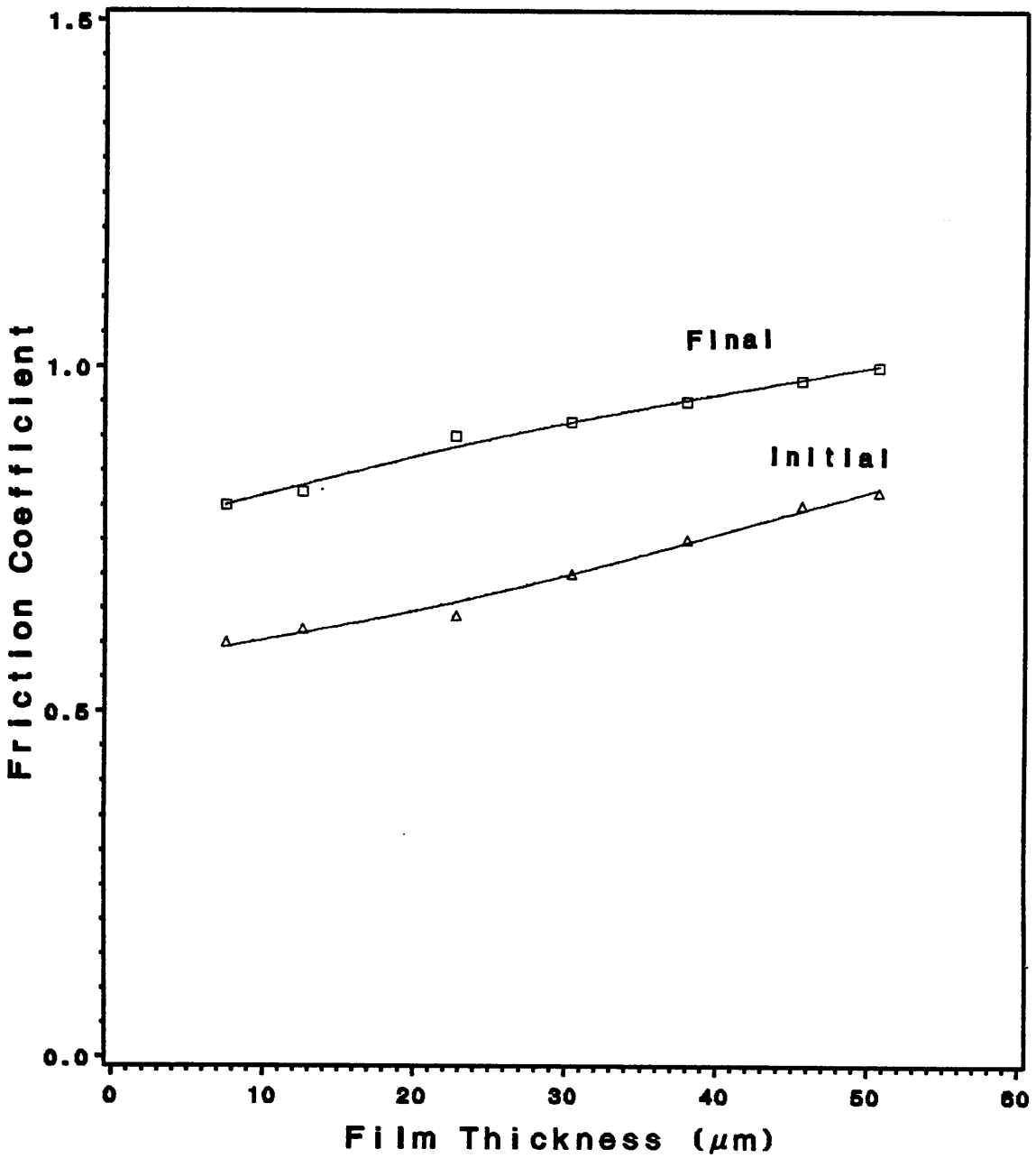

Figure 8. Friction Results.

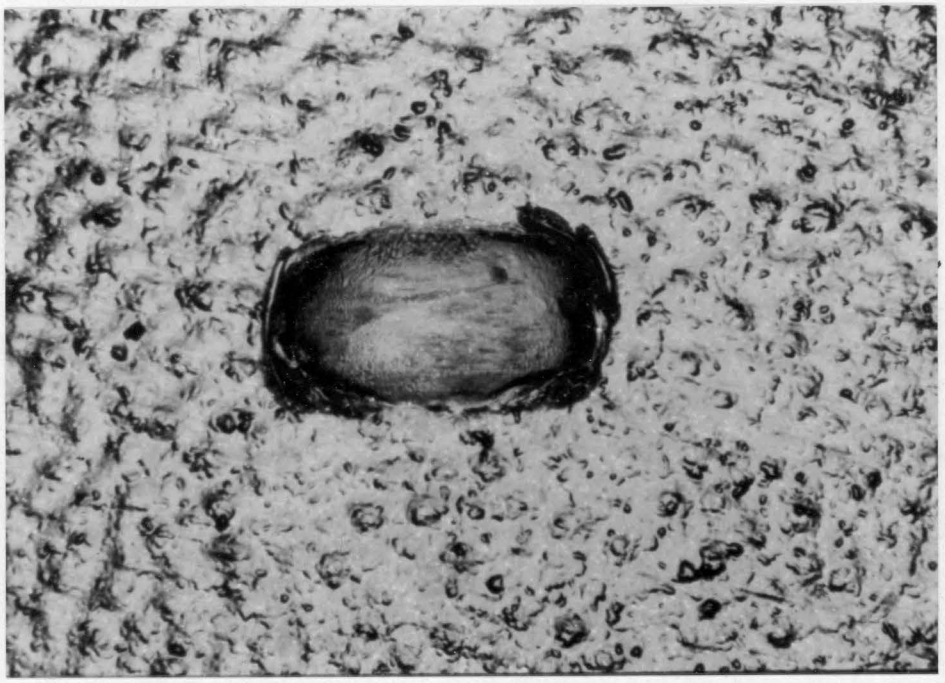

(a)

305 μm

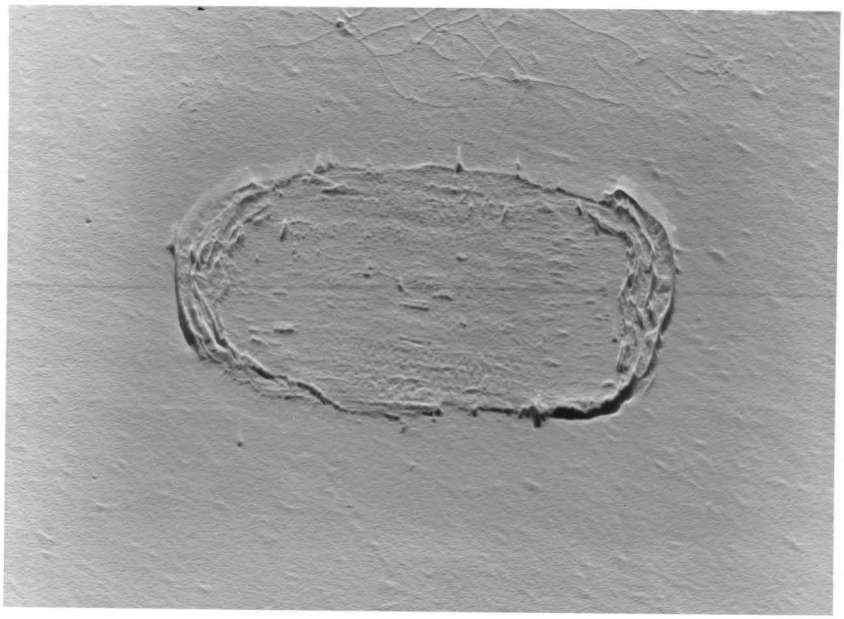

(b)

305 μm

Figure 9. Optical and SEM Photographs for the 7.9 μm Film.

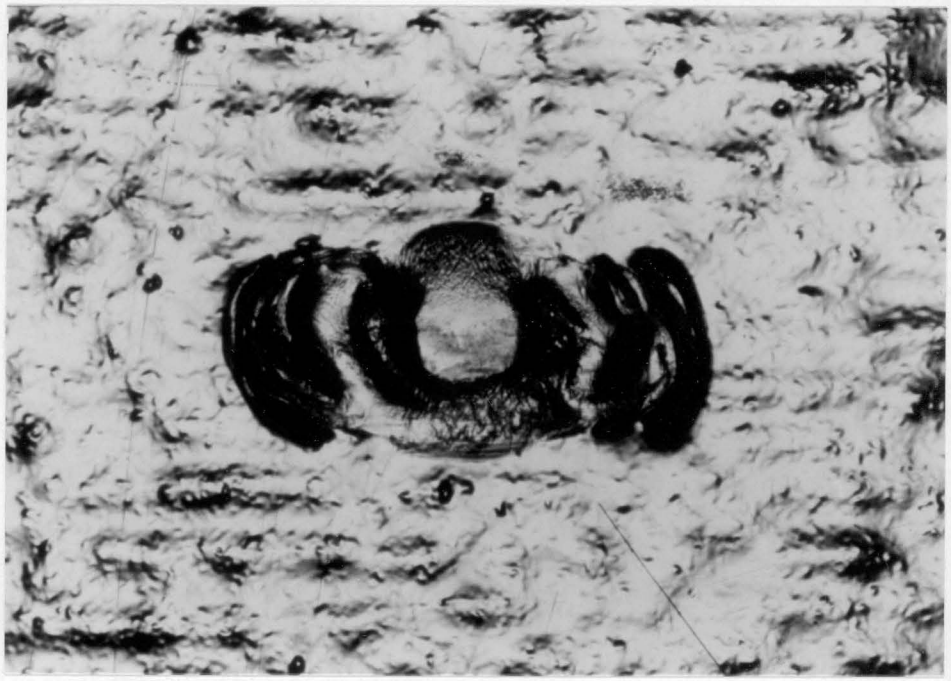

(a)

305 μm

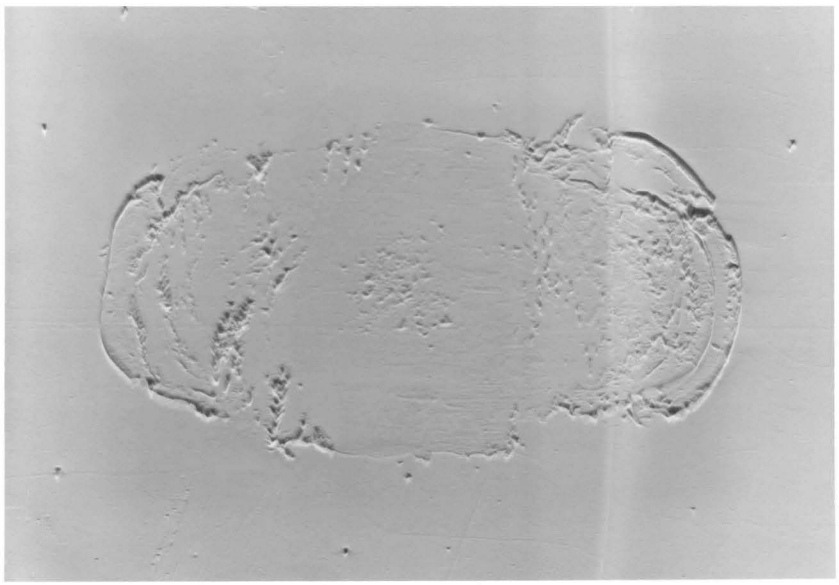

(b)

305 μm

Figure 10. Optical and SEM Photographs for the 13 μm Film.

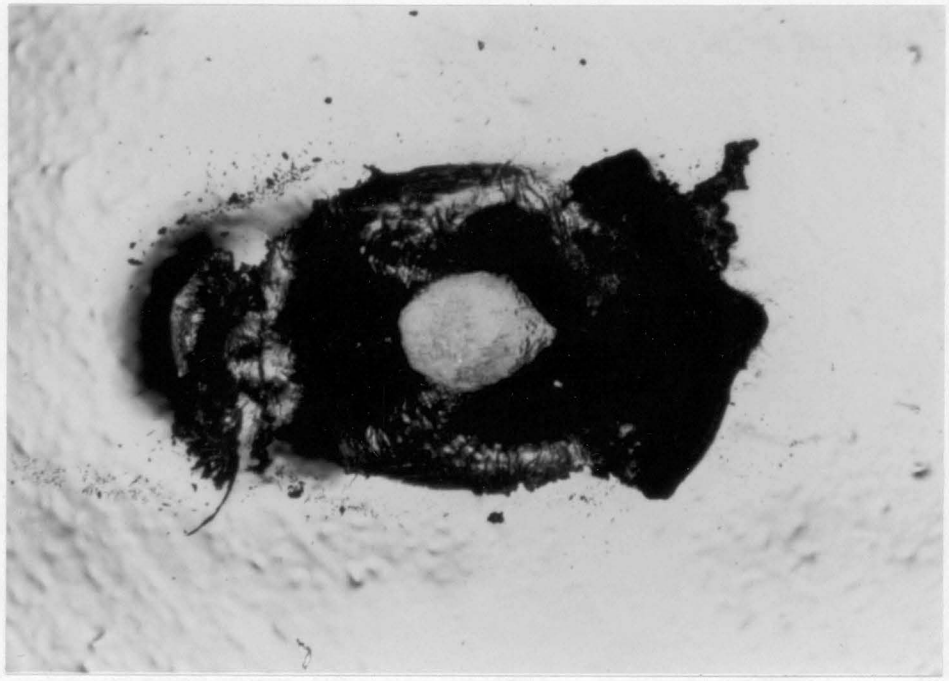

(a)

305 μm

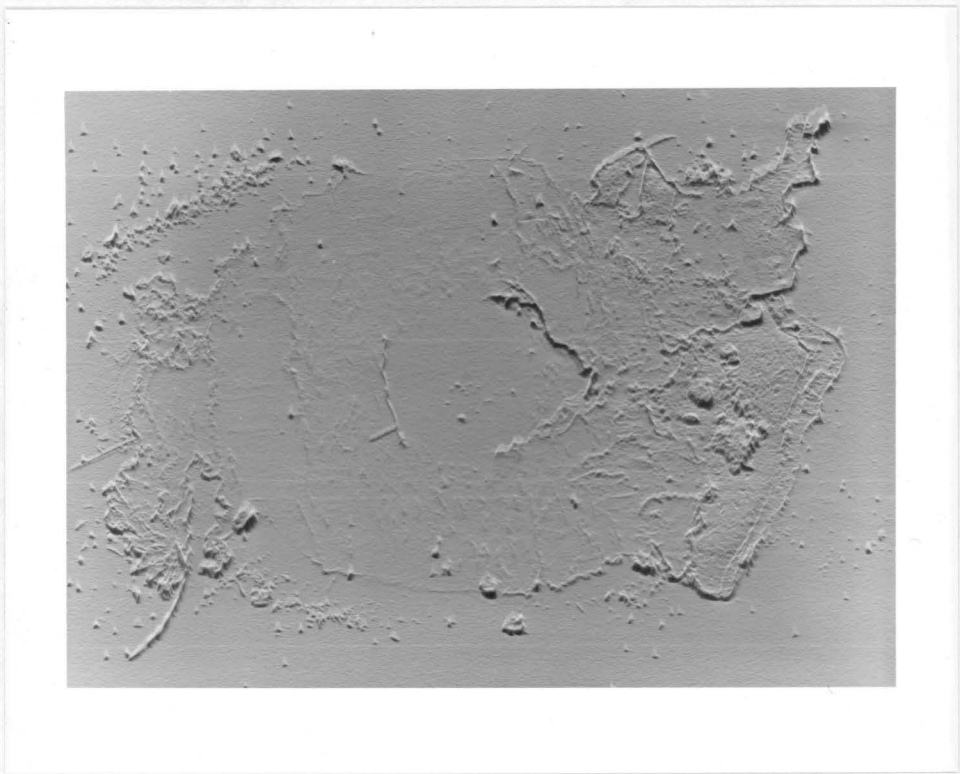

(b)

305 μm

Figure 11. Optical and SEM Photographs for the 23 μm Film.

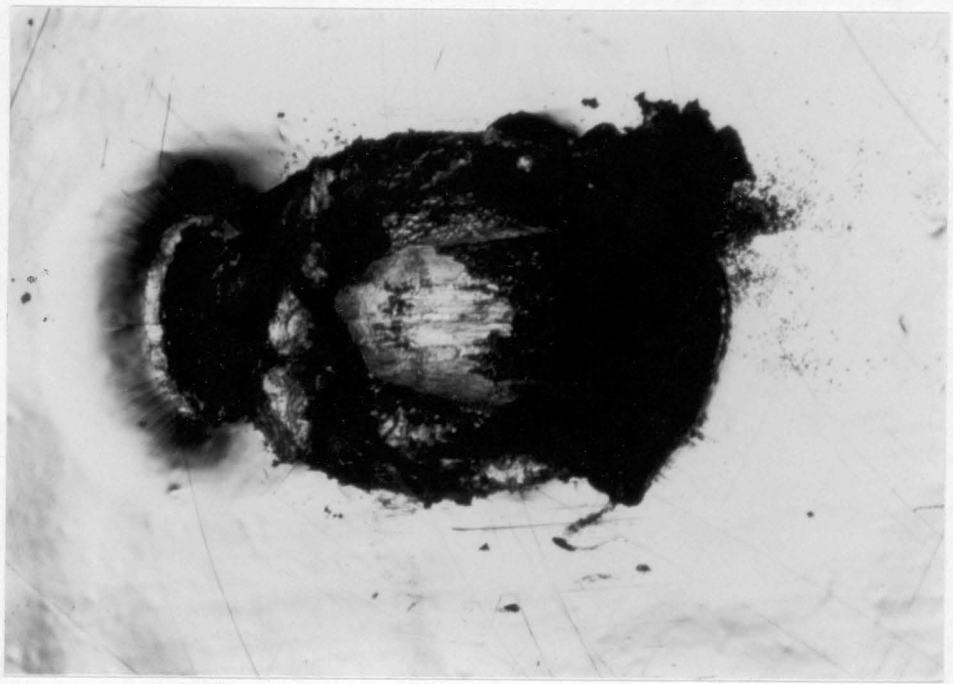

(a)

305 μm

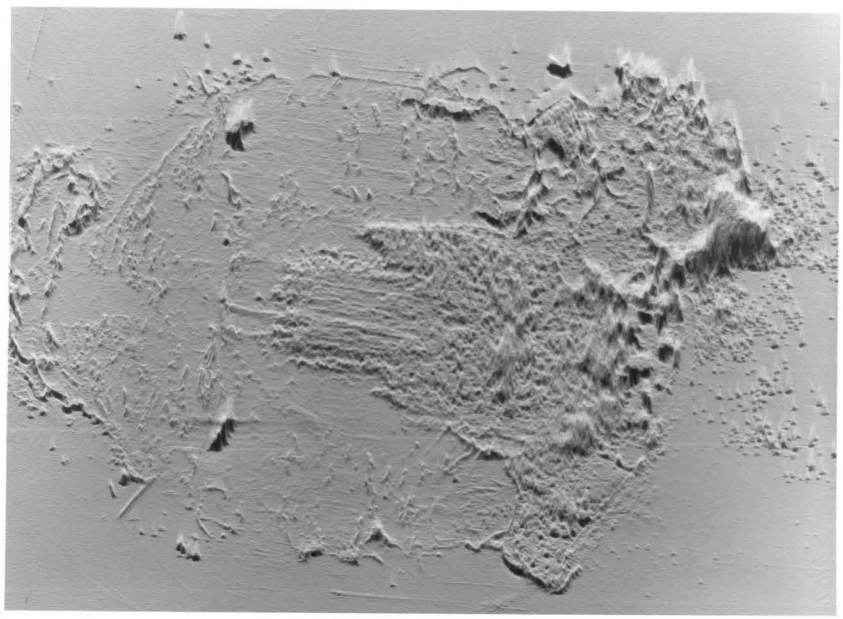

(b)

305 μm

Figure 12. Optical and SEM Photographs for the 31 μm Film.

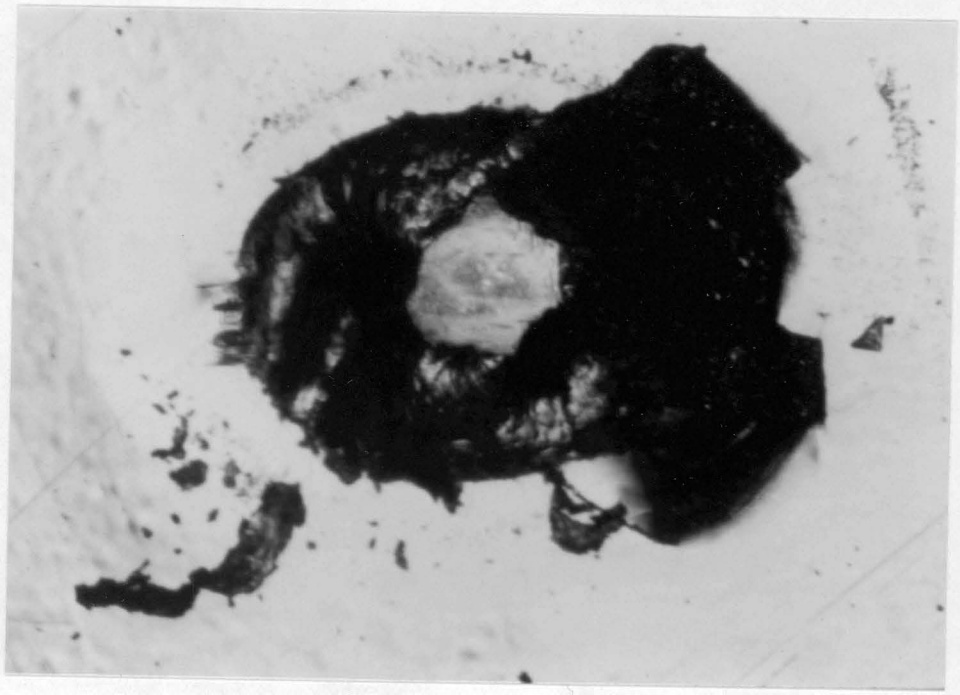

(a)

305 μm

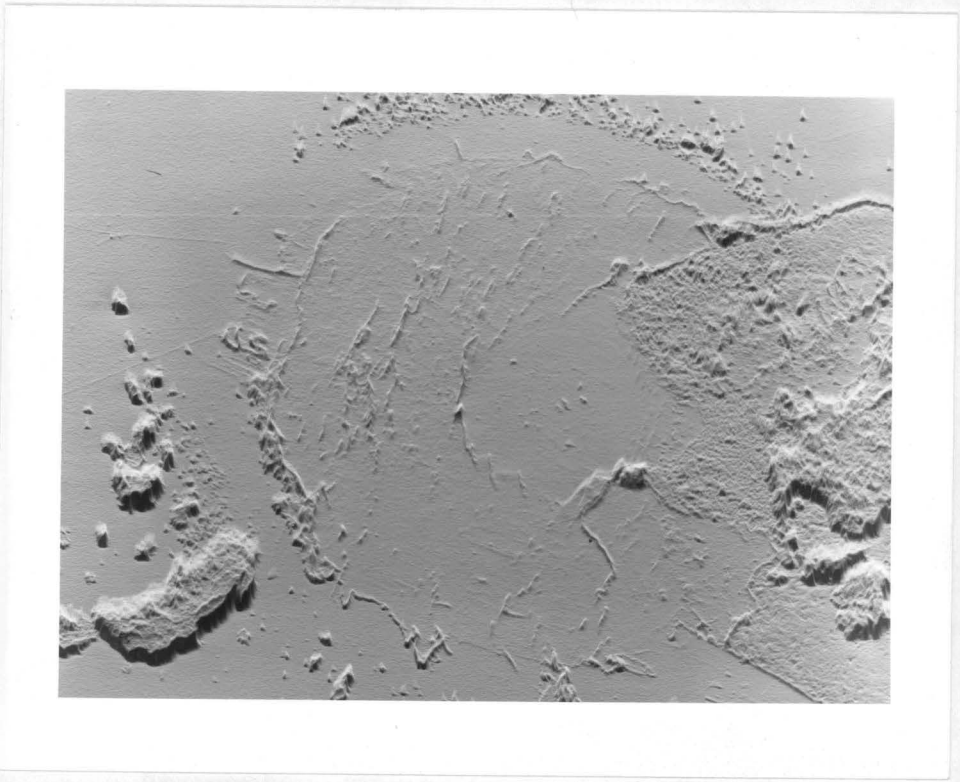

(b)

305 μm

Figure 13. Optical and SEM Photographs for the 38 μm Film.

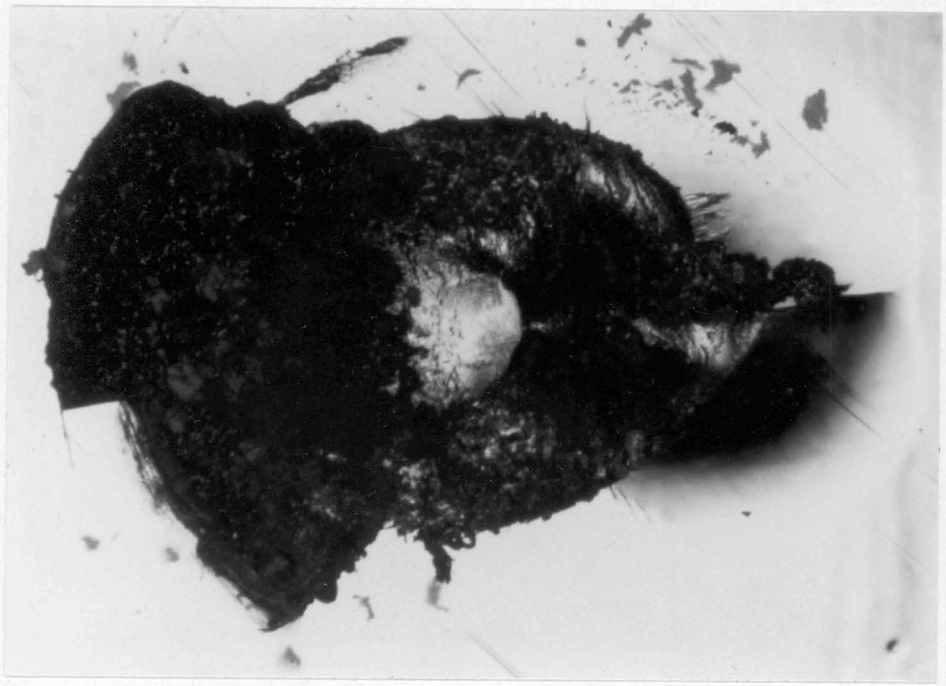

(a)

305 μm

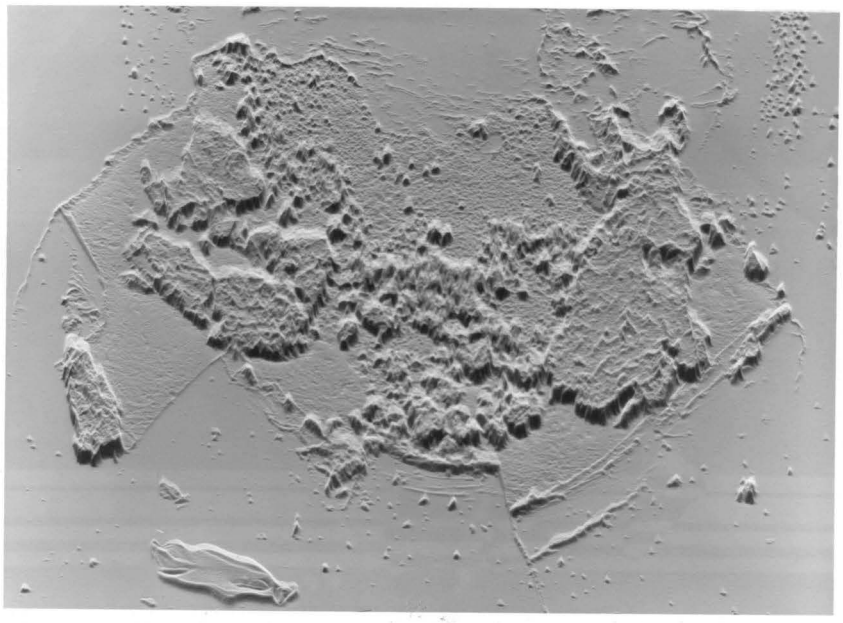

(b)

305 μm

Figure 14. Optical and SEM Photographs for the 46 μm Film.

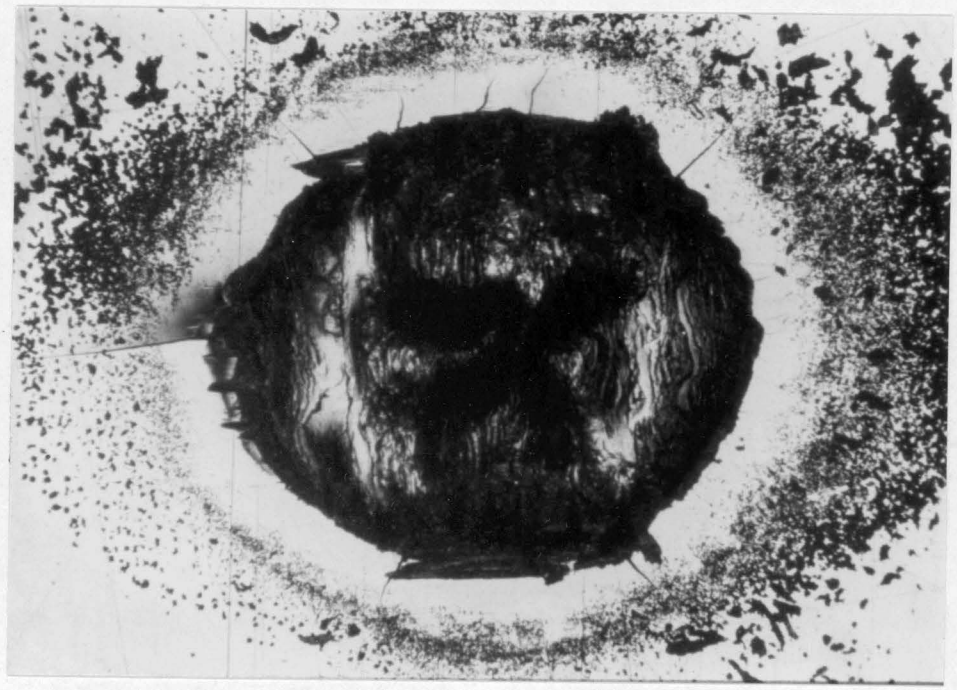

(a)

305 μm

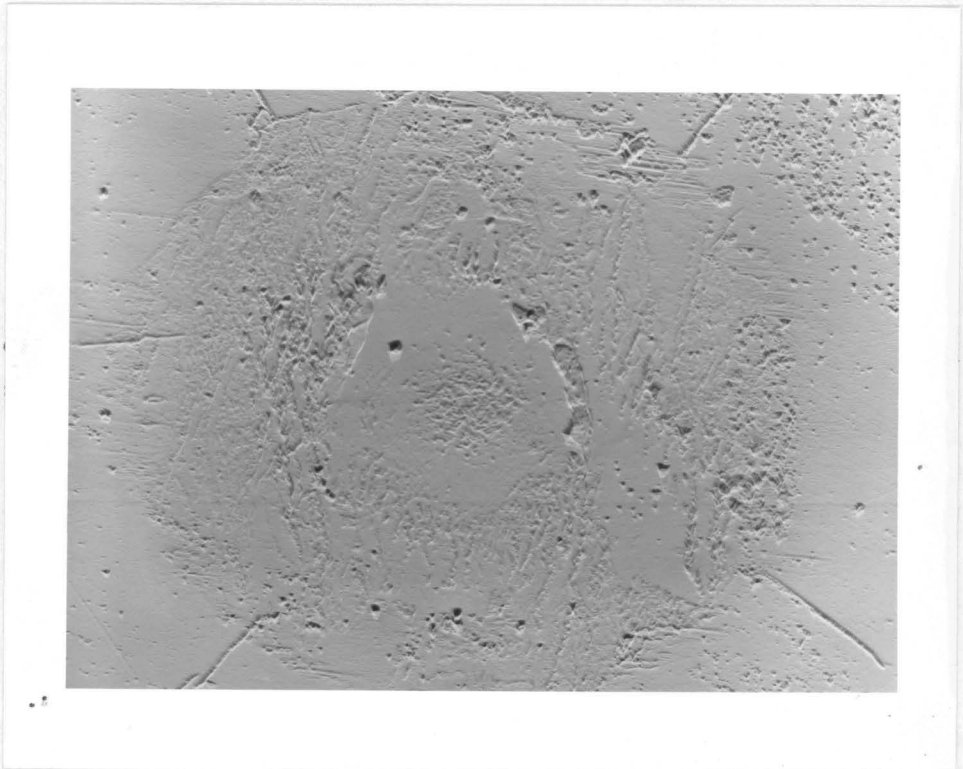

(b)

305 μm

Figure 15. Optical and SEM Photographs for the 52 μm Film.

using the external light source positioned at an angle with the coating surface. Another common characteristic is the black region surrounding this central region which can be seen in the optical photographs. Comparison with the SEM photographs tends to indicate that this is an optical phenomenon most probably due to a loss of reflectivity. Both optical and SEM pictures show debris surrounding the wear scars. However such debris is totally absent for the 7.9 and the 13 μm thicknesses. The debris is in the form of very fine particles even though some larger, plate-like, particles can be seen especially in the thinner films. No debris is seen within the wear scar itself. Some debris transfer occurs to the ball. This is shown in Figure 17. The transferred debris is loosely attached and very easily removed. Some debris, however, adhered to the ball of the 52 μm film but it was easily removed with a solvent. No damage of any type was observed on the ball. The wear scar tend to be larger and more circular with increasing film thickness. This can be seen in Figure 18 where the growth of the wear scar with film thickness is shown.

The 52 μm film (Figure 15) shows three distinct regions in its wear scar. The central region shows plastic deformation with small cracks and ridges perpendicular to the direction of motion. The second, or middle region, surrounding the central region shows radial cracks. The outer region shows the loose debris. The middle region is less visible for the thinner films and none of them showed the radial cracks. The 52 μm film shows a well defined ring of debris surrounding the wear scar which is absent in thinner films even though debris particles have been formed.

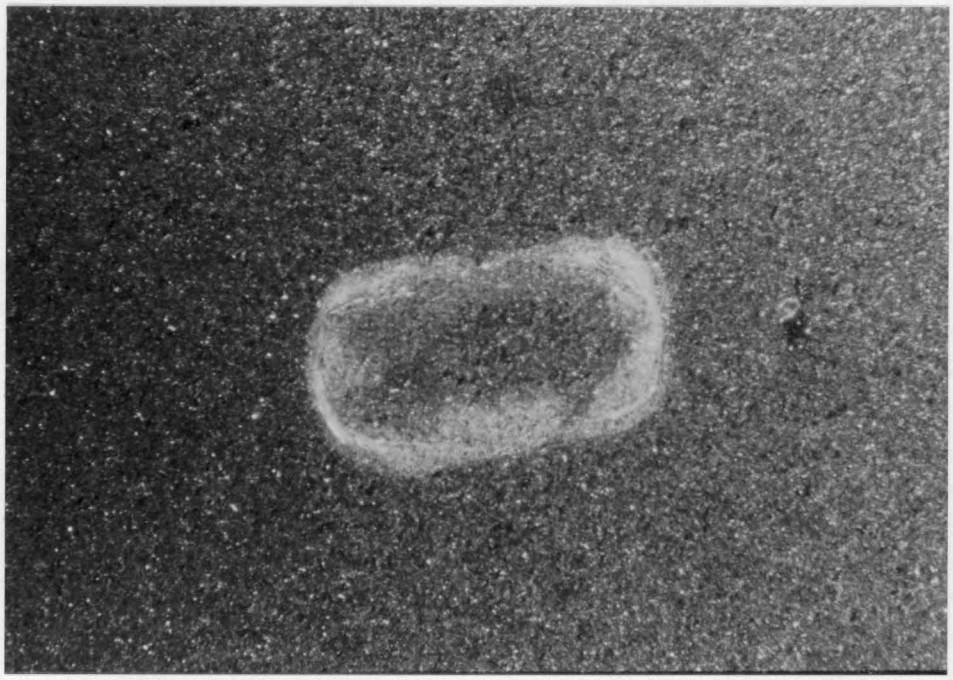

(a)

305 μm

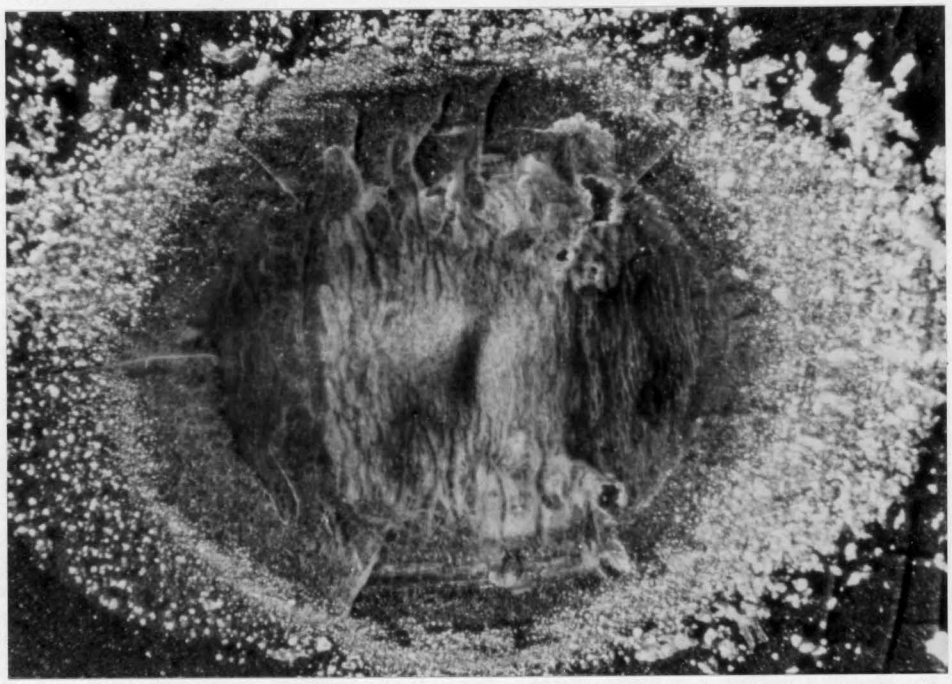

(b)

305 μm

Figure 16. Comparison of the Wear Scars for the 7.9 (a) and the 52 (b) μm Films.

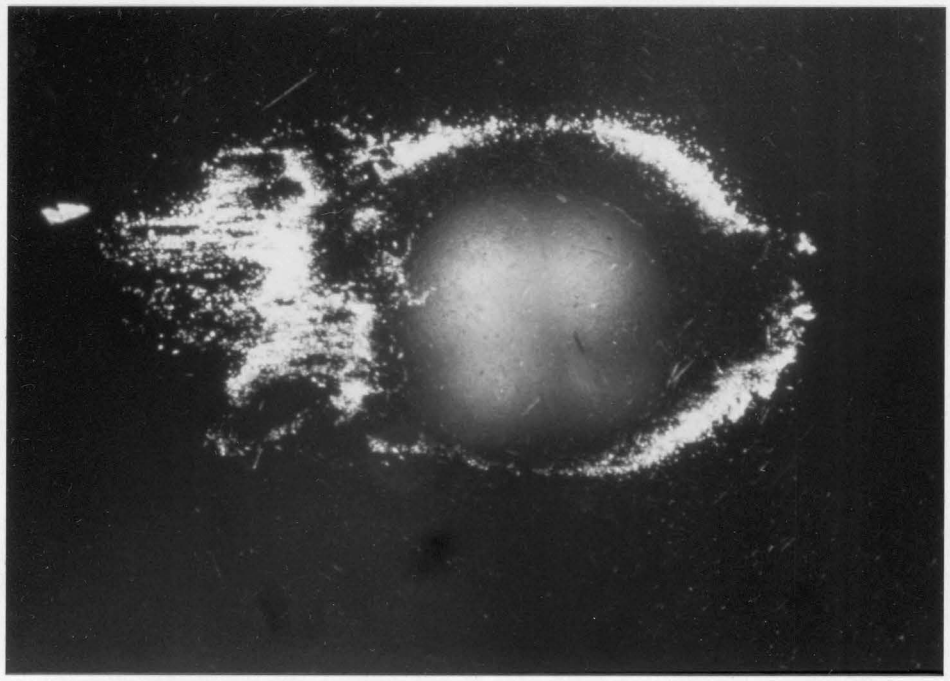

(a)

305 μm

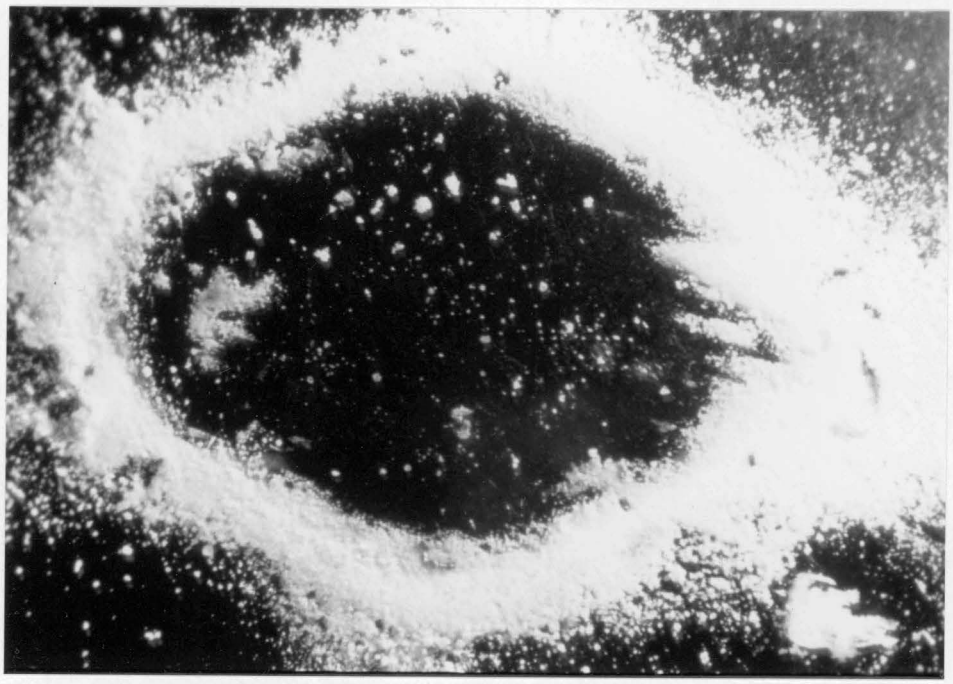

(b)

305 μm

Figure 17. Debris Transfer to the Steel Ball for the 23 (a) and the 52 (b) μm Films.

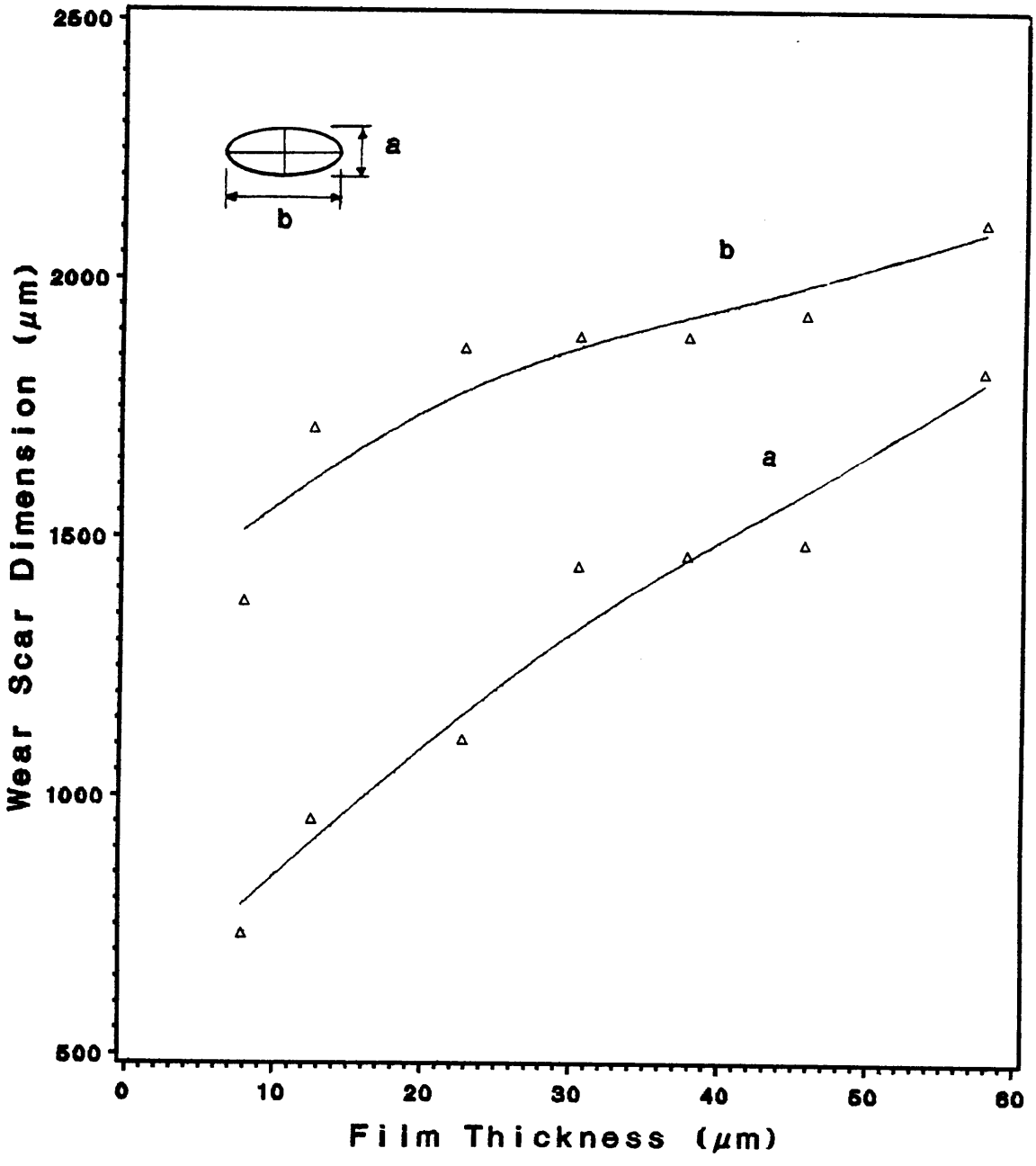

Figure 18. Wear Scar Growth With Film Thickness.

4.2 Results of the Wear-Time Experiments.

In this set of experiments the progress of fretting damage with time, before film failure, was evaluated to try to determine what governed the relationship between film thickness and film life. Two film thicknesses were chosen: 38 and 52 μm. The 38 μm film was chosen because it had a life long enough to allow the possibility of studying time effects while it still was below 40 μm. The 52 μm film was chosen because of its extraordinary long life. The extent of the fretting damage was evaluated by using optical and SEM photographs as well as computer-generated three-dimensional maps of the wear scars. All the experimental data for both thicknesses are shown in Appendix D.2.

4.2.1 Results for the 38 μm Film.

At this thickness, the polystyrene film lasted an average of almost 600 seconds. The lower limit of the 95 percent confidence interval was 426 seconds. To stay on the safe side it was decided to run the test a maximum of 360 seconds. Twelve tests, 30 seconds apart, were run. The 270-second test showed complete metal contact several seconds before the scheduled end. The results from this test were omitted because the purpose of these tests was to observe the progression of events leading to film failure. The 360-second test showed metal contact just at the end of the test. Hence the results represent the wear scar at the time metal contact just started.

Table 5 shows the results of the WEAR program which uses the computer-generated three-dimensional maps as the data file for its calculations. Wear and debris volumes

Table 5. WEAR Program Results for the 38 μm Film.

Test Time (sec)	Wear Volume (mm^3)	Debris Volume (mm^3)	Volume Difference (mm^3)	Maximum Depth of Penetration (μm)
30	0.009	0.030	-0.021	6.75
60	0.030	0.013	0.017	11.45
90	0.013	0.016	-0.003	10.13
120	0.027	0.015	0.012	22.22
150	0.031	0.012	0.018	12.44
180	0.009	0.005	0.004	7.61
210	0.172	0.186	-0.014	35.31
240	0.027	0.006	0.021	14.57
300	0.183	0.397	-0.213	27.88
330	0.102	0.150	-0.048	19.09
360	0.684	0.634	0.050	50.64

are plotted in Figure 19, and Figure 20 shows how far the ball penetrated in the film with time. Both wear and debris volumes as well as depth of penetration kept increasing until breakthrough. As the ball went deeper into the film, the wear scar size increased as it can be seen in Figure 21. The fact that the wear scar kept increasing while the coefficient of friction remained constant indicates that friction does not depend on the apparent area of contact.

The volume difference shown in Table 5 is found by subtracting the debris volume from the wear volume. In some cases this difference is negative indicating that more debris is generated than material is worn. However this is not the case. The large debris volumes are due to the approximation the computer does in creating the three-dimensional

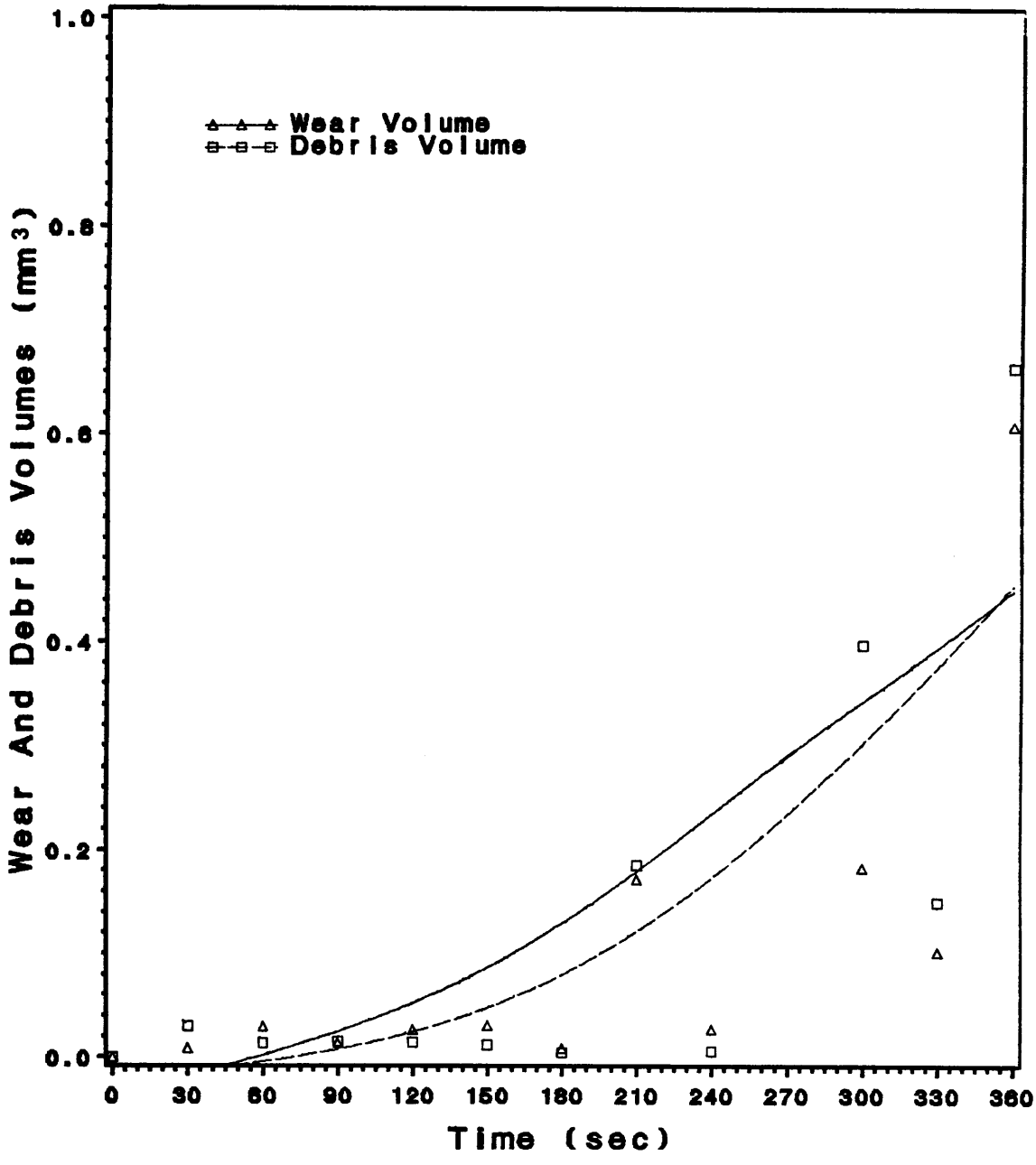

Figure 19. Wear and Debris Volumes for the 38 μm Film.

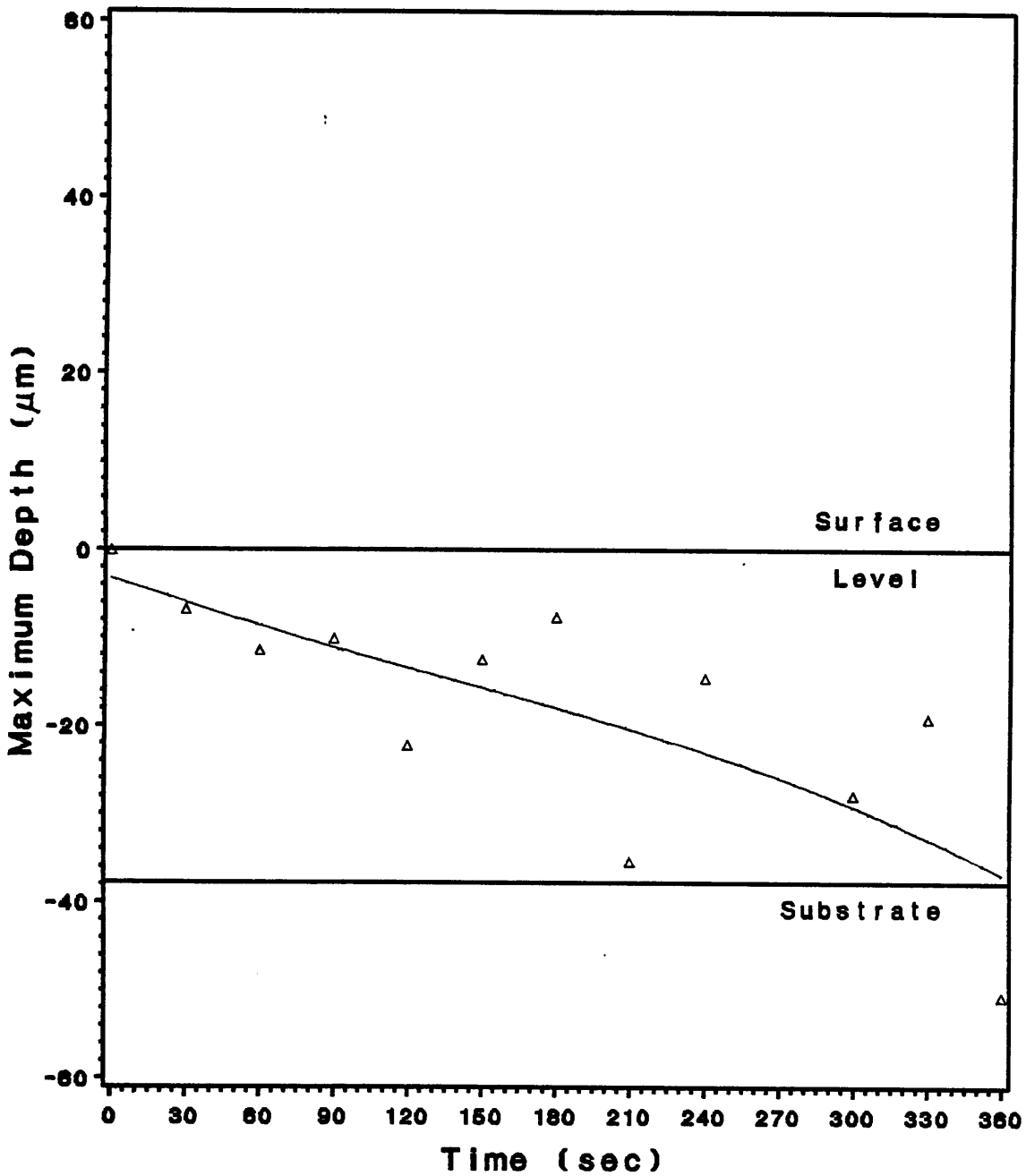

Figure 20. Progression In Time of the Maximum Depth of Penetration for the 38 μm Film.

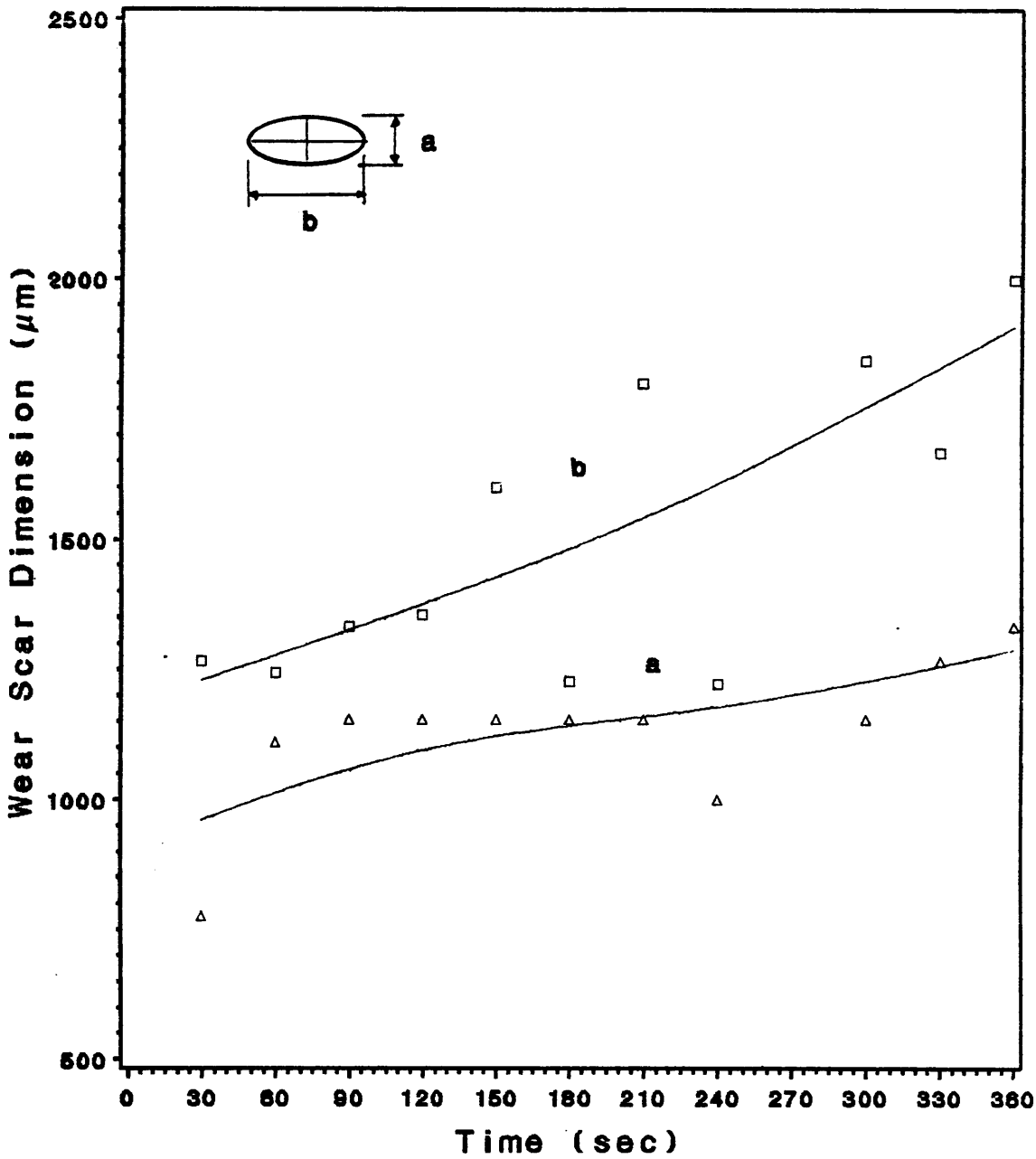

Figure 21. Growth of the Wear Scar With Time for the 38 μm Film.

maps. Linear interpolation is used to connect the points between the different traces. Therefore when connecting the two traces, the program draws a line from one point to another. Since the debris is in the form of particles of different size, it is not possible to determine exactly where a debris particle starts and ends. Therefore the interpolation may join several particles together as part of one single solid with a volume much larger than the sum of the volumes of each single debris particle. To overcome this difficulty more traces closer together must be used. However, the program used for displaying the maps (MOVIE.BYU) can only handle a maximum of 5000 points. Also the distance between traces must be the same for all traces. These considerations limit the number of traces that can be used.

Figure 22 shows the growth of the wear scar as a function of time. The wear scar profiles were created using the computer technique described in section 3.3.3. The figure shows that the wear scar grows more horizontally than vertically. This is an indication that the stresses, as a consequence of the ball motion, are higher near the surface and rapidly fade away with depth.

Figures 23 through 29 show optical and SEM photographs for various time intervals. Figure 30 shows the computer-generated three-dimensional maps for four different time intervals. The vertical magnification is 20 times the horizontal. Examination of the photographs and of the computer-generated maps shows that the wear scar shape goes from an oval shape to a more circular one with time. The 30-second wear scar does not show any debris formed and no debris is transferred to the steel ball. Debris starts to form after and some flake of loose materials can be seen on the edges of the wear scar for the 90-second wear scar. A highly deformed central region is clearly visible from the very short time tests. In this regions no wear particles are present but cracks and ridges

perpendicular to the direction of sliding are formed. For the short time tests, wear debris is present just outside this central region. With longer testing time the wear particles move further away and tend to form a ring. Longer testing times show the debris becoming smaller in size and more distributed around the wear scar. The three-dimensional maps indicate that more wear debris is piled up on one side of the wear scar. This side is the one toward the driving mechanism of the MARK III fretting machine. The reason for this pile-up is unknown. With time darker regions develop within the wear scar. Again these dark regions appear so because of optical effects. They generally seem to develop more in one direction than another. Some small radial cracks seem to form outside the wear scar after a testing time of about 300 seconds. This is in contrast with the result from the life-thickness experiments in which no radial cracks were seen for films thinner than 52 μm.

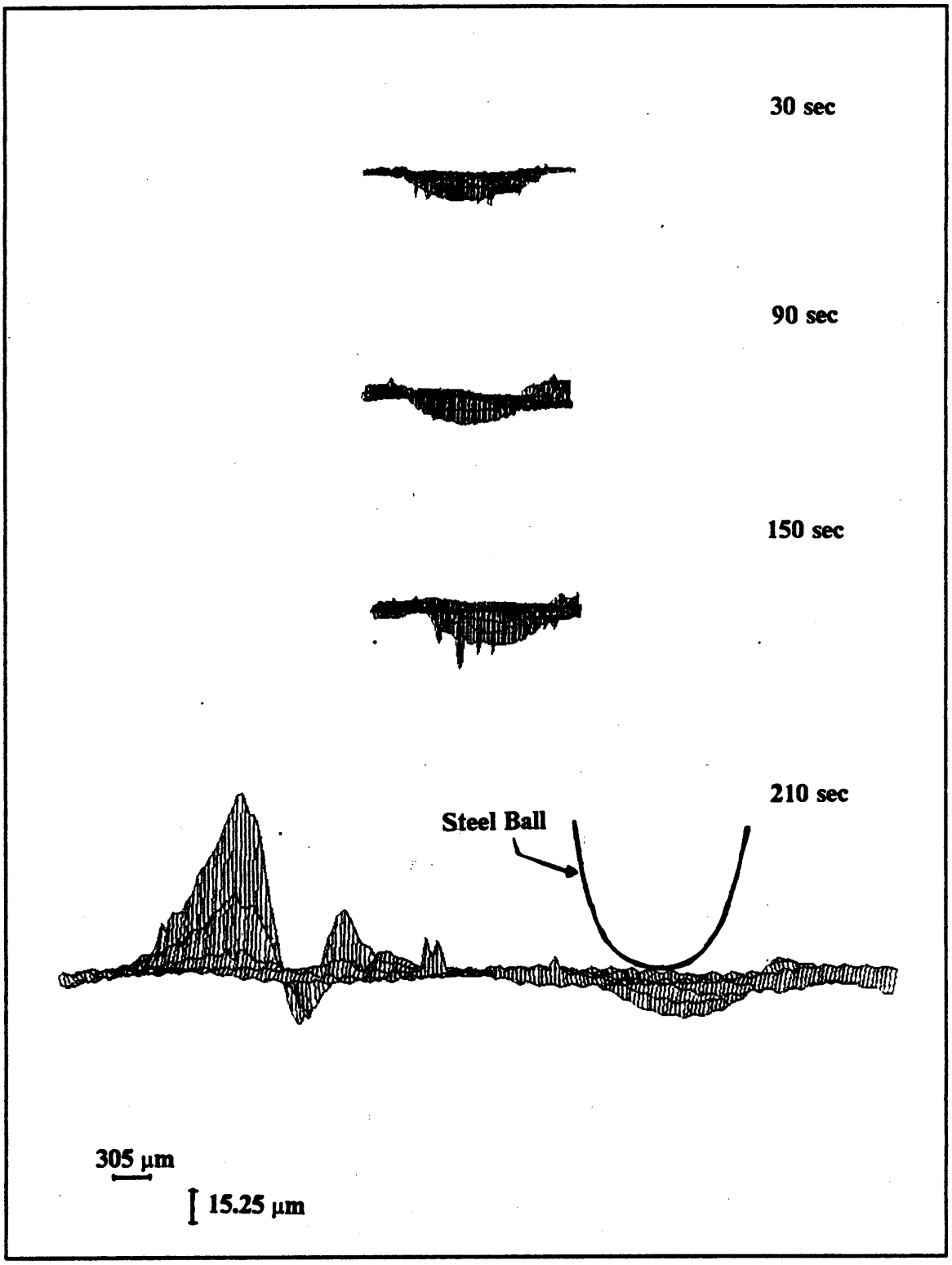

Figure 22. Computer-Generated Profiles of the Wear Scars for Different Testing Times of the 38 μm Film.

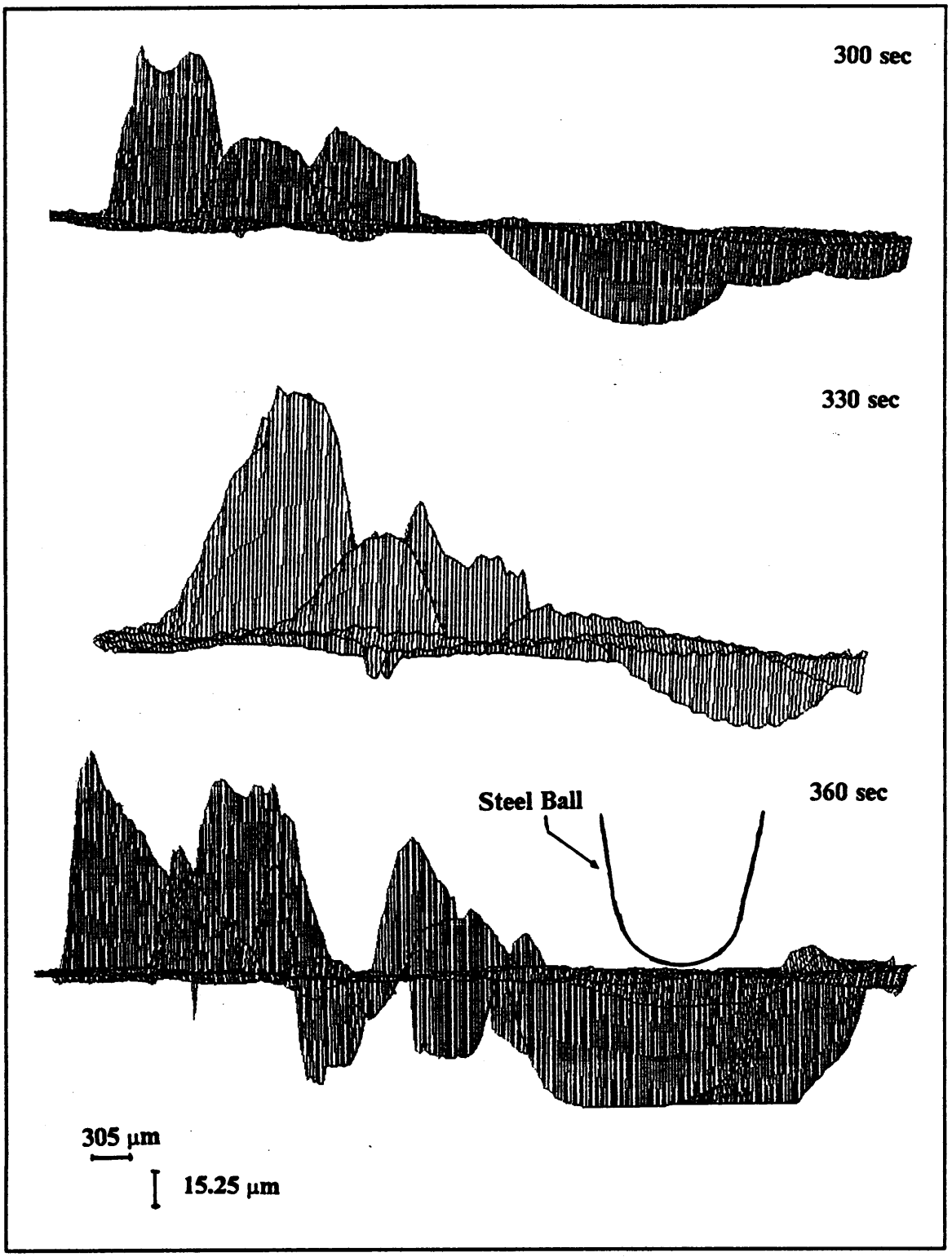

Figure 22. Continued.

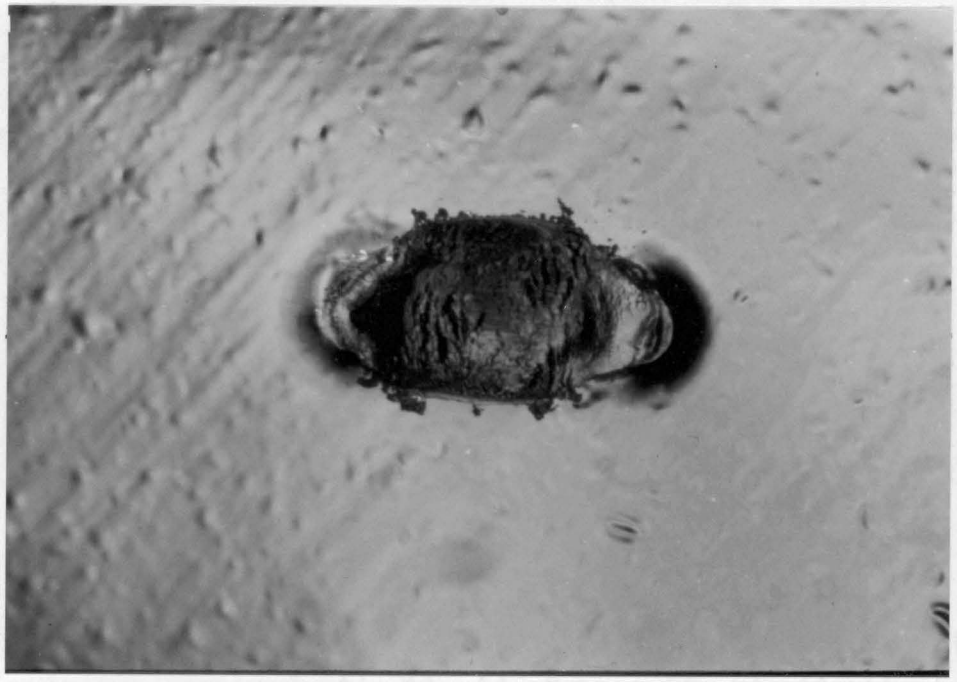

(a)

305 μm

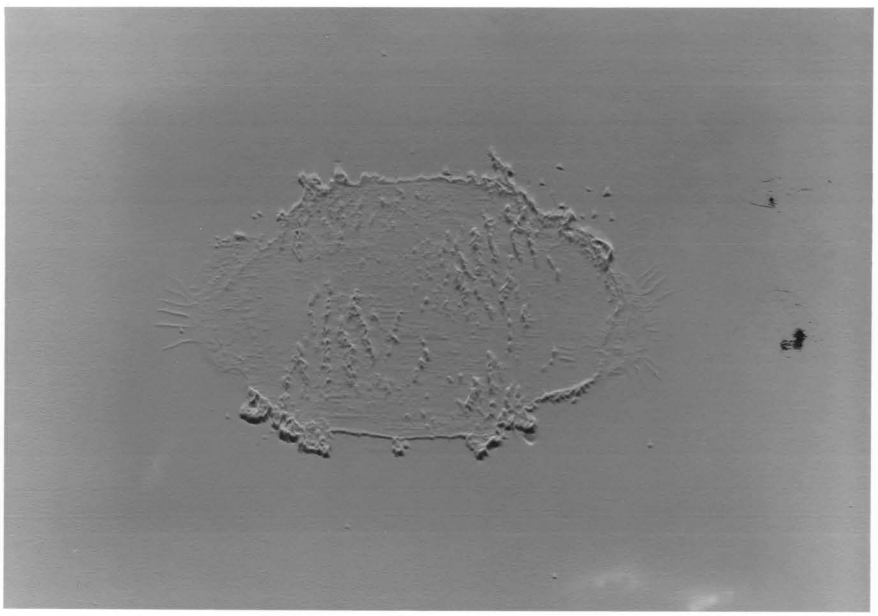

(b)

305 μm

Figure 23. Optical and SEM Photographs After 30 sec of Testing for the 38 μm Film.

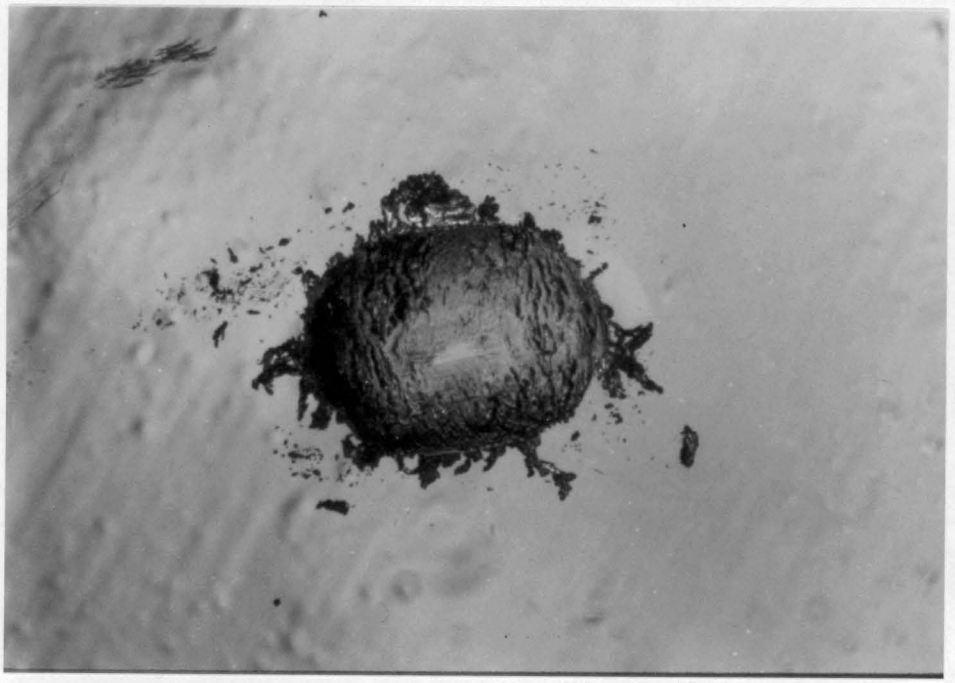

(a)

305 μm

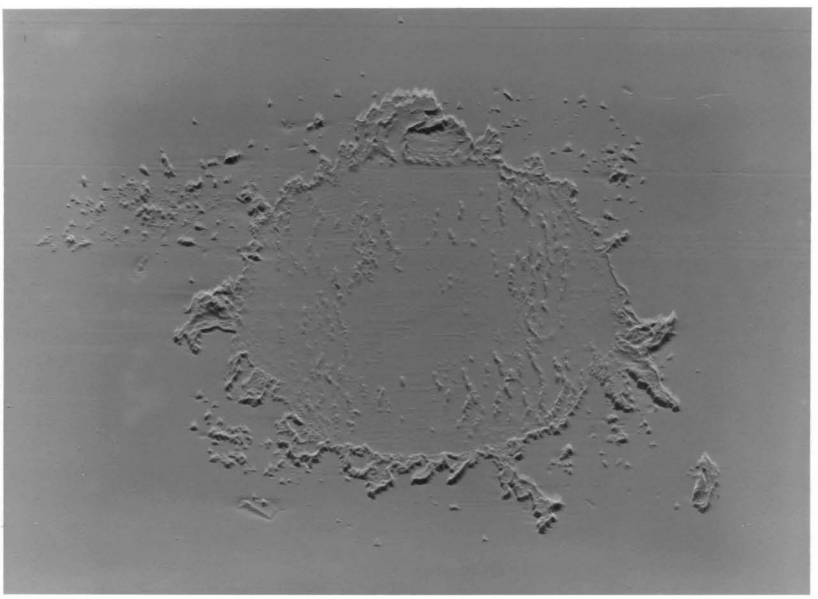

(b)

305 μm

Figure 24. Optical and SEM Photographs After 90 sec of Testing for the 38 μm Film.

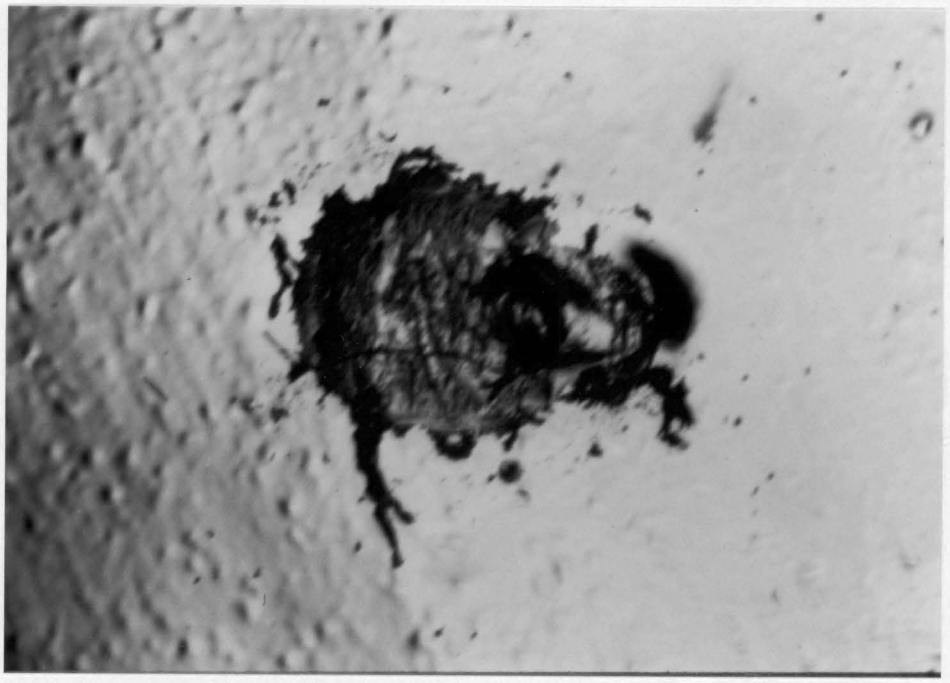

(a)

305 μm

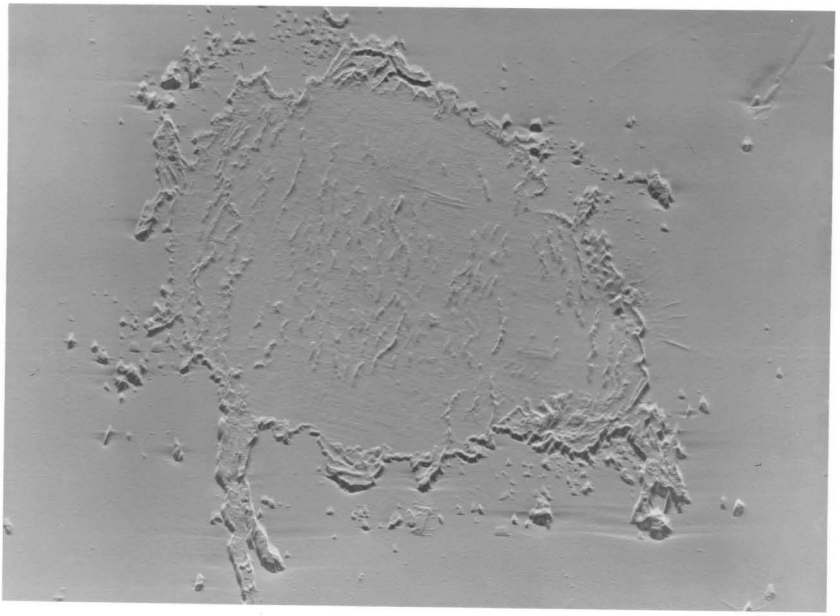

(b)

305 μm

Figure 25. Optical and SEM Photographs After 150 sec of Testing for the 38 μm Film.

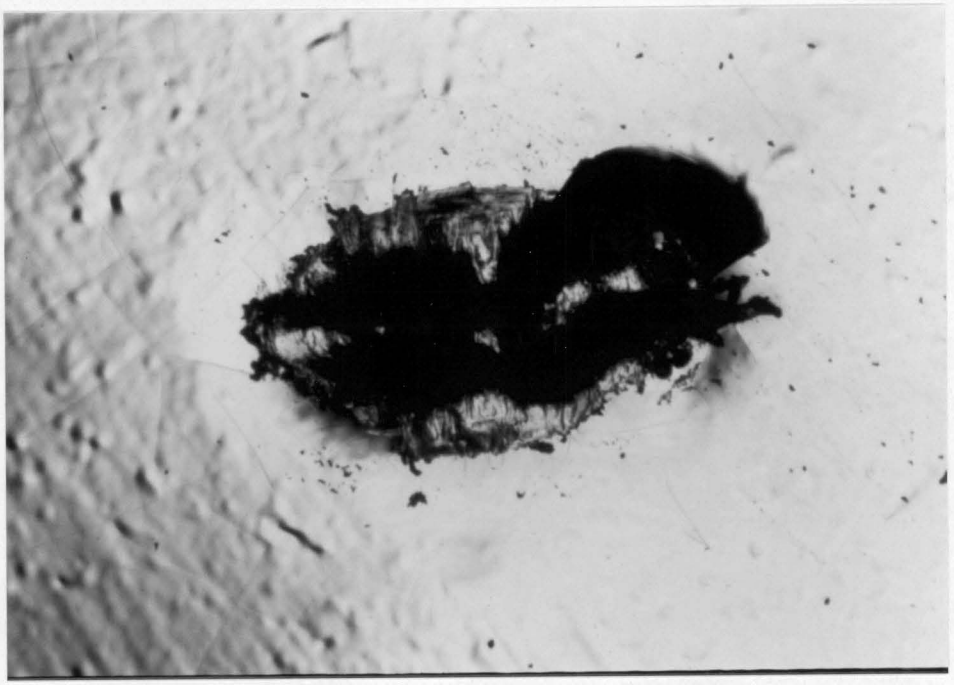

(a)

305 μm

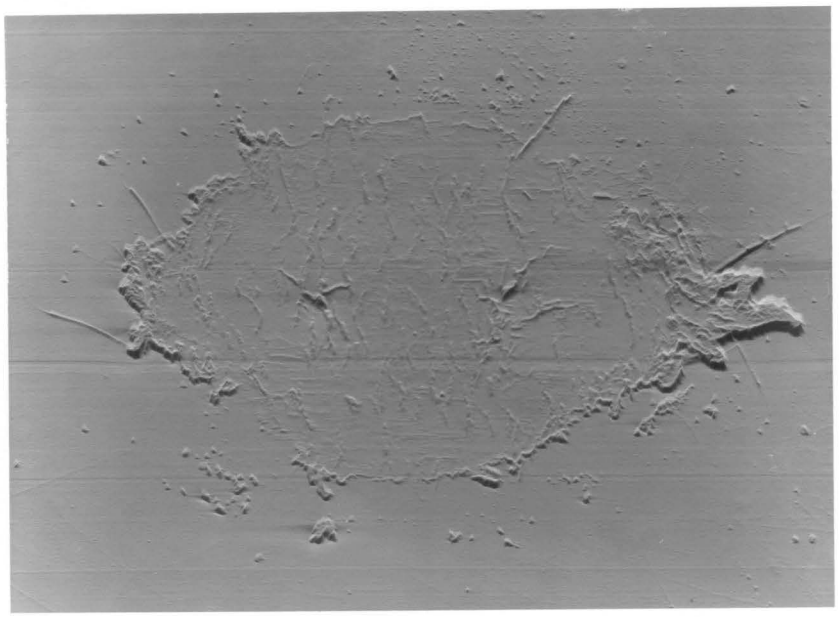

(b)

305 μm

Figure 26. Optical and SEM Photographs After 210 sec of Testing for the 38 μm Film.

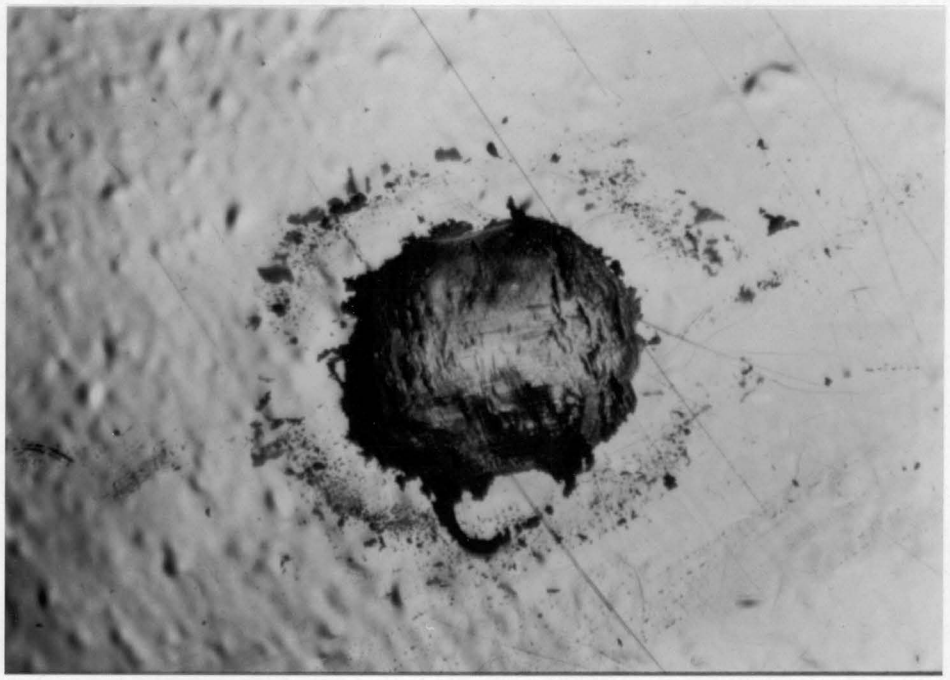

(a)

305 μm

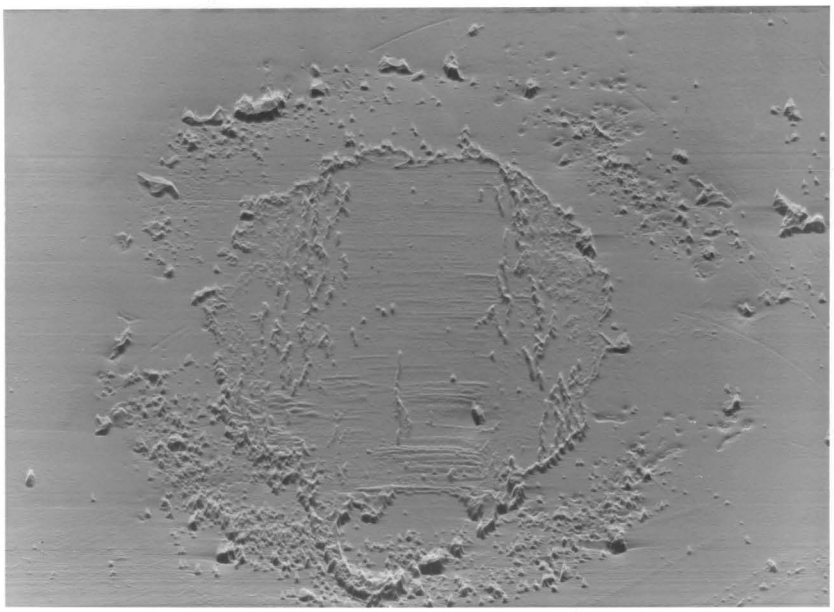

(b)

305 μm

Figure 27. Optical and SEM Photographs After 240 sec of Testing for the 38 μm Film.

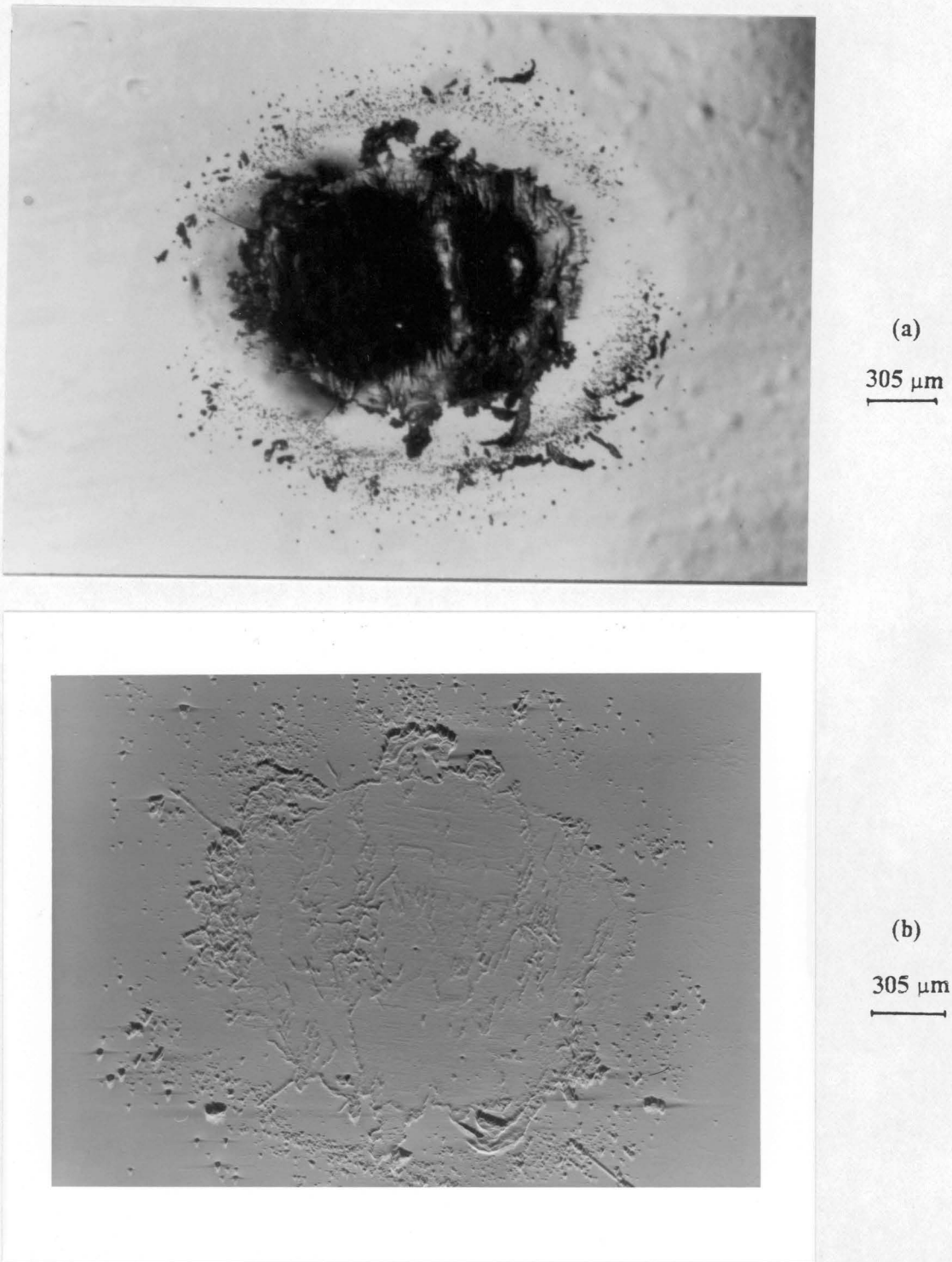

Figure 28. Optical and SEM Photographs After 300 sec of Testing for the 38 μm Film.

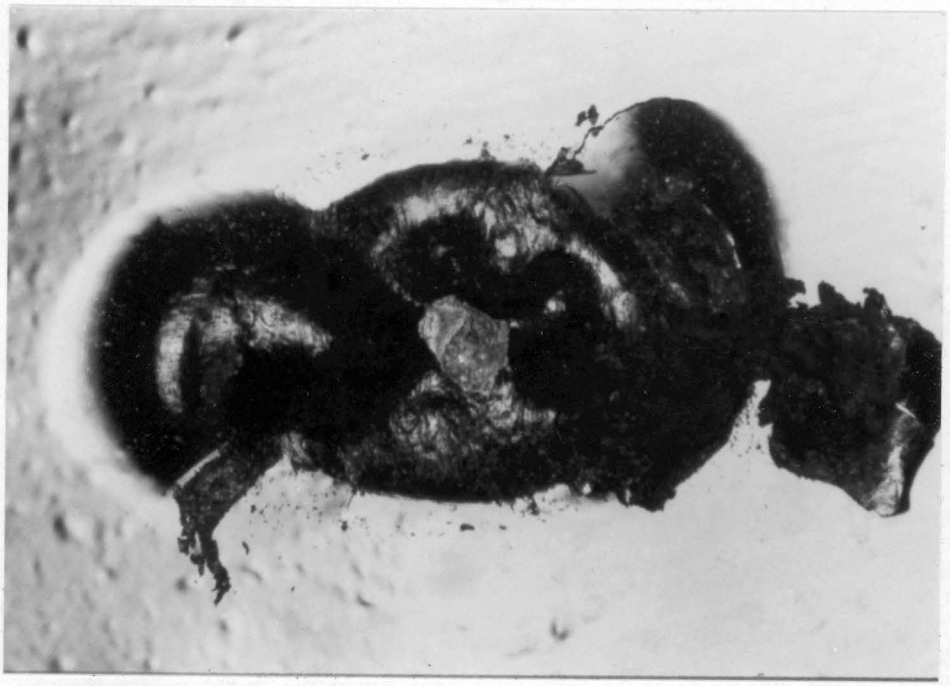

(a)

305 μm

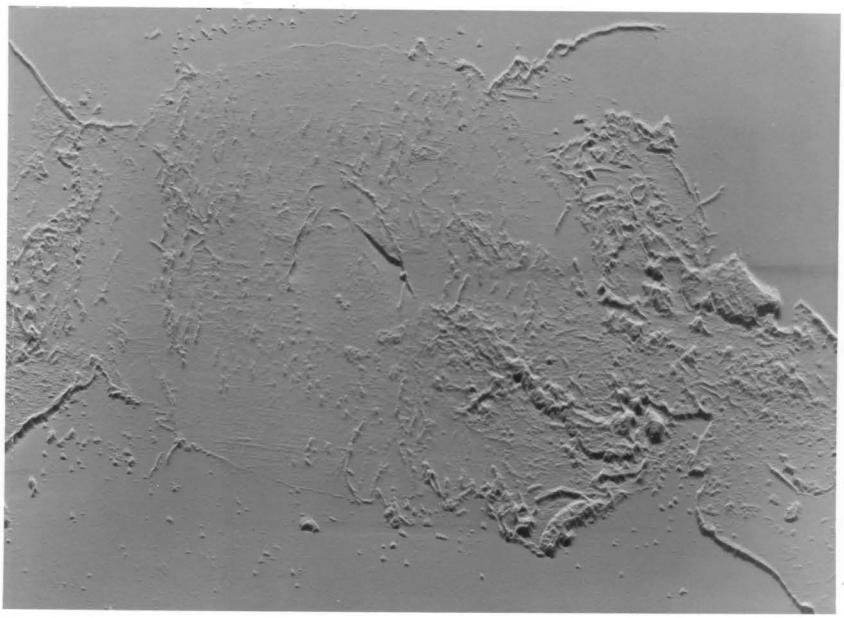

(b)

305 μm

Figure 29. Optical and SEM Photographs After 360 sec of Testing for the 38 μm Film.

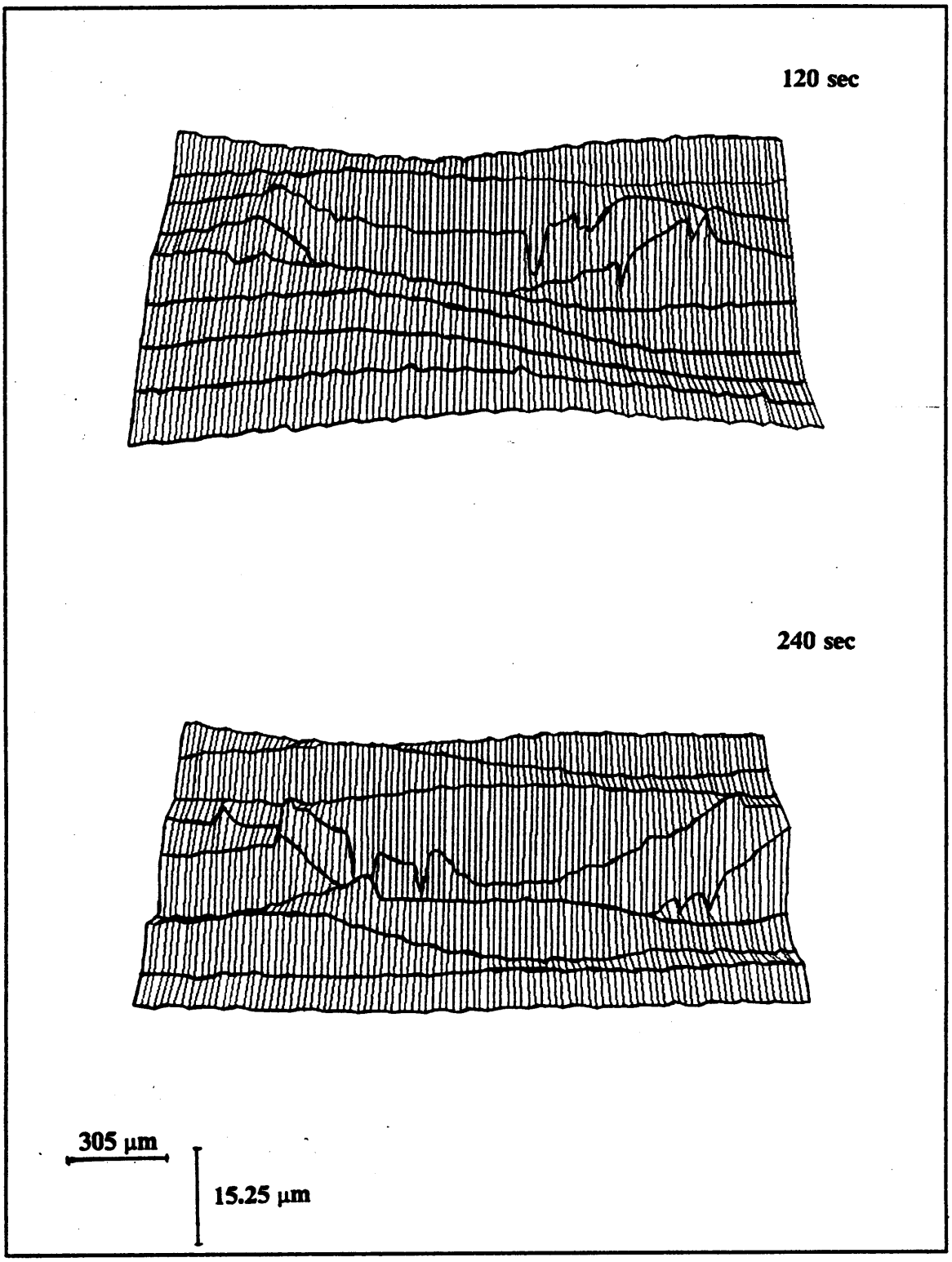

Figure 30. Computer Representation of the 38 μm Film Wear Scar at Different Time Intervals.

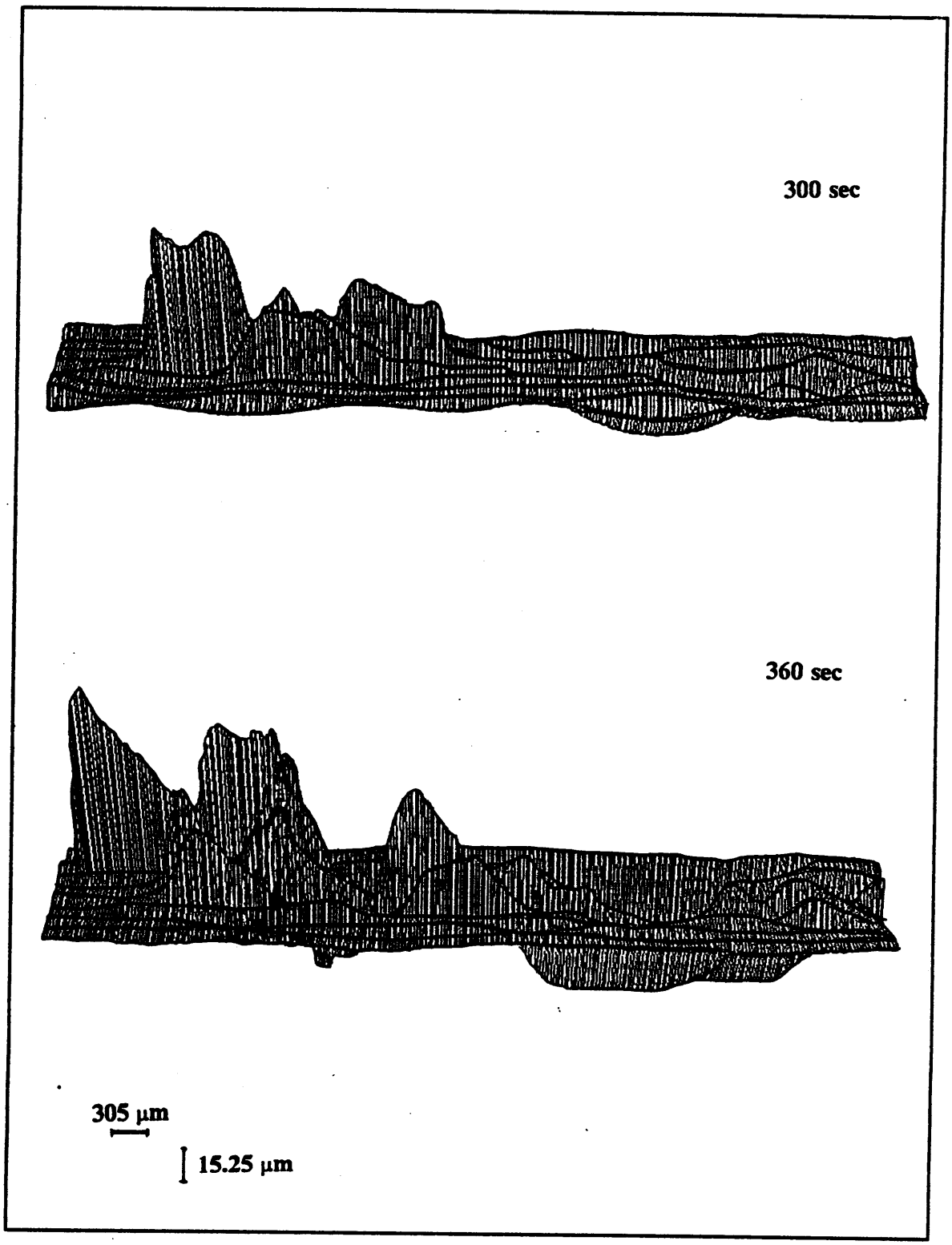

Figure 30. Continued.

4.2.2 Results for the 52 μm Film.

Table 6. WEAR Program Results for the 52 μm Film.

Test Time (sec)	Wear Volume (mm^3)	Debris Volume (mm^3)	Volume Difference (mm^3)	Maximum Depth of Penetration (μm)
30	0.006	0.004	0.002	6.77
60	0.015	0.009	0.006	10.61
90	0.035	0.026	0.009	15.27
120	0.039	0.016	0.023	12.31
150	0.026	0.013	0.013	10.53
300	0.041	0.020	0.021	14.68
600	0.047	0.011	0.036	19.86
900	0.049	0.041	0.008	19.99
1200	0.174	0.255	-0.081	20.84
1800	0.383	0.699	-0.314	36.68
2400	0.465	0.968	-0.502	32.04
3000	0.840	1.040	-0.199	45.31
3600	0.712	0.540	0.172	50.29
4200	0.148	0.359	-0.211	22.73
4800	0.570	0.622	-0.053	44.13
5400	0.509	0.613	-0.105	43.73

Sixteen time intervals were used to evaluate the fretting behavior at this thickness. The longest time interval was 5400 seconds, well below the lower limit of the 95 percent confidence interval, while the shortest testing time was 30 seconds. Table 6 shows the WEAR program results for the 52 μm film. The wear and debris volumes growth in

time is shown in Figure 31. The fact that there is more debris than worn material is due to the approximation used in creating the maps as explained before. Figure 32 and Figure 33 show the progression of the ball penetration in time, and the wear scar growth, respectively. Both the wear and debris volumes and the depth of penetration level off approximately after 3000 seconds. The same tendency but to a lesser degree is also observed for the wear scar dimensions. This is in contrast with what was observed for the 38 μm film where wear and debris volumes, depth of penetration, and wear scar dimensions kept increasing with each time interval never levelling off. This indicates that indeed a different wear regime is reached for the 52 μm film.

Figure 34 shows the computer-generated profiles of the wear scars at different time intervals. The wear scar for the 52 μm film grows more horizontally than it does vertically. Figures 35 through 43 show the optical and SEM photographs for different time intervals. Figure 44 shows the three-dimensional maps of the wear scars at different time intervals. Wear debris starts to form only after 60 seconds of running time. However, in contrast to the 38 μm film, the wear scar shape is more circular from the beginning. A complete ring of wear debris is present all around the wear scar after 600 seconds of testing time. The dark regions are not visible until after 900 seconds. It is also after this time that radial cracks start to form. These cracks are longer and better defined than the one seen in the 38 μm film. The cracks do not seem to grow with time but are about the same length for all remaining tests. The center of the wear scar shows the same type of deformation as the other films. However the degree of deformation seems to increase with time. After 1200 seconds, cracks start to form also in directions not perpendicular to the direction of motion. The three-dimensional maps indicate that with time the wear debris piles up just on one side of the wear scar.

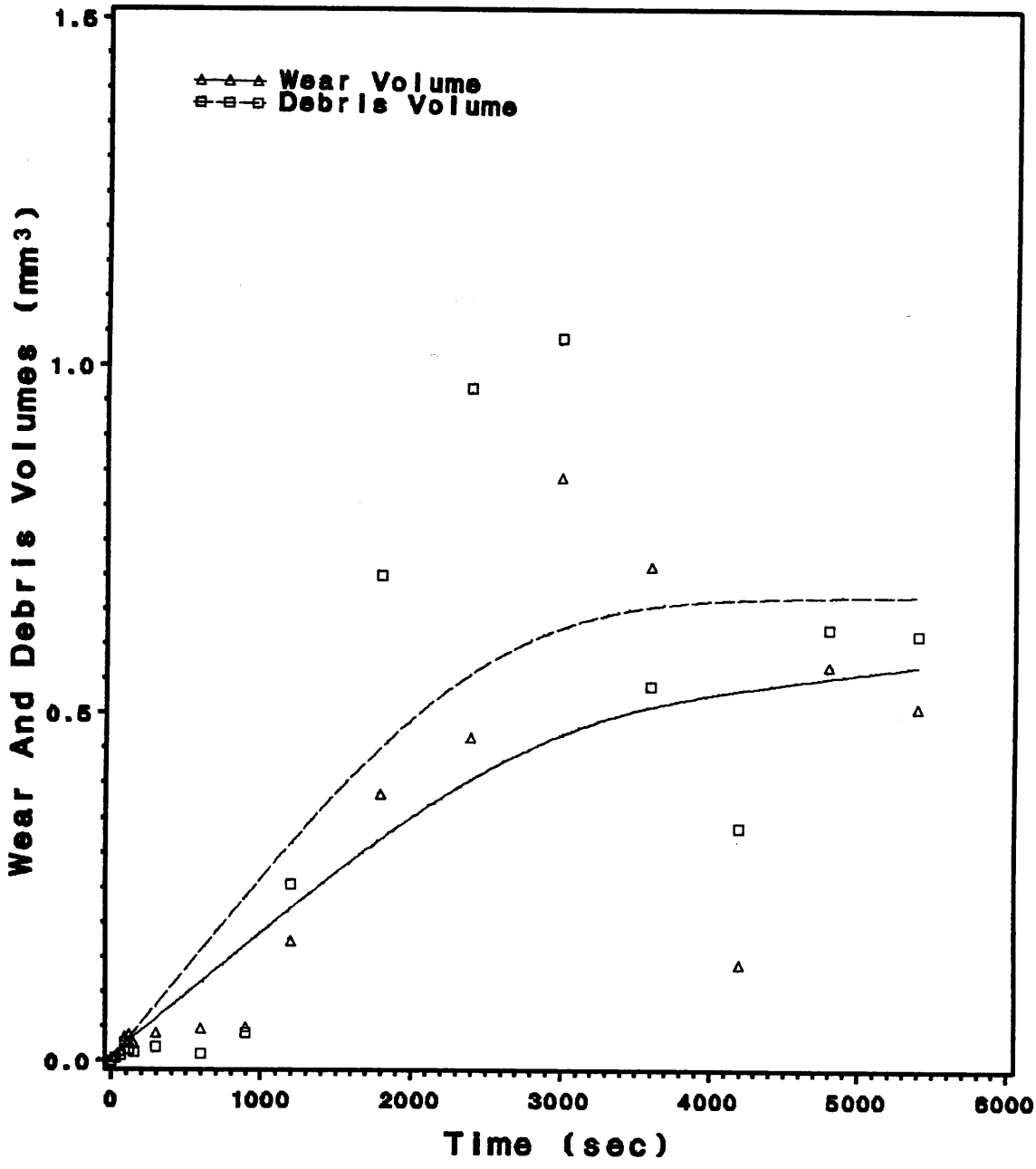

Figure 31. Wear and Debris Volumes for the 52 μm Film.

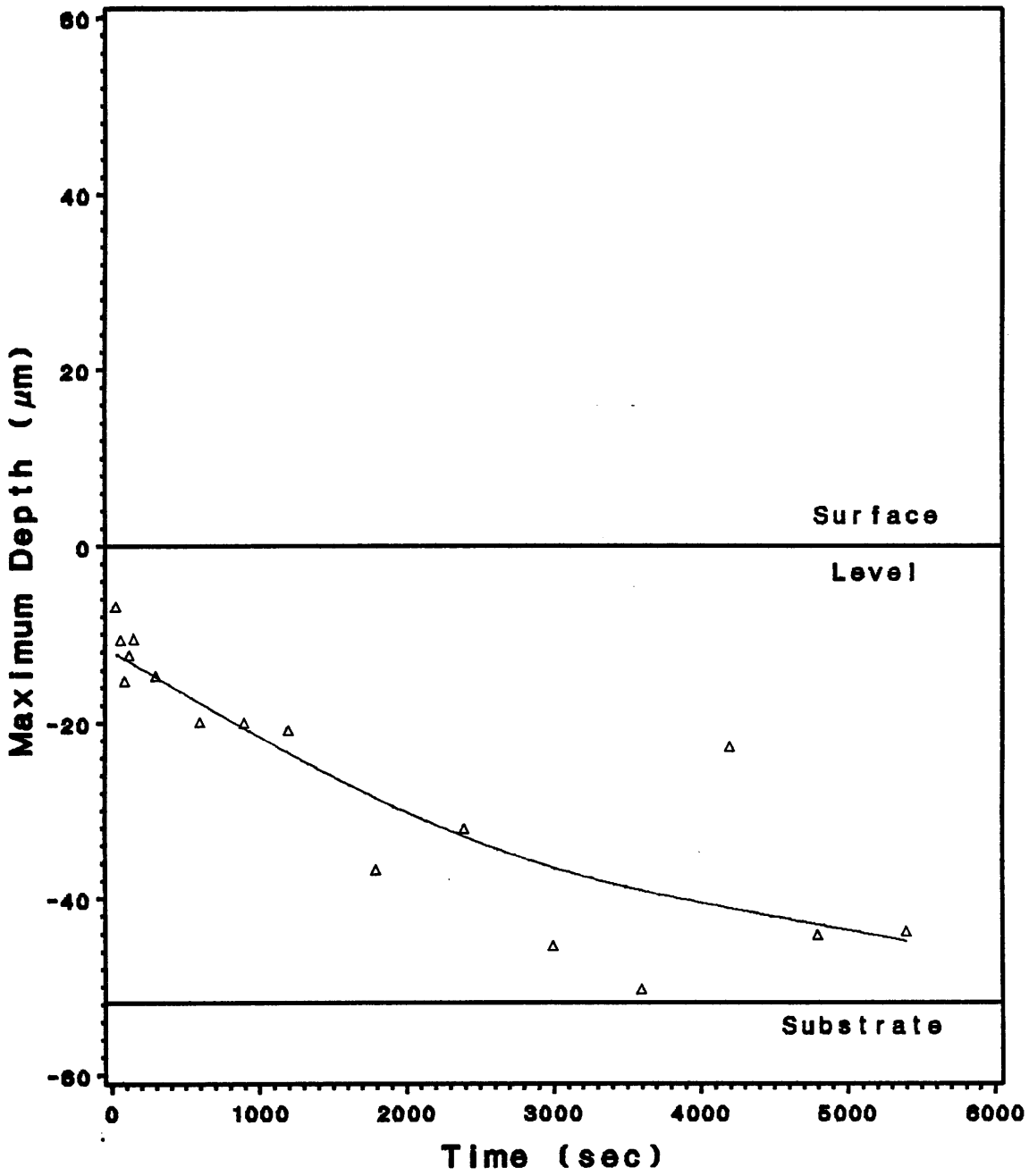

Figure 32. Progression In Time of the Maximum Depth of Penetration for the 52 μm Film.

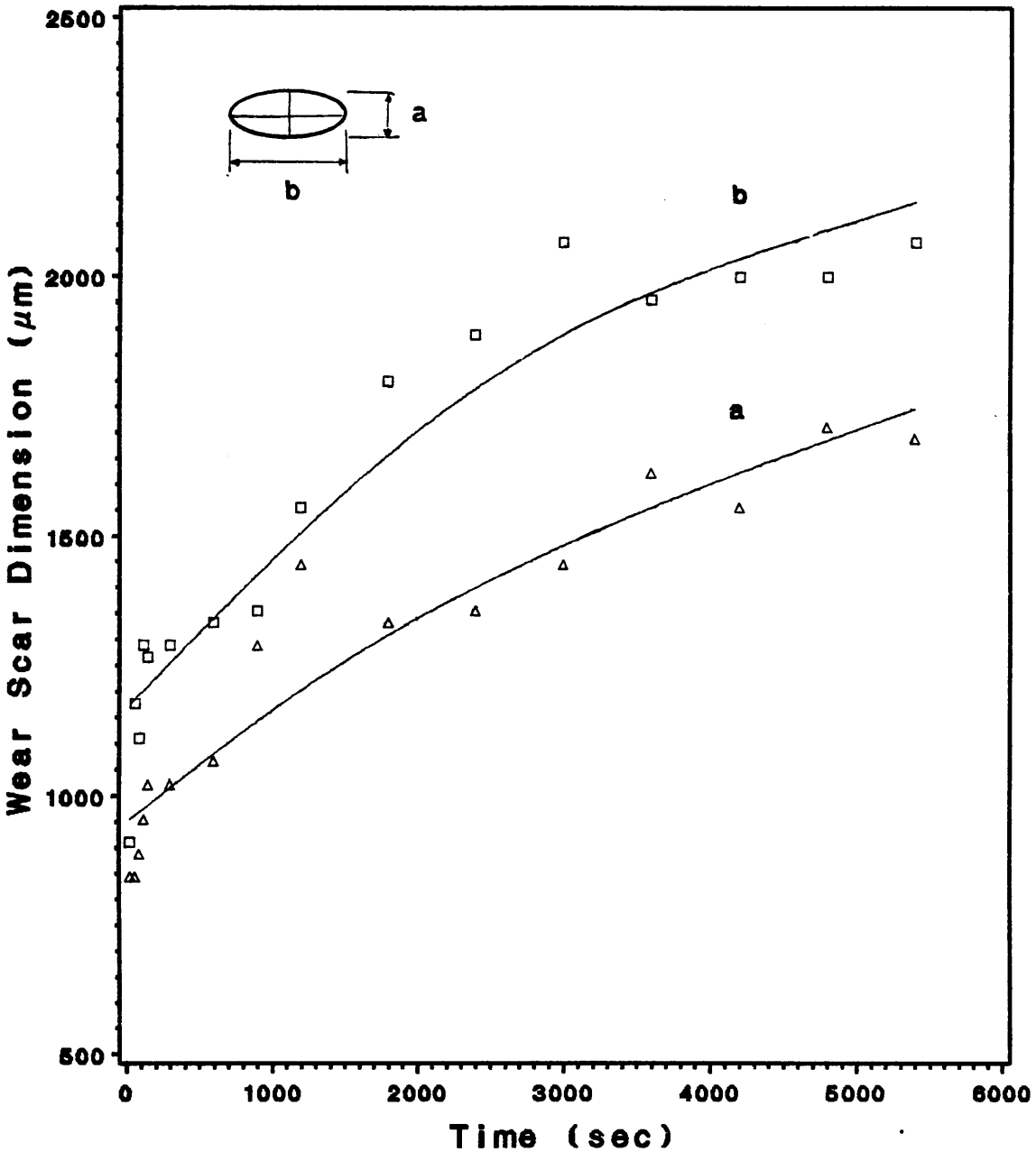

Figure 33. Growth of the Wear Scar With Time for the 52 μm Film.

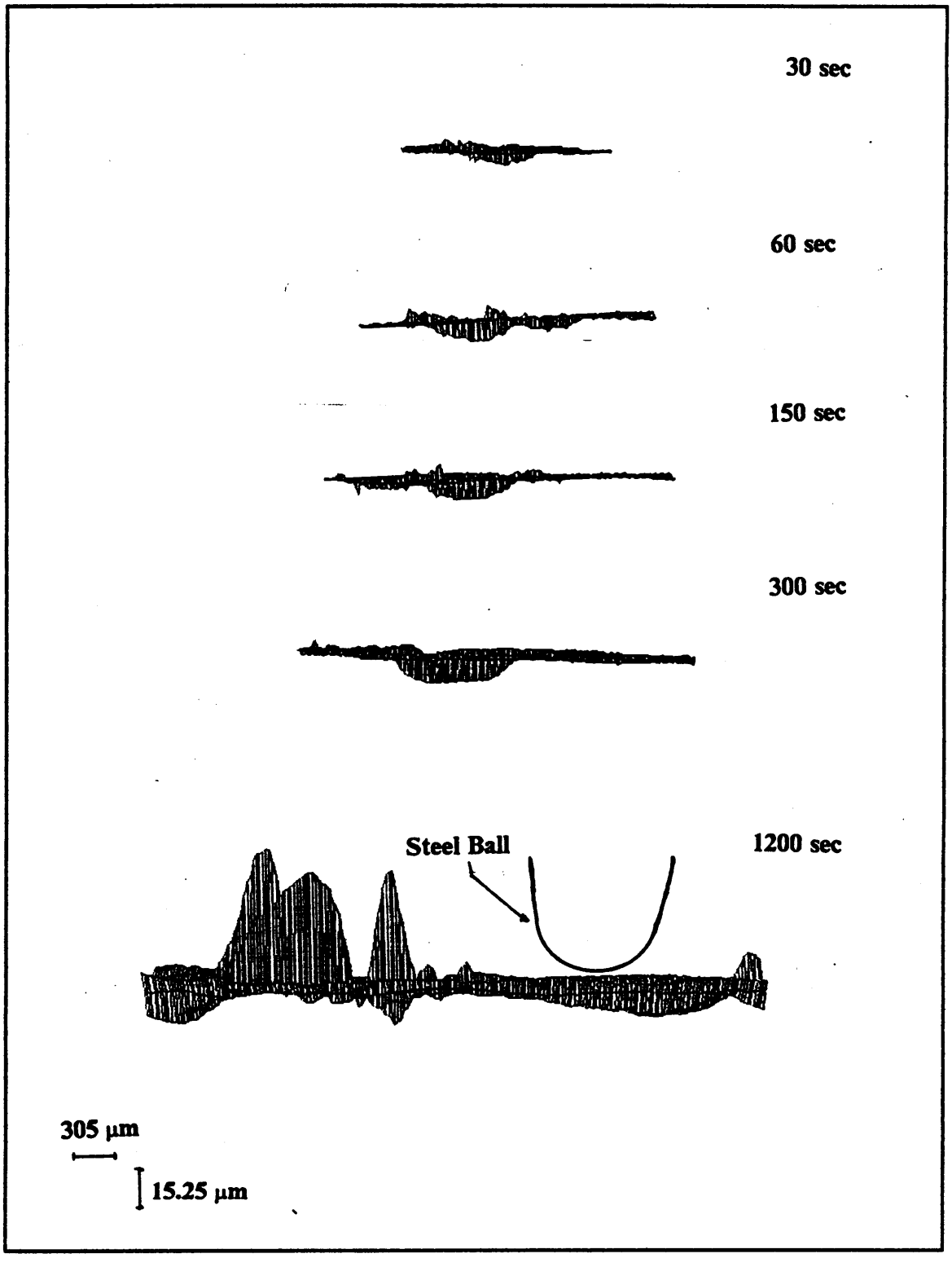

Figure 34. Computer-Generated Profiles of the Wear Scars for Different Testing Times of the 52 μm Film.

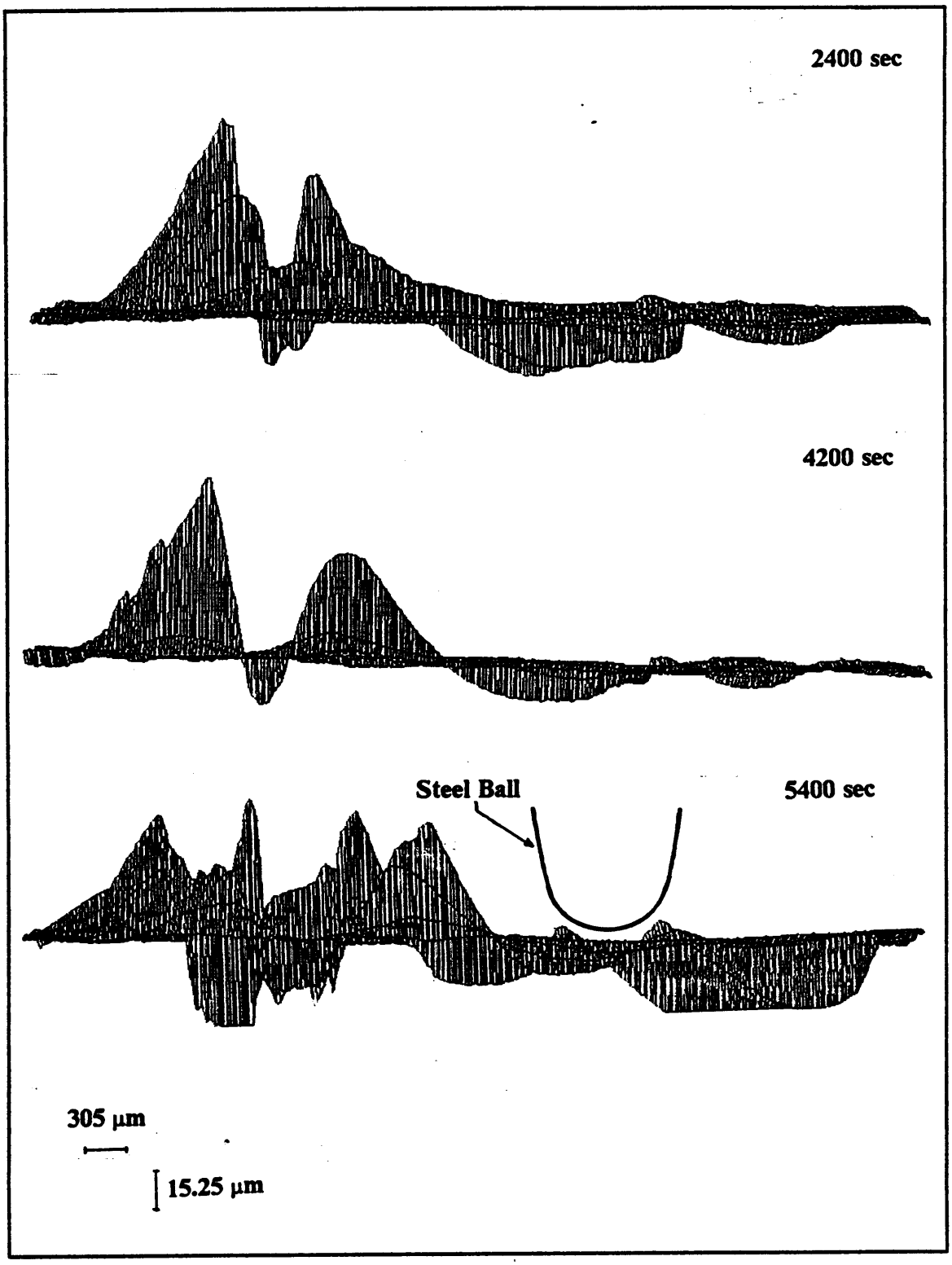

Figure 34. Continued.

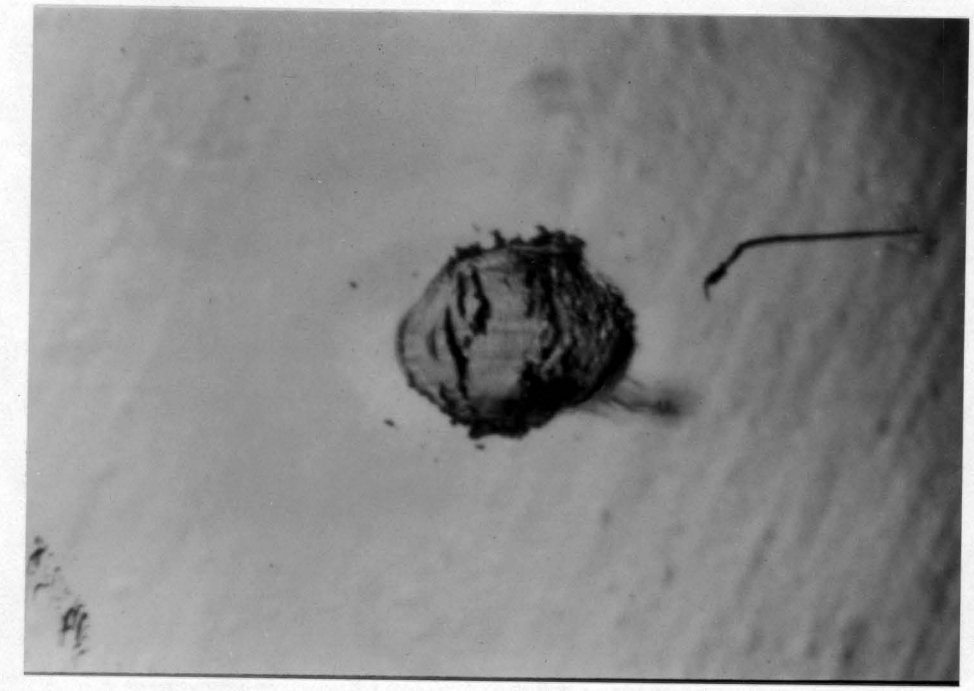

(a)

305 μm

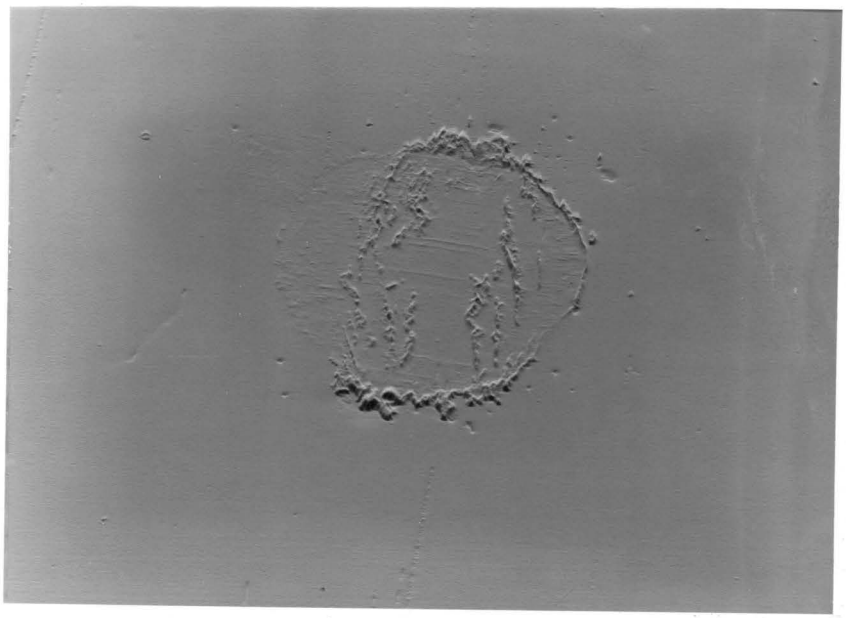

(b)

305 μm

Figure 35. Optical and SEM Photographs After 30 sec of Testing for the 52 μm Film.

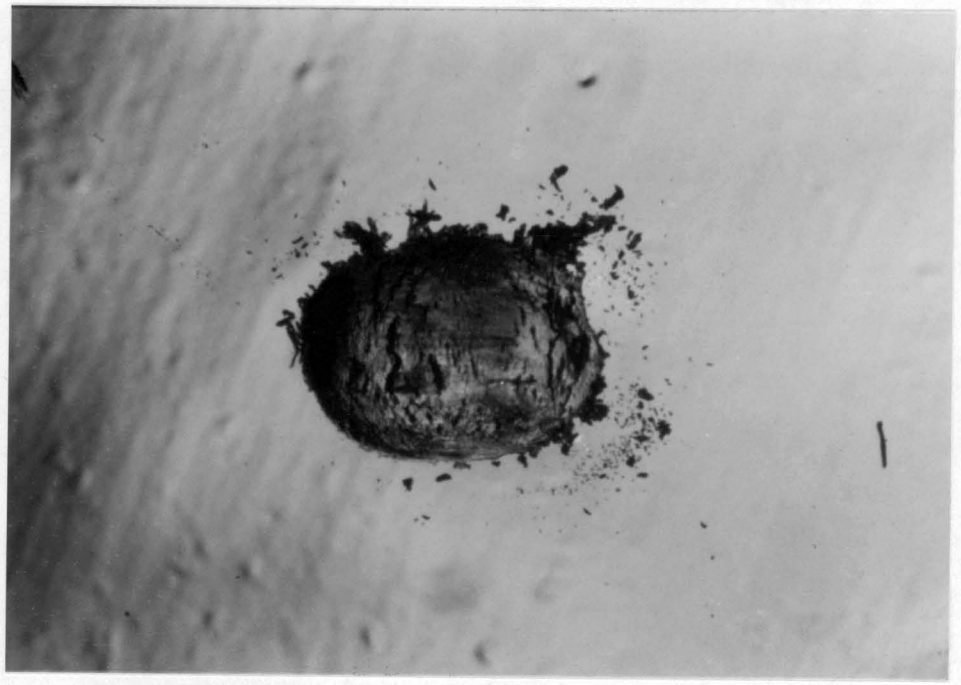

(a)

305 μm

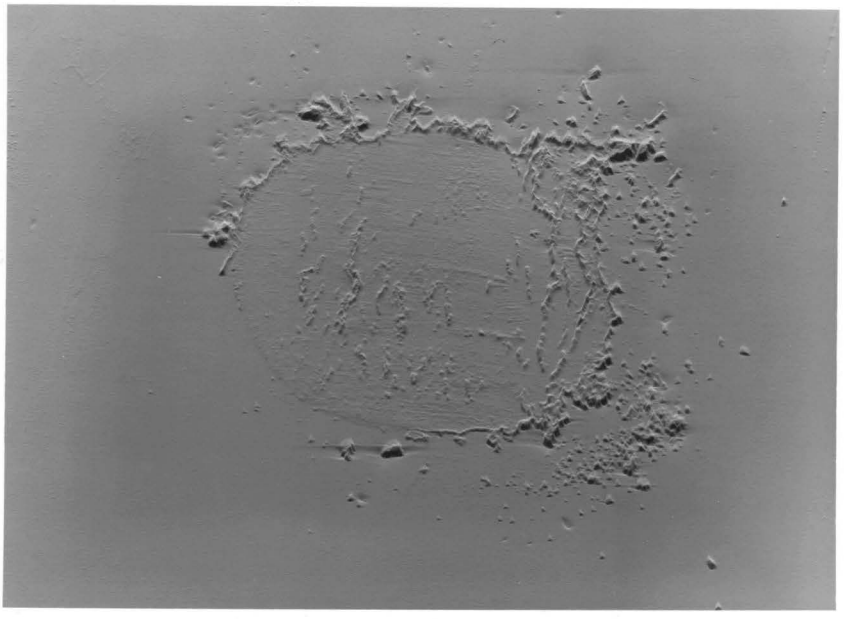

(b)

305 μm

Figure 36. Optical and SEM Photographs After 120 sec of Testing for the 52 μm Film.

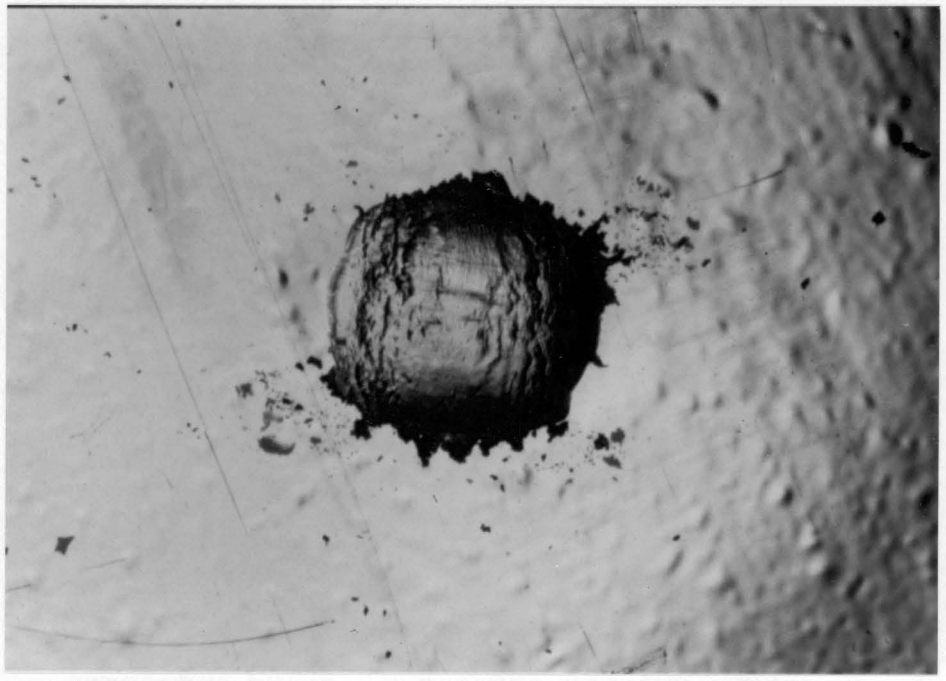

(a)

305 μm

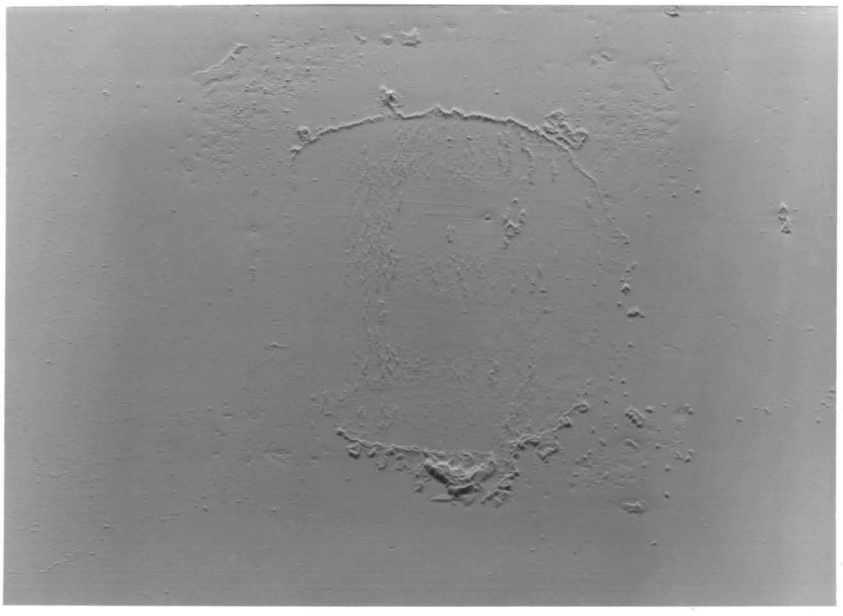

(b)

305 μm

Figure 37. Optical and SEM Photographs After 300 sec of Testing for the 52 μm Film.

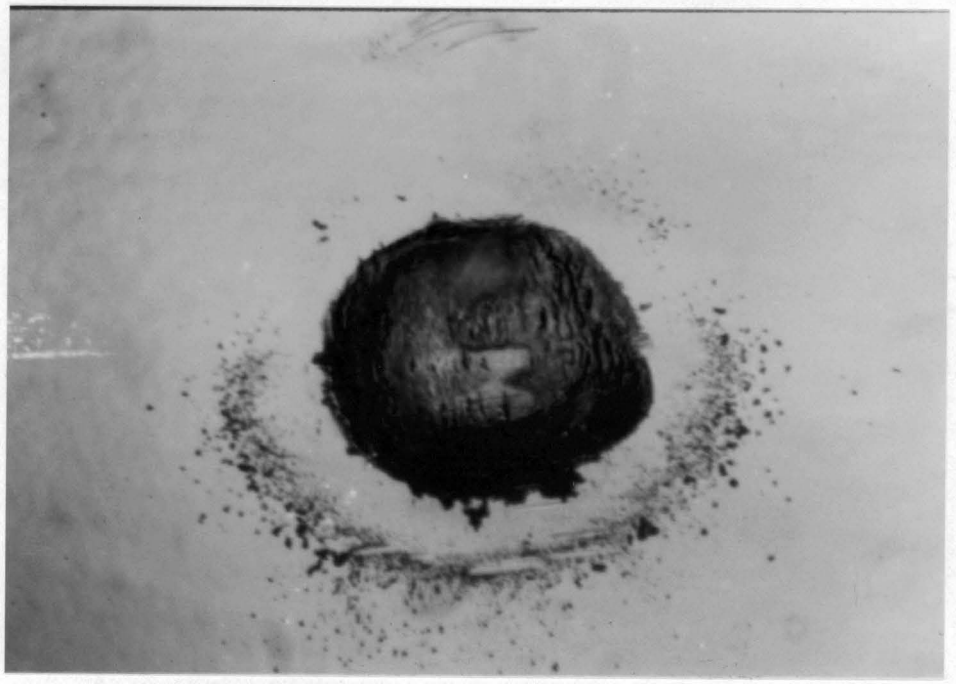

(a)

305 μm

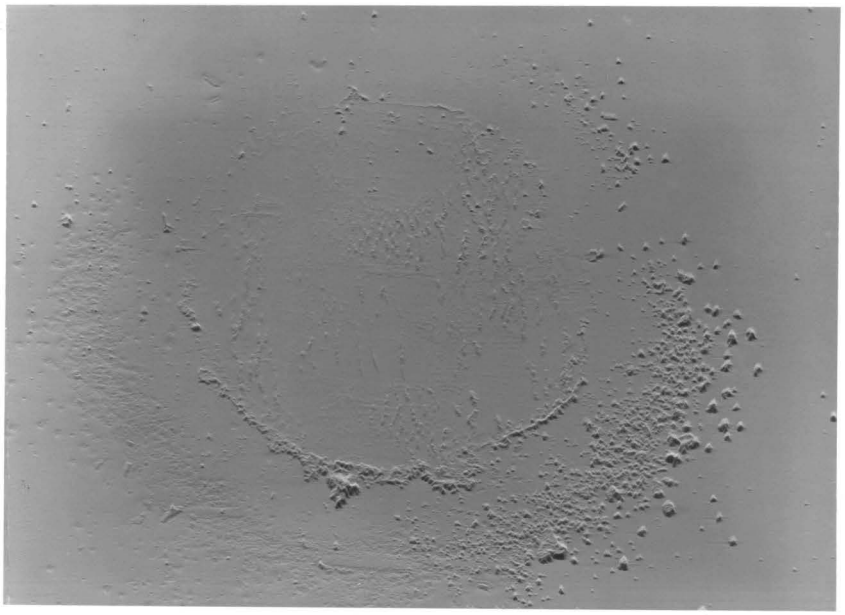

(b)

305 μm

Figure 38. Optical and SEM Photographs After 600 sec of Testing for the 52 μm Film.

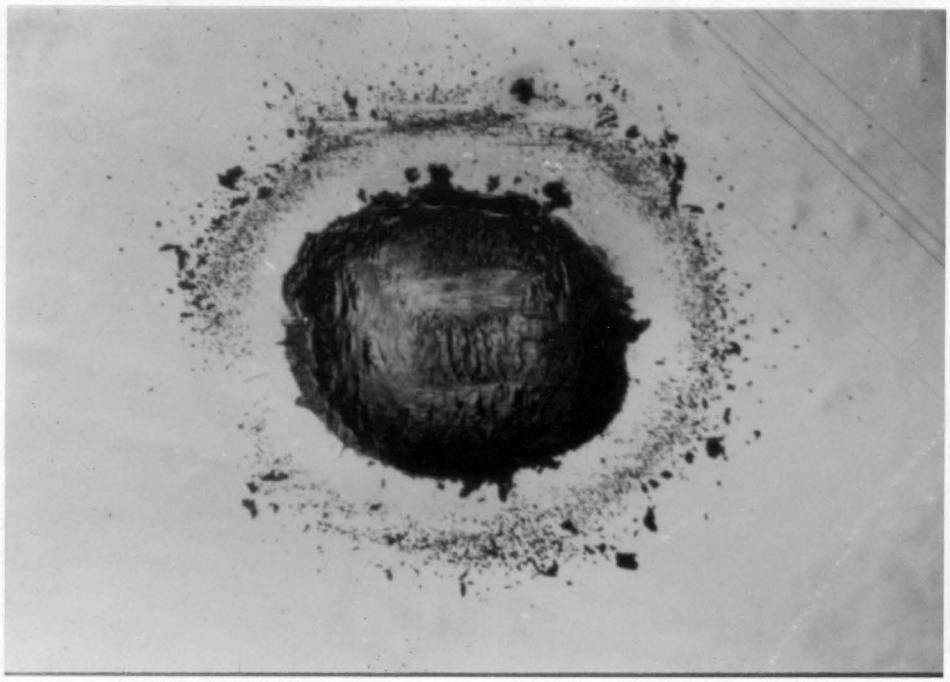

(a)

305 μm

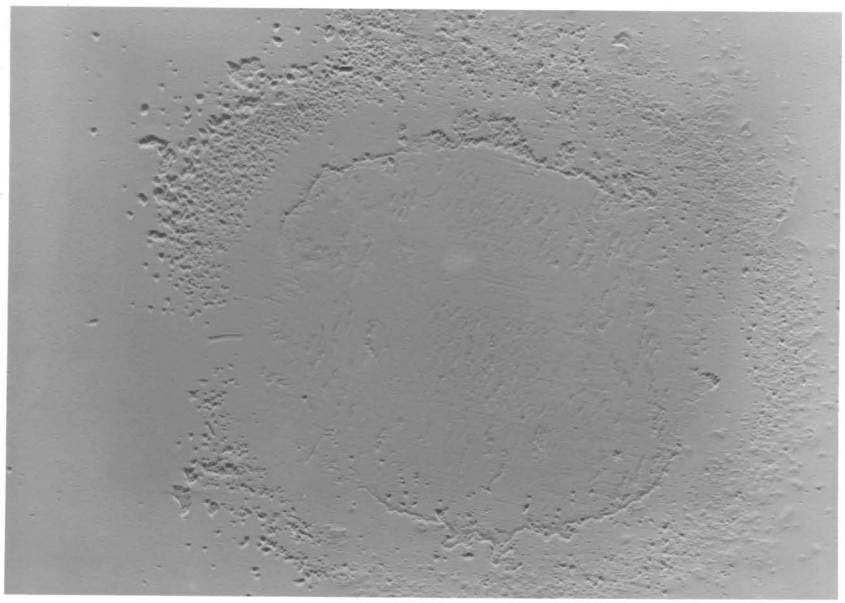

(b)

305 μm

Figure 39. Optical and SEM Photographs After 900 sec of Testing for the 52 μm Film.

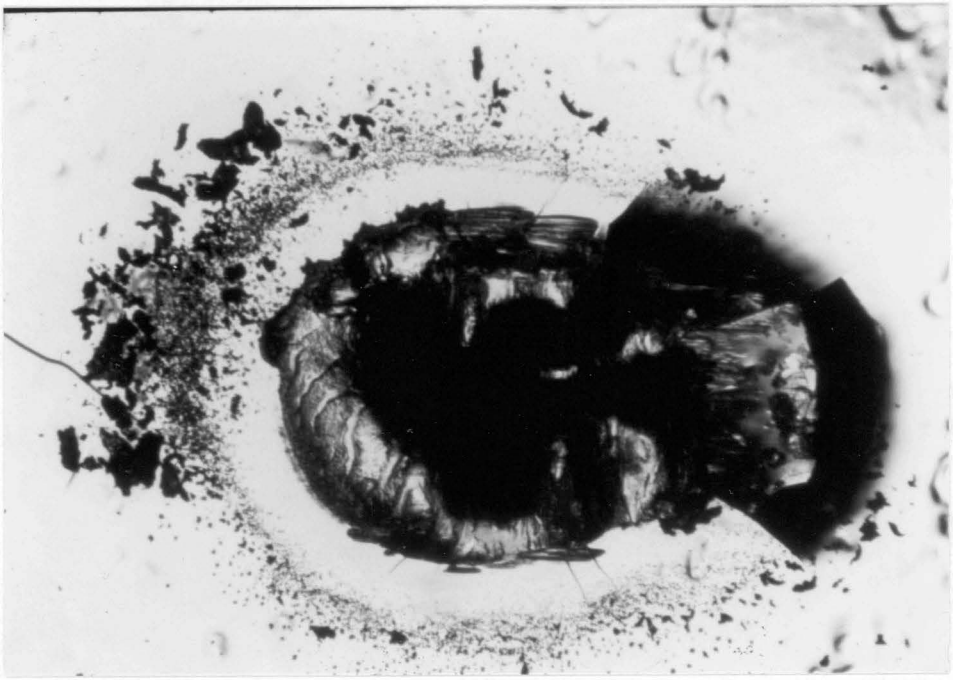

(a)

305 μm

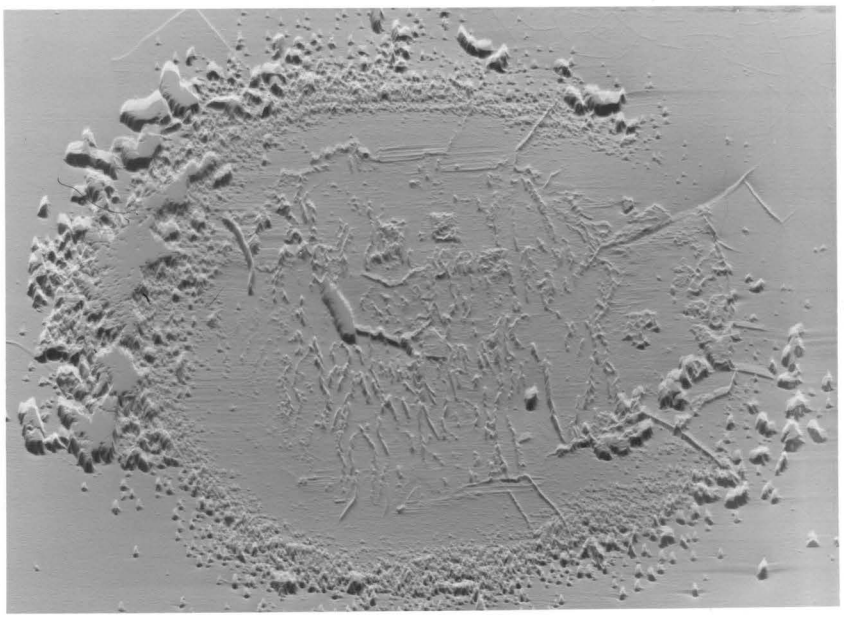

(b)

305 μm

Figure 40. Optical and SEM Photographs After 1200 sec of Testing for the 52 μm Film.

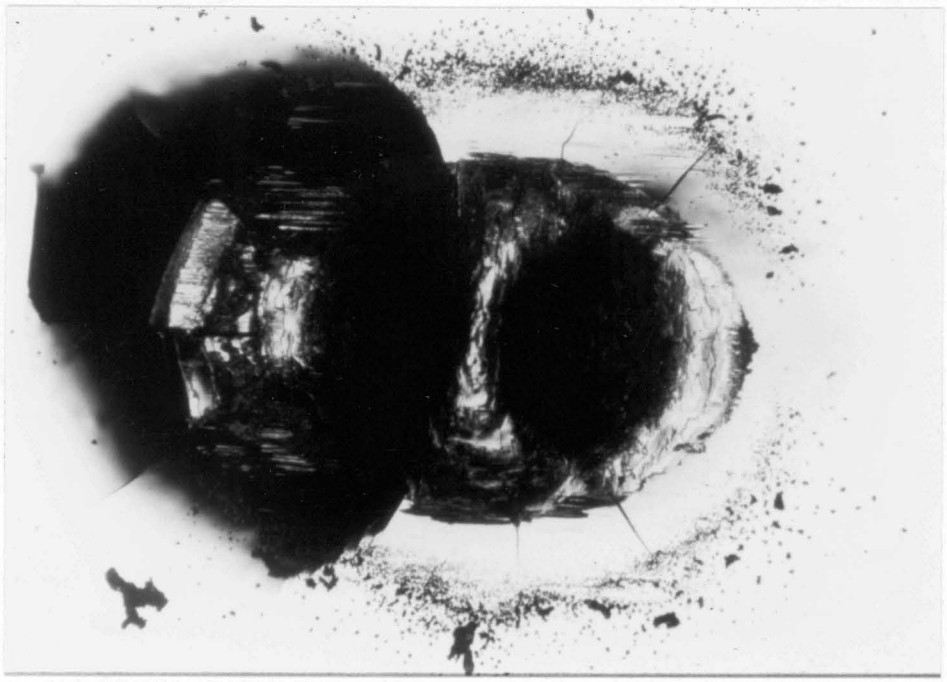

(a)

305 μm

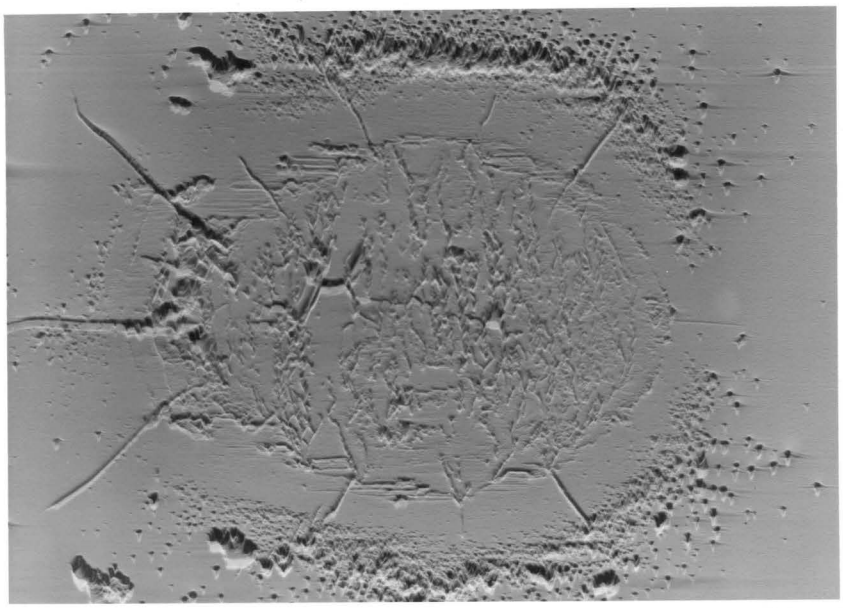

(b)

305 μm

Figure 41. Optical and SEM Photographs After 3000 sec of Testing for the 52 μm Film.

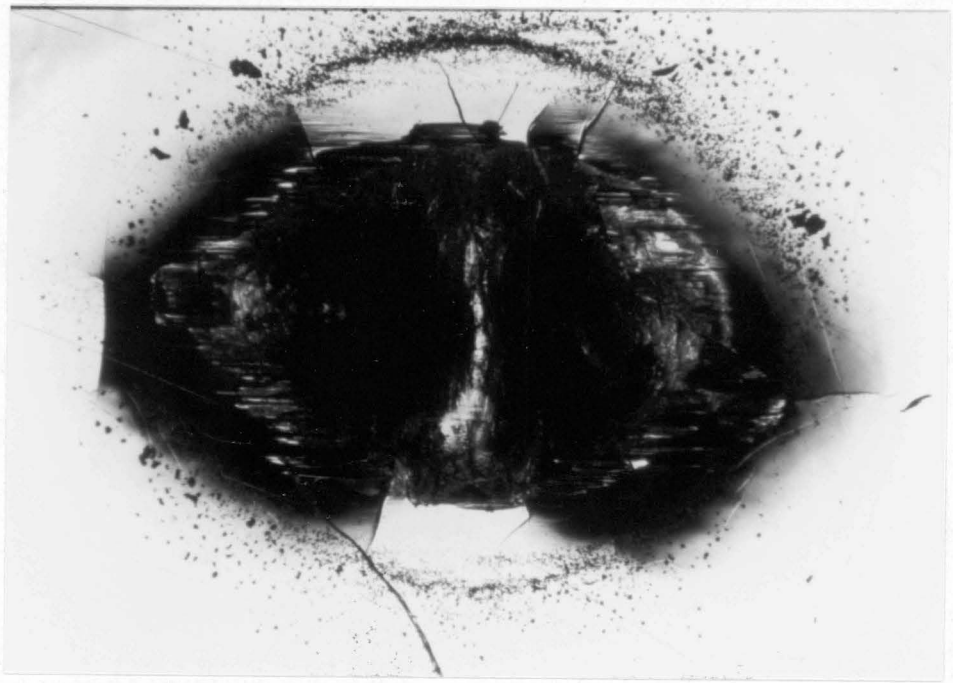

(a)

305 μm

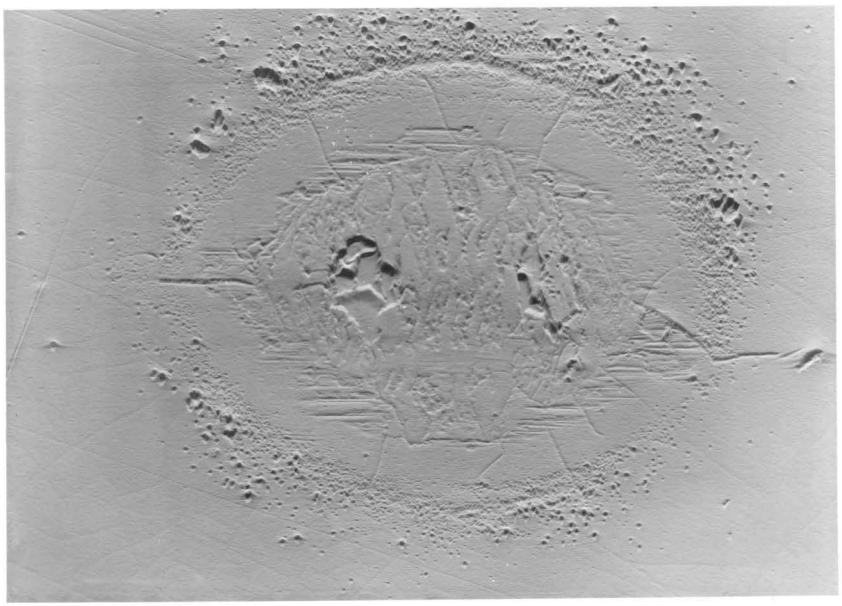

(b)

305 μm

Figure 42. Optical and SEM Photographs After 4200 sec of Testing for the 52 μm Film.

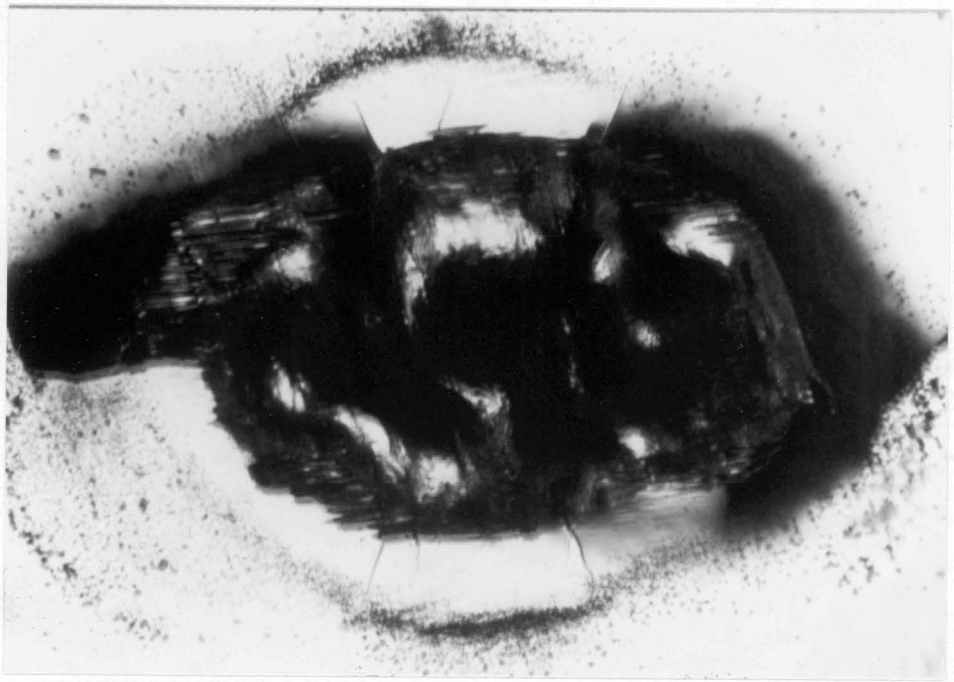

(a)

305 μm

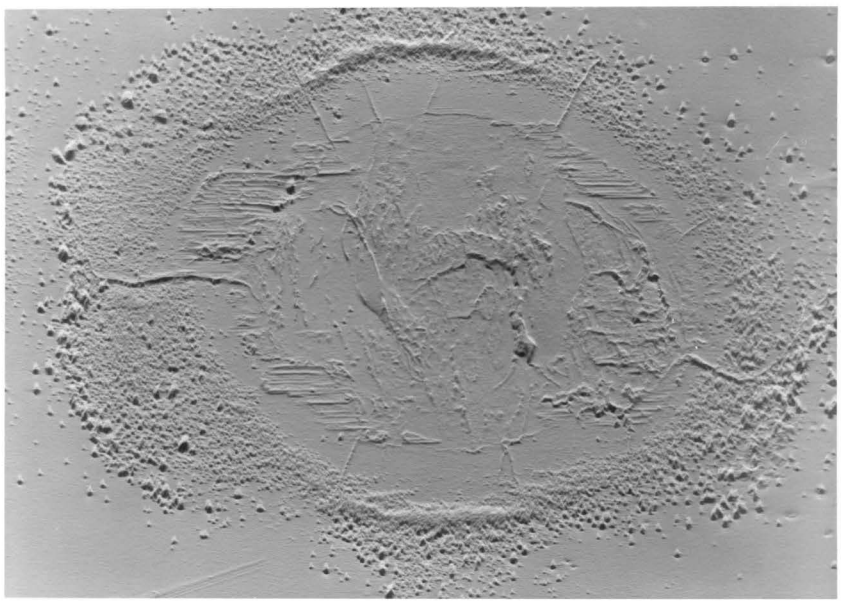

(b)

305 μm

Figure 43. Optical and SEM Photographs After 5400 sec of Testing for the 52 μm Film.

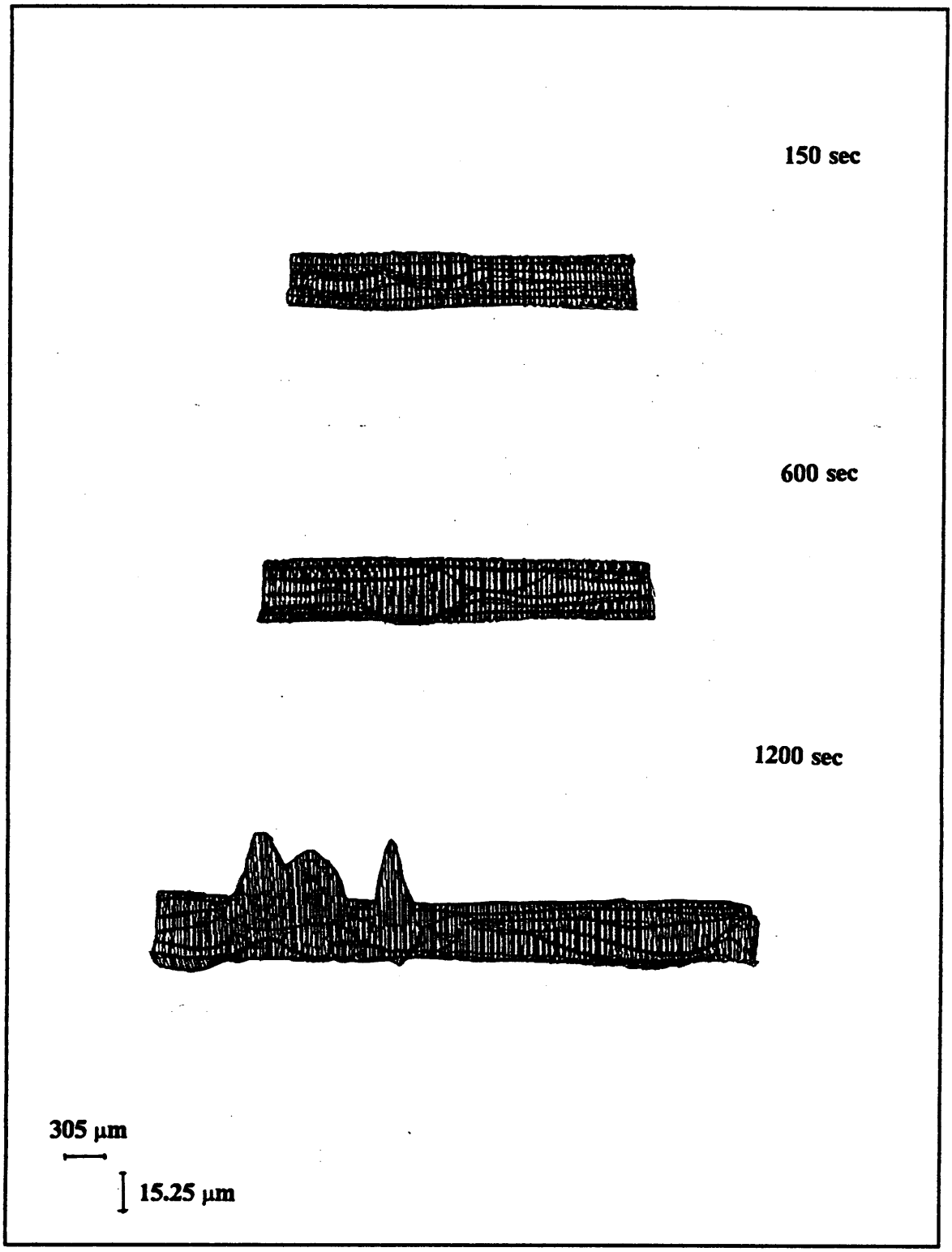

Figure 44. Computer Representation of the 52 μm Film Wear Scar at Different Time Intervals.

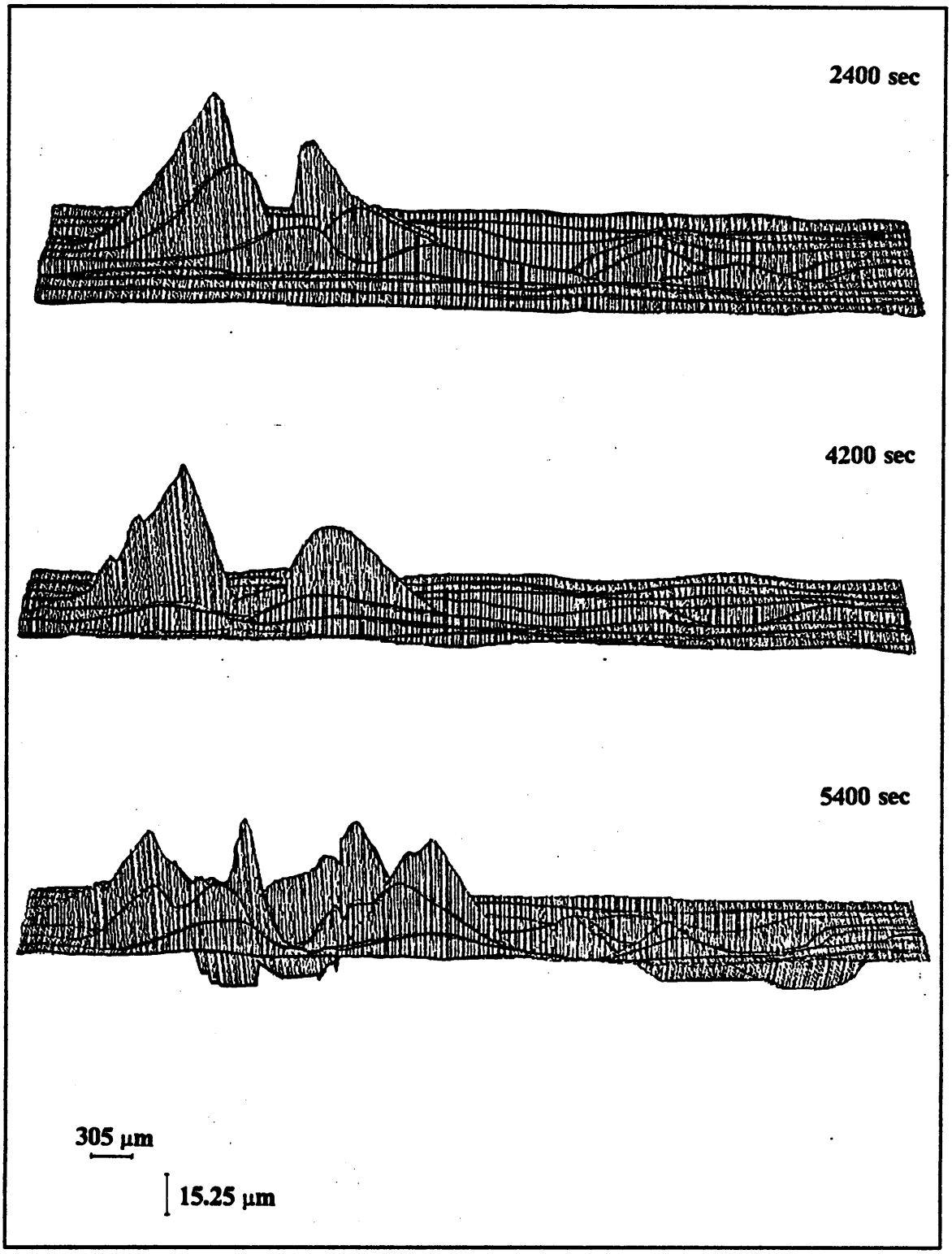

Figure 44. Continued.

5.0 Discussion.

It is a well known fact that in fretting both mechanical and chemical factors are important (see section 2.1.1). But their interaction is not clear. Uhlig [18] proposed that the frictional work done during fretting created enough energy to promote rapid oxidation. In another instance, Puzio [4], and Rorrer [5] identified dehydrochlorination as the main cause for the failure of a PVC coating under fretting. It is possible that the mechanical energy developed during fretting triggered the dehydrochlorination process. But, especially in the case of fretting of polymeric coatings, the extent of the interaction between mechanical work and chemical reactions may be much larger. It is possible, for instance, that the polymer coating fails because of mechano-degradation. That is, the chemical bonds are broken in the absence of thermal energy by the presence of a strong stress field. Of course the products from the mechano-degradation may differ from those of the thermo-degradation. This concept of mechanically triggered chemical reactions is an old one; but its application to tribological systems is very recent. It is a concept which is gaining a lot of followers especially in eastern Europe. Tribochemistry is the field that studies mechanically-initiated degradation. Another important effect of me-

chanically excited bodies is the emission of electrons. Electrostatic effects are studied in the area called tribophysics.

This chapter discusses the results obtained in this work in terms of the possible mechanisms and variables that may have influenced the outcome of the experiments. Mechanical, chemical, tribochemical, and tribophysical aspects of the system studied are presented and discussed.

5.1 Mechanical Aspects.

Polymers exhibit a combination of solid and liquid type behavior. Mechanical parameters depend rather strongly on time. This type of behavior is called viscoelasticity. Materials which are viscoelastic show a phase difference between stress and strain when subjected to sinusoidally oscillating stresses or strains. In order to take this difference into account, complex moduli, viscosities, or strains must be introduced in the analysis. The complex moduli, for instance, account for both storage and loss components while a complex strain accounts for both the immediate elastic recovery as well as creep. Viscoelastic behavior results from high chain mobility. Glassy polymers, at room temperature, are frozen into a state where there is very little or no chain mobility. It is at temperatures higher than T_g that enough chain mobility is present to cause viscoelastic behavior. However, it has been shown that high stresses can transform the mechanical response from glass-like to rubber-like by increasing chain mobility [62].

For a polymer coating on a rigid substrate the stresses will be high for thin films since, in thin films, there is less material to support the same load. Also, thin films are more rigid because of the effect of the substrate and surface asperities of the substrate can act as stress concentrators. As a consequence, the ball does not penetrate very far into the coating; this results in a small contact area and high stresses. Therefore, the sliding of the ball causes the coating to be subjected to large plastic deformations. For thicker films, the ball penetrates further which results in a large contact area and low stresses. Hence most of the ball motion causes elastic deformation of the polymer coating. Some of the energy required for elastically deforming the coating is dissipated into heat because of the material hysteresis losses. Because the friction force is higher for the thicker films more energy has to be dissipated into the polymer coating in the form of heat. The combination of hysteresis losses, increased frictional heat, and poor heat conduction out of the film into the substrate because of the increased thickness, causes an increase in the coating temperature. The distinction between thin and thick, for a given polymer, depends only on load. This study was conducted at a constant load. Hence if a different load is used different thicknesses will be identified as thin or thick. However the same general behavior should be observed.

In this study fretting is simulated by loading a steel ball on a coated steel disk and reciprocating the ball at a small amplitude. This results in normal and shear stresses acting on the surface of the polymer coating. The normal stress (σ_x) is given by the normal load (N) divided by the contact area (A_c) while the shear stress (τ_{xy}) is given by the friction force (F_f) divided by the contact area (A_c) or:

$$\sigma_x = \frac{N}{A_c} , \qquad (5.1)$$

and

$$\tau_{xy} = \frac{F_f}{A_c} \ . \tag{5.2}$$

The normal load is constant at 22.3 N and the friction force has been measured during the experiments. The contact area is estimated from the wear scar measurements (see Appendices D.1.3 and D.2) according to the following:

$$A_c = \frac{1}{2}\left[\frac{\pi}{4}(a)(b - 305)\right] , \tag{5.3}$$

where a and b are the short and long diameters in micrometers of the elliptic wear scar. The sliding distance, 305 μm, is subtracted from the long diameter so that the distortion caused by the ball motion is minimized. The reason for the 1/2 factor will become clear later. The distortion-energy theory, also known as the von Mises-Hencky theory, has been applied in order to evaluate whether the above described stresses are sufficient to cause yielding of the polymer coating. According to this theory a material will yield whenever its tensile strength is exceeded by the von Mises stress (σ') defined as:

$$\sigma' = \sqrt{\sigma_x^2 + 3\tau_{xy}^2} \ . \tag{5.4}$$

Table 7 shows the von Mises stress for different film thicknesses at breakthrough and for different testing times. Values close to the lower end of the polystyrene tensile strength range (34.5 to 82.7 MPa) are reached for the 7.9 (31 MPa) and the 13 (26 MPa) μm films. Instead the stress for the 23 μm film is down to 15 MPa. Slightly higher values are found for the 30 seconds test of the 38 and 52 μm films: 40 and 47 MPa respectively. However, after 60 seconds of testing the stresses are down to 26 MPa for the

Table 7. von Mises Stress for Different Film Thicknesses and Testing Times.

Film Thickness (μm)	von Mises Stress, σ′ (MPa)		
	30 sec	60 sec	Film Failure
7.9	—	—	31
13	—	—	26
23	—	—	15
38	40	26	12
52	47	28	8.3

38 μm film and 28 MPa for the 52 μm film. Thicker films and longer testing times yield even lower stresses. It is therefore possible that yielding governs the surface deformation mechanism for the thin films and at the beginning of the fretting process for the thicker films. This is especially true since the area of contact calculated as described before is the "apparent" area of contact. It is assumed that complete contact occurs between the two mating surfaces. Due to surface irregularities the "real" area of contact is only a portion of the apparent area of contact. If the real area of contact is used even higher stresses result.

Comparison of the photographs of the wear-time experiments for the 38 and the 52 μm films after 300 seconds of testing shows that the thicker film produces a larger more circular wear scar. This can also be seen in Figure 45 where the wear scar dimensions for the first 300 seconds are compared. The dimensions of the wear scar for the thicker film are consistently larger than those for the thin films. Therefore the contact area for

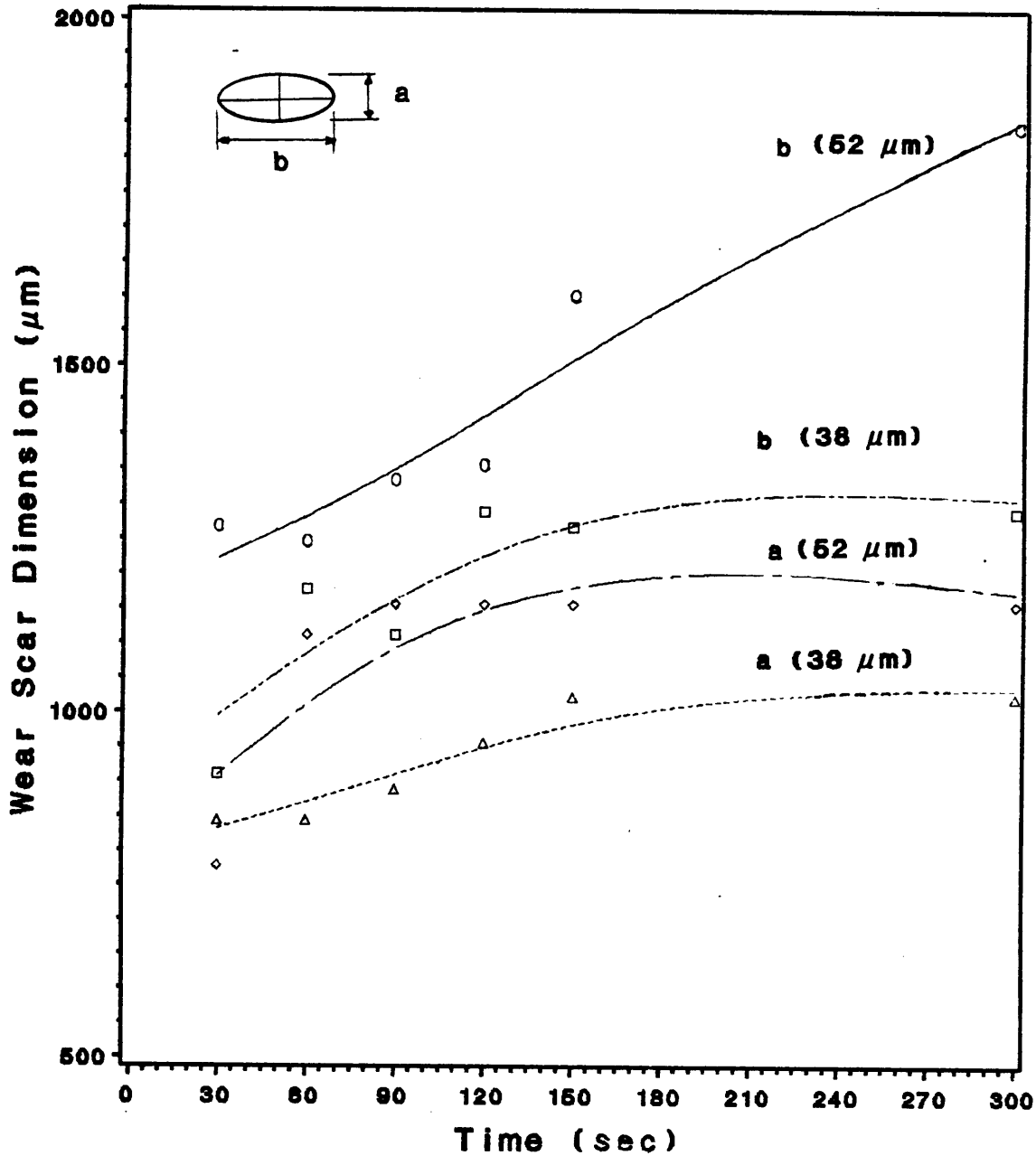

Figure 45. Wear Scar Growth During the First 300 sec for the 38 (a) and the 52 μm Films.

the thick film is larger and the load is distributed over a larger area. Thick films have a more circular shape than thin films. This is due to the fact that the contact area grows larger while the slip amplitude remains fixed. The increased contact area reduces the stresses within the coating and a milder wear rate results. This is shown in Figure 46 where the wear volume for the the first 300 seconds are compared.

Plastic deformation is the irreversible change of the shape of a body under the influence of a stress. For metals it mainly occurs through the development and motion of dislocations in the solid. Amorphous, glassy polymers, such as polystyrene, generally follow one of two types of deformation mechanisms: normal yielding or shear yielding. Normal yielding is also known as crazing. Crazing consists of an intricate array of fine cracks developing on the surface of the material at right angles to the principal tensile axis. A glassy polymer generally deforms through crazing. However, if an hydrostatic pressure is introduced shear yielding may become the preferred deformation mechanism [63]. Ihara, Shaw, and Bhushan [64] used a finite element technique to analyze the contact stress and strain of an elastic film on a rigid substrate when indented by a rigid sphere. They varied film thickness and friction and kept load and contact area constant. They found the maximum stress to be always on the surface and compressive in nature. However, for thin films and high friction the stress becomes tensile just beyond the trailing edge of the loaded area.

A study of the effect of crazing on the mechanical behavior of polystyrene films in tension was conducted by Moreno, Moet, and Baer [65]. They showed that macroscopic plastic deformation of the polystyrene films was a direct consequence of craze formation and thickening especially for high strains (> 3 %). Craze thickening under cycling loading is caused by molecular chain disentanglements of craze fibrils [63]. Crazing

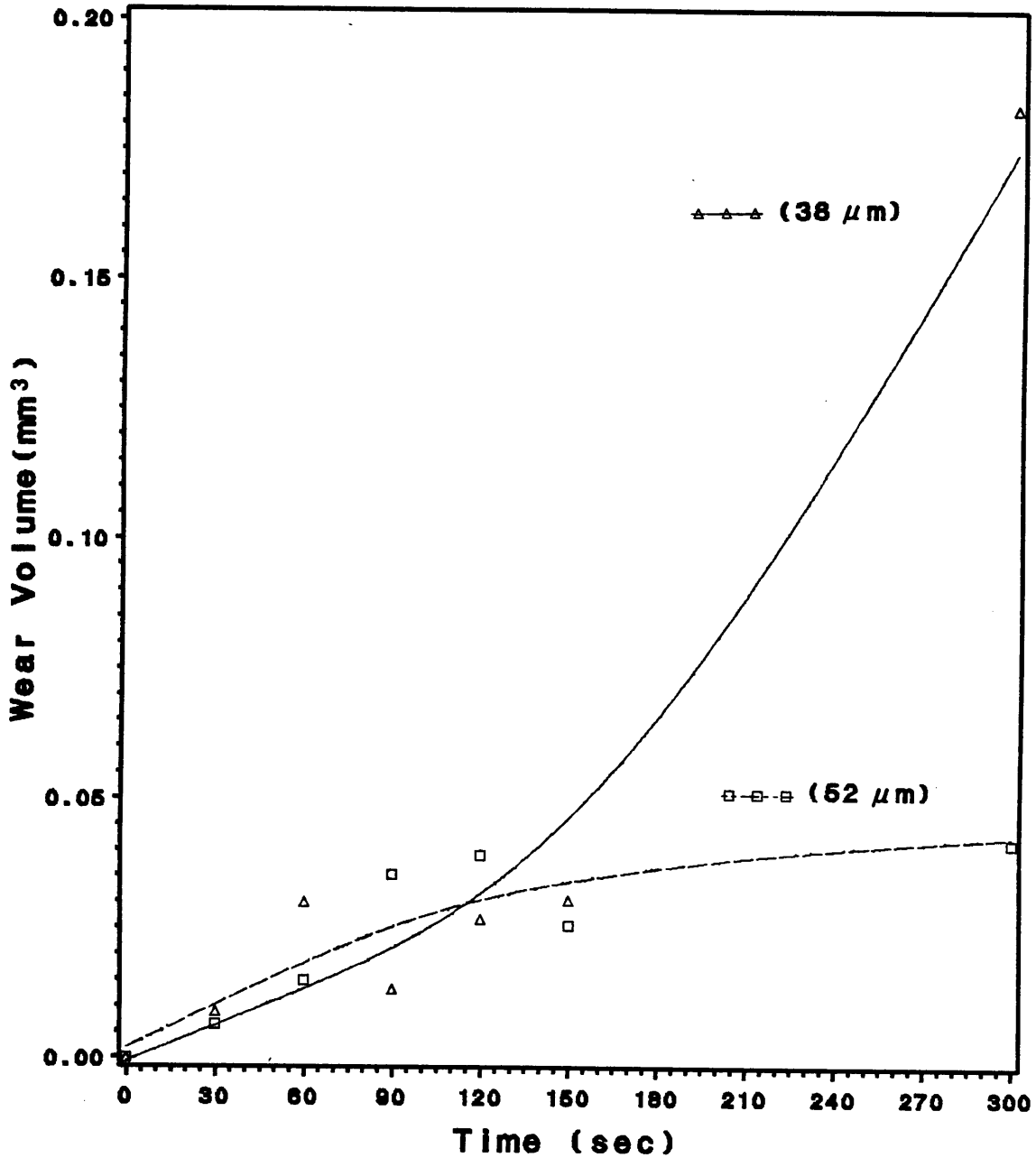

Figure 46. Wear Volume During the First 300 sec for the 38 and the 52 μm Films.

causes dilatation while shear yielding is a constant volume process. The dilatation in the crazed material causes a change of the optical properties. Craze boundaries are highly reflective while the craze itself has a lower refractive index. Gent [66] proposed a theory for craze formation. According to his theory stress concentration at a flaw causes devitrification (from glassy to rubbery) of the polymer. As a result a thin band of softened material forms which can then undergo cavitation with deformation characteristic of crazing. Thus, crazing is favored by high temperatures and high stress concentrations and restricted by hydrostatic pressure and the occurrence of creep.

The photographs presented in Chapter 4 do not show enough evidence for determining the actual mechanism of deformation. According to the above discussion one would expect crazing in the highly deformed central region. Since the particular set-up used for the SEM is not capable of distinguishing between a crack and a ridge, a scratch was made on a coated disk and photographed in the SEM machine. This way it was possible to determine how the cracks would be represented on a SEM photograph. The SEM photographs show small cracks perpendicular to the direction of motion, which is also the direction of the principal tensile stress, in the central region. Figure 47 shows the cracks for the 38 and the 52 μm films. There is no difference between the cracks of the thin film and the ones of the thick film. It is possible that the cracks are the result of a fatigue process since the central region is exposed to stresses continuously changing from tension to compression.

The optical photographs show black regions within this central region but they also extend outside in the undeformed region. The black regions present at the edges are most probably due to delamination of the film and loss of adhesion with the substrate. Figure 48 shows the photographs of the 38 and the 52 μm films after 30 seconds of

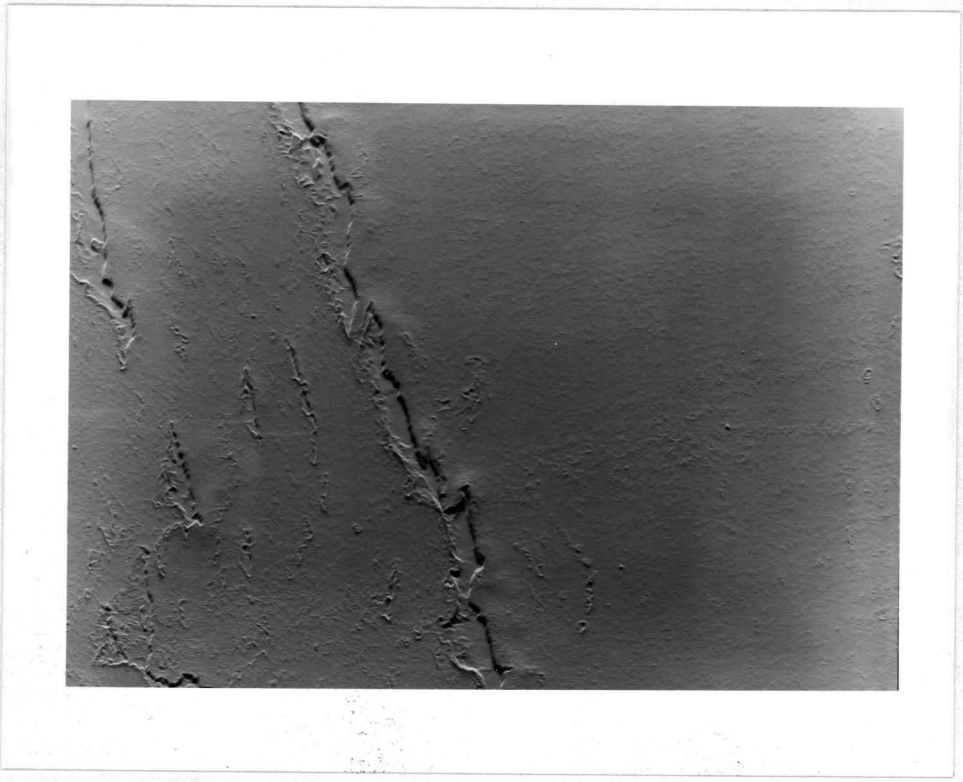

(a)

305 μm

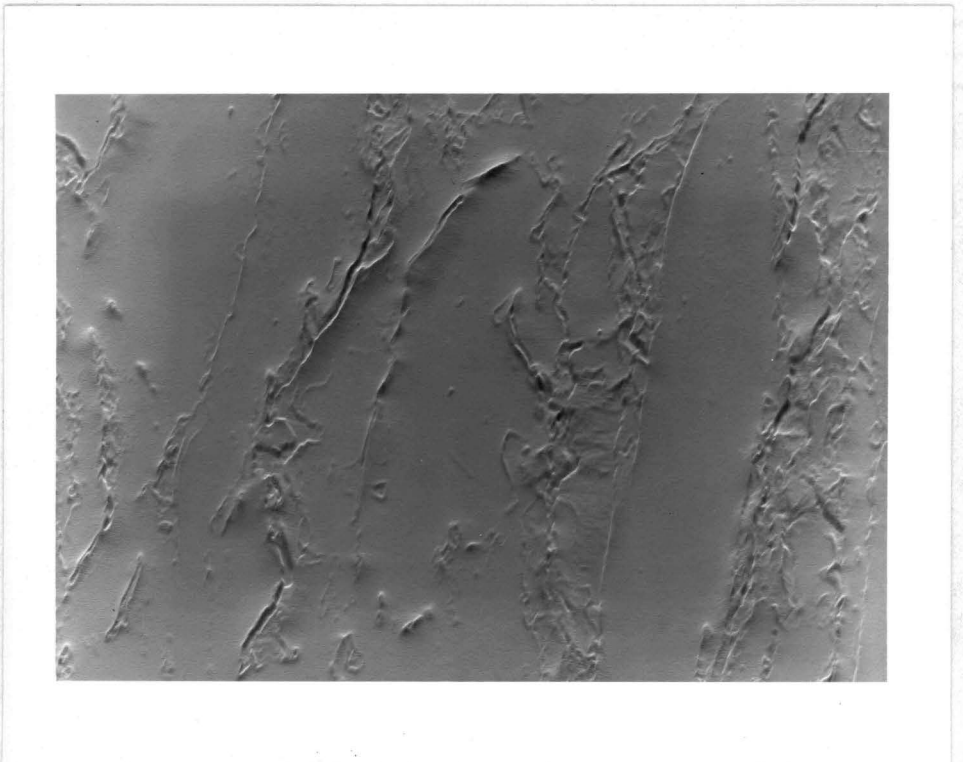

(b)

305 μm

Figure 47. Central Region Cracks for the 38 (a) and the 52 (b) μm Films.

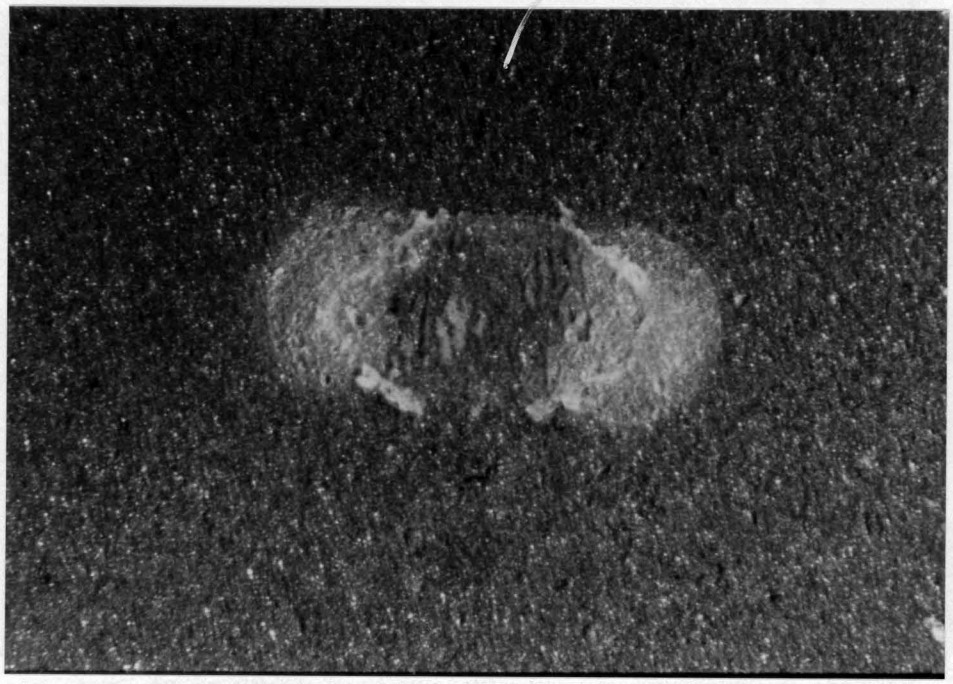

(a)
305 μm

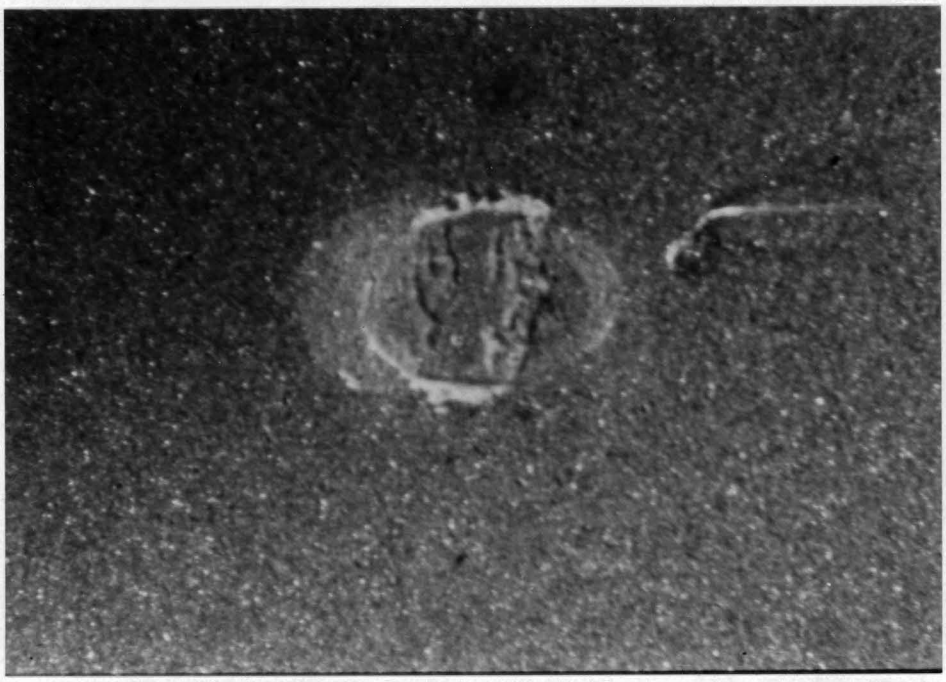

(b)
305 μm

Figure 48. Comparison of Wear Scar After 30 sec of Testing for the 38 (a) and the 52 (b) μm Films.

testing. The delaminated region is clearly visible for the 38 μm film while it is totally absent for the 52 μm film. A more dramatic representation of this region is shown in Figure 49. The delaminated regions are probably the result of the fact that higher stresses are present at the edge of the wear scar as a result of the change in the direction of motion of the ball. The situation is depicted in Figure 50.

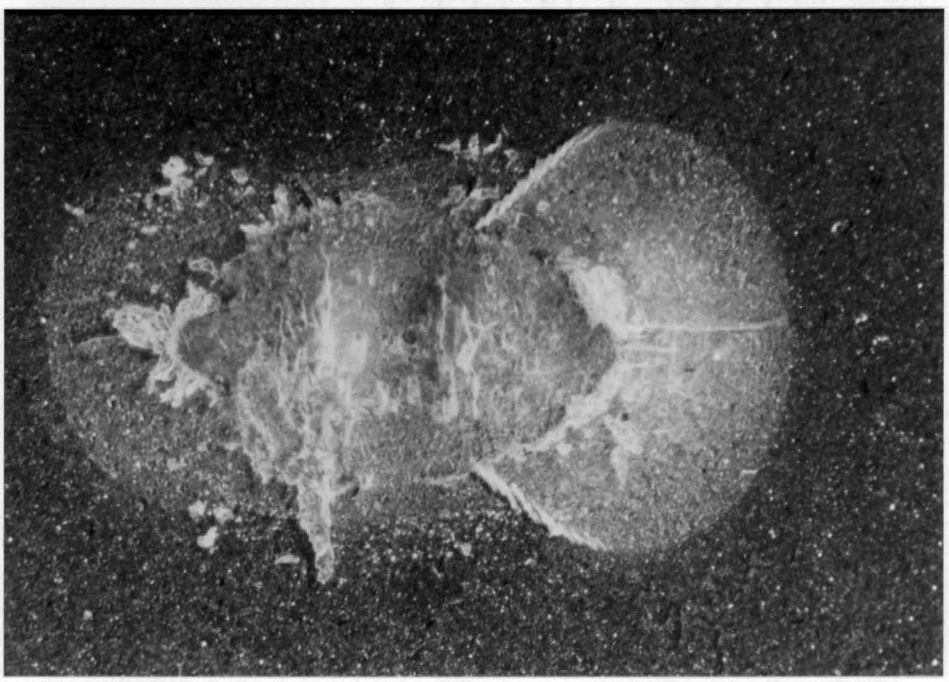

Figure 49. Delaminated Region of the 38 μm Film After 300 sec of Running Time.

When the ball is only statically loaded (Figure 50.a) the resulting contact area is circular, providing an uniformly distributed support. When the ball is in steady-state motion (Figure 50.b), only the front half of the ball supports the load causing high stresses in the coating. This is also the reason for the 1/2 factor used in equation (5.3). The situation becomes even worse when the ball is changing direction. Figure 50.c shows that as the ball changes direction the support must switch from one half of the ball to the other. As a consequence the ball is forced to penetrate deeper in the coating. As the motion progresses the load is redistributed until steady-state is reached again. This combined with the viscoelastic recovery of the polymer pushes the ball back up. For thin films high enough stresses exist at the polymer-substrate interface at the beginning of a test to cause breaking of the adhesive bonds between the coating and the substrate. In the thicker film the delaminated region develops later since the stresses at the polymer-steel interface are lower initially. However, even though several different mechanisms can explain the observed phenomena, the possibility of some degree of crazing and/or shear yielding is not to be excluded.

The two very thin films (7.9 and 13 μm) did not produce any wear debris prior to film failure. Hence the polymer coating must have been pushed away. The photographs taken, Figure 9 for the 7.9 μm film and Figure 10 for the 13 μm film, show a very smooth central region and material seem to have been pushed on the edges of the wear scar. The stress analysis done previously showed that stresses high enough to cause yielding and plastic flow may exist for these films. Thicker films formed wear debris prior to failure. The debris was also transferred to the contacting ball. However, the 38 and 52 μm films did not produce any wear debris during the first 30 seconds of testing. Also the wear debris tended to become smaller with longer testing times. The delay in debris formation was most probably due to the fact that, as shown before, the stresses

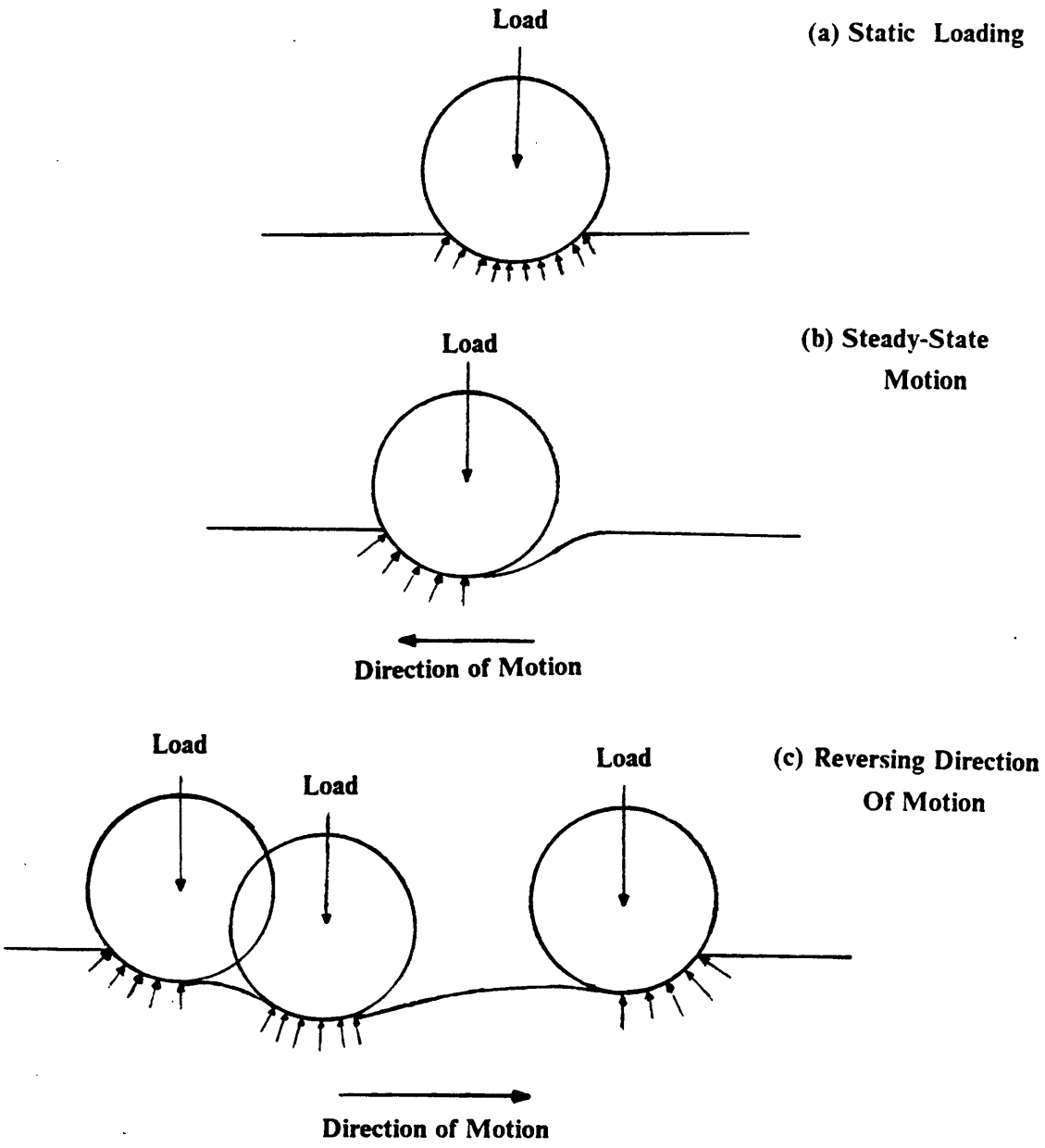

Figure 50. Load Distribution and Film Displacement During Sliding of The Ball.

of the 30-second tests for both the 38 and the 52 μm films were high enough to cause yielding of the coating surface. Therefore material was pushed away without forming any debris. Another possibility is the presence of a thin oxide layer on the ball surface. When the ball was forced to reciprocate on the coated disk, the oxide layer acted as a lubricant thus reducing stresses. Later, when the stresses on the surface were lower, or the oxide layer had been worn out, adhesion and ploughing between asperities of the steel ball and of the polymer occurred and debris particles were formed. With time the polymer surface tended to smooth out and smaller debris were formed. Also, as the ball oscillates some crushing of the debris and subsequent size reduction occurred. The uncrushed, big particles were being pushed toward the outside by the ball motion and are visible on the outer part of the debris ring. Further, smaller debris may have formed as a consequence of fatigue processes.

Examination of the photographs show that three distinct regions develop. A central or plastic region where plastic deformation and wear occurs. Outside is the elastic region where the material is subjected to elastic deformation. The wear debris defines the borders of this region. Further out is the undisturbed or zero-stress region. The plastic region and the wear debris formation have already been discussed above. The elastic region is subjected to tensile, compressive and shear stresses. It is a region where fatigue plays an important role. For the 52 μm film radial cracks form in this region between 900 and 1200 sec, long after any other film, except the 46 μm film which however, did not show any cracking, has failed. These radial cracks are most probably due to fatigue.

5.2 *Chemical, Tribochemical, and Tribophysical Aspects.*

The polymer films were formed using a solvent-coating technique (see section 3.1.3). Prest and Luca [67] studied the effect of such a technique. They found that, as a consequence of this technique, the polymeric chains are preferentially oriented in the plane of the film. This orientation is more evident with decreasing film thickness. The alignment is a function of both molecular weight and temperature and is the result of the fact that the relaxation time of the concentrating solution is rapidly increasing. Hence, the stressed segments have less time to respond to the decrease in volume. The ability of the chain to adapt and relieve the localized stresses is therefore restricted. These stresses are caused by both a collapse of the film, contracting the molecules into a smaller volume, and the creation of intermolecular entanglements. The orientation reflects both the stresses supported by the entanglements and the alignment of localized segments. A non-equilibrium state has been frozen-in during the evaporation of the solvent. Thus the solvent casting process leads to a somewhat oriented system. Further orientation can occur during the first stages of sliding. The initially high stresses imposed by the sliding ball tend to try to align the molecular chains in the direction of motion and since the temperature is low the chains can not move to adjust and some further alignment occurs.

Uncrosslinked polymers, such as polystyrene, adhere mainly through van der Waals forces. However, entanglements represent temporary stable physical coupling points capable of transmitting mechanical stresses [68]. Local disentanglements are, therefore, a weakening phenomenon. Entanglements can be resolved either by force, that is chain scission, or by long loading times at elevated temperatures [69]. Chain scission and

subsequent disentanglement can lead to polymer degradation but require very high stresses and/or temperatures. There is very little support for the opinion that chain scission governs the failure mode of amorphous polymers. Structural weakening under loading seems to be caused more by disentanglement due to chain slip, and void opening processes [70].

In the particular case of this study, the sliding of the ball causes the surface of the polymer coating to be subjected to both constant and alternating loading. Heinicke [71] observes that in a sliding situation, most of the mechanical work done against friction is converted into heat. This is especially true for polymers. Experiments have shown that temperature peaks as high as 1000 °K have been observed for a very short time ($\cong 10^{-4}$ sec) at moderate to high sliding velocities. He also notes that under the effect of a constant load the interatomic bonds are elastically deformed, their natural frequency is shifted, and interatomic distances and valence angles are changed. All of this causes a reduction of the bond energy and the temperature dependence of the tribochemical reaction is lowered. If, on the other hand, the material is subjected to alternating stresses, the elastic energy is constantly redistributed among the different macromolecule of the system depending on frequency of action and relaxation time of the material. Energy can be absorbed up to a certain level and then it is redistributed. This leads to the creation of non- equilibrium excited vibration states in certain section of a macromolecule. Heinicke argues that this fact alone can lead to the breaking up of main valence bonds. Heinicke's observations, combined with the chain orientation due to the solvent-casting technique used and sliding of the ball, lead to a picture of a highly strained, non-equilibrium chain conformation. Molecular stresses are therefore unevenly distributed inside the polymer. Thus it is possible that some bonds are overloaded and broken. This leads to a degradation of the polymer and ultimately to the formation of

molecules of polystyrene of lower molecular weight. Eventually, aggregates of these molecules form plate-like wear particles since this is a surface phenomenon.

The tribochemical degradation of carbon-chained polymers leads to the formation of activated radicals. Experiments have shown that when polystyrene is mechanically degraded the following radicals form [72]:

$$\sim CH(C_6H_5)\text{—}H_2\dot{C} + \dot{C}H(C_6H_5)CH_2 \sim .$$

These activated radicals have excess free energy and therefore will form secondary reactions. They could react with the steel ball in the form of film transfer, or they could react with each other and form bigger particles. However, this is unlikely because of the crushing effect of the sliding ball. A third possibility is for the radicals to react with the bulk polymer. The free radical might be able, with the right conditions of temperature and time, to graft onto the bulk polymer. The result of such a reaction would be a second film of less strength but nevertheless capable of offering some protection. For this film to be able to form enough time must be given for the reactions to take place. A thicker film, simply because there is more material to wear away, gives enough time for this secondary film to form and extend the film life even longer. The fact that both the wear volume and maximum depth of penetration level off after about 3000 seconds seems to support this theory. This secondary film is probably starting to form some time before, as soon as the coating is at the right temperature and enough active radicals have been formed, but it needs to grow to a certain extension in order to be effective. Further breaking of grafted chains will produce smaller particles of even lower molecular weight. The drop in molecular weight of the degrading polymer will be faster at the beginning of the process and will tend to stabilize with time. However, mechanical properties are

relatively unaffected by a drop in molecular weight until a certain value after which the mechanical properties drop sharply. Therefore, at the beginning of this process the secondary film is about as good as the original one but later on it is broken much more easily.

Ohara [73], in his study on the molecular processes during friction of various polymers, including polystyrene, points out that molecular processes are affected not only by mechanical factors, but that electrostatic effects are also very important. It could be possible then that under the effect of rubbing free charges develop and are absorbed by the polymer. Polystyrene is an electron acceptor therefore it is capable of absorbing free charges. Once saturated the polymer must discharge. The discharging process can lead to surface destruction, deformation of surface molecules and generation and/or relaxation of surface strain. Thin films have a lower capacitance simply because there is less material and they are subjected to more frequent discharges. Thick films can absorb more charges, therefore the surface of the coating is less effected by this phenomenon. In order to measure the occurrence of contact a 1.5 mV voltage was put across the film. The circuitry is such that the contacting ball is charged positively while the disk holder and the disk itself are negatively charged. The effect of a positive charge is to inhibit the emission of electrons, thus reducing electrostatic effects. A negative charge has just the opposite effect. Therefore the 1.5 mV voltage should have only a very small, negligible effect on the phenomena described before.

6.0 Conclusions.

Two sets of experiments were carried out to determine the effect of film thickness on a polystyrene coated steel disk under fretting. The polystyrene coating was applied on a 1045 steel disk and fretted against a 52100 steel ball. A normal load of 22.3 N, a slip amplitude of 305 μm, and a frequency of vibration of 20 Hz were used for both sets of experiments. Seven film thicknesses ranging from 7.9 to 52 μm were used for the first set of experiments. Twelve tests were run for each film thickness in order to evaluate the film life. The second set of experiments was used to study the progression in time of the fretting damage. Two film thicknesses, 38 and 52 μm, were used. Tests were run to precise time intervals covering the film life prior to failure. Optical and scanning electron microscopy and computer graphics were employed to study the fretting interface.

Obviously the processes involved in the use of polymeric films are very complex and influenced by a combination of physical, chemical, thermal, and mechanical effects. This is demonstrated not only in the results of this work, and the one presented in the thesis referred to, but in pubblications based on this type of work [74,75]. More research is needed to fully understand the phenomena.

The following general conclusions were drawn from this study:

1. Polystyrene coated disks were found to be effective in preventing fretting corrosion and fretting wear since the steel counterface did not show any damage.
2. The fretting conditions simulated in this study were severe enough to cause the failure of all polystyrene films.
3. A drastic increase in film life occurred at thicknesses above 40 μm. Above this thickness stress and temperature conditions of the coating changed enough to cause a milder fretting regime. There were several factors involved and they were of mechanical, chemical, and tribochemical nature.
4. Film roughness decreased with film thickness while friction increased.
5. Thick films were smoother and more elastic than thin films since the effect of the substrate was less. This resulted in a more conforming and larger contact area.
6. The absence of wear debris and the fact that the polymer tensile strength was exceeded by the von Mises stress indicates that yielding has occured for the 7.9 and the 13 μm films and for the 30-second tests of the 38 and 52 μm films. Yielding is the cause for the failure of the two thinnest films.
7. Thicker films failed probably because of a combination of degradation, shear yielding, crazing, and fatigue. The thicker the film the more important the last two mechanisms become.

7.0 Recommendations.

The following recommendations are put forth as a consequence of this study:

1. Computerize the data recording system of the MARK III fretting machine. The addition of the LVDT has made possible to record all of the involved variables by electrical signals. The addition of a clock in combination with the starting and the ending of the tests would yield a very efficient and accurate computer based data acquisition system. This would make data manipulation and analysis much easier.
2. Equip the MARK III with an automatic frequency setter which would make the start of the test procedure much more accurate and repeatable.
3. Develop methods to determine properties of the polymer coating such as compressive strength, shear strength, chain orientation, and dielectric constant just to mention a few.
4. Analyze the chemistry of the wear debris formed to determine the extent of the tribochemical reactions discussed in this work. The use of electron spin resonance spectroscopy could determine whether or not free radicals are formed during fretting.

5. Study the temperature effects at the interface. Temperature effects when polymers are involved are very important. The use of an infrared microscope would be appropriate.
6. Study the extent of the electrostatic effects discussed in this work.
7. Determine the effect of the contact detection circuit on the electrostatic charging and discharging. An easy way to do it would be to simply reverse the circuit polarity.
8. Explore the effects of different loads and environments.
9. Research the extent of the interactions between physical, chemical, thermal, and mechanical effects. This study indicates that all of this effects are important and interconnected.

List Of References.

1. Frantz, R. D., "An Experimental Study of Fretting Corrosion at a Bearing/Cartridge Interface," Masters Thesis, Mechanical Engineering, Virginia Polytechnic Institute and State University, February 1983.

2. Furey, M. J., Eiss N. S. Jr., Mabie H. H., "Fundamental Studies on the Effects of Thin Polymeric Surface Films in Reducing Fretting Corrosion and Wear," *Research Proposal, U. S. Army Research Office*, Mechanical Engineering Department, Virginia Polytechnic Institute and State University, Blacksburg, Virginia, August 1983.

3. Sweitzer, K. A., "The Effects of Thin Polymeric Surface Films on Fretting Corrosion," Masters Thesis, Mechanical Engineering, Virginia Polytechnic Institute and State University, September 1984.

4. Puzio, D., "A Study of Chlorinated Polymer Coatings in a Fretting Interface," Masters Thesis, Mechanical Engineering, Virginia Polytechnic Institute and State University, November 1985.

5. Rorrer, R. A. L., "The Effects of Load, Frequency, Slip Amplitude, Humidity, and Film Thickness of Polyvinyl Chloride on Fretting Corrosion," Masters Thesis, Mechanical Engineering, Virginia Polytechnic Institute and State University, December 1985.

6. Day K. A., "The Use of Thin Polymeric Coatings to Prevent Fretting Corrosion and Metallic Contact in Steel-On-Steel Systems," Masters Thesis, Mechanical Engineering, Virginia Polytechnic Institute and State University, March 1986.

7. Collins J. A., "Fretting, Fretting Fatigue and Fretting Wear," *Failure of Materials in Mechanical Design*, John Wiley & Sons, New York 1981.

8. *Glossary of Terms and Definitions in the Field of Friction, Wear and Lubrication--Tribology*, OECD Publications, Paris 1969, p. 35.

9. Barwell, F. T., "Friction and Wear, Detection and Measurement," *Lubrication and Wear of Living and Artificial Joints*, The Institute of Mechanical Engineers, London, 1966-67, Vol. 181, Pt. 3, pp. 36.

10. Waterhouse, R. B., and Lamb M., "Fretting Corrosion of Orthopedic Implant Materials by Bone Cement," *Wear*, 60, 1980, pp. 357-368.

11. Ko, P. L., Tromp, J. H., Weckwerth M. K., "Heat exchanger Tube Fretting Wear: Correletion of Tube Motion and Wear," *Materials Evaluation Under fretting Conditions*, ASTM Special Technical Publication 780, 1982, pp. 86-105.

12. Kayaba, T., and Iwabuchi A., "The Fretting Wear of 0.45 % Carbon Steel and Austenitic Stainless Steel from 20 to 650 °C in Air," *Wear*, 74, 1981-1982, pp. 229-245.

13. Waterhouse, R. B., "Fretting," *Treatise on Materials Science and Technology*, Vol. 13, Academic Press, 1979, pp. 259-286.

14. Eden E. E., Rose W. N., Cunningham F. C., "The Endurance of Metals," *Proceedings of the Institute of Mechanical Engineers*, Part 4, London, 1911, pp. 839-880

15. Tomlinson, G. A., "The Rusting of Steel Surfaces in Contact," *Proceedings of the Royal Society of London*, Series A, Vol. 115, London, 1927, pp. 472-483.

16. Tomlinson, G. A., Thorpe, P. L., Gough, H. J., "Investigation of the Fretting Corrosion of Closely Fitted Surfaces," *Proceedings of the Institute of Mechanical Engineers*, Vol. 141, London, 1939, p. 223.

17. Feng, I-Ming, and Rightmire, B. G., "An Experimental Study of Fretting," *Proceedings of the Institute of Mechanical Engineers*, Vol. 170, London, 1965, p. 1055.

18. Uhlig, H. H., "Mechanism of Fretting Corrosion," *Journal of Applied Mechanics*, 21, December 1954, pp. 401-407.

19. Milestone, W. D., "Fretting and Fretting-Fatigue in Metal-to-Metal Contacts," ASME paper 71-DE-38, 1971.

20. Hurricks, P. L., "The Mechanism of Fretting - A Review," *Wear*, 15, 1970, pp. 387-409.

21. Robinson, R., "Fretting Corrosion on Rolling Bearings: Cause and Avoidance," *Design Engineering*, August 1983, pp. 23-27.

22. Sproles, E. S. Jr., and Duquette, D. J., "The Mechanism of Material Removal in Fretting," *Wear*, 49, 1978, pp. 339-352.

23. Waterhouse, R. B., and Taylor, D. E., "Fretting Debris and the Delamination Theory of Wear," *Wear*, 29, 1974, pp. 337-344.

24. Suh, N. P., "The Delamination Theory of Wear," *Wear*, 25, 1973, pp. 111-124.

25. Campbell, W. E. "Fretting," *Boundary Lubrication, An Appraisal of World Literature*, Chapter 7, ASME, 1969, pp. 119-131.

26. Ohmae, N., and Tsukizoe, T., "The Effect of Slip Amplitude on Fretting," *Wear*, 27, 1975, pp. 281-294.

27. Toth, L., "The Investigation of the Steady Stage of Steel Fretting," *Wear*, 2, 1972, pp. 277-286.

28. Feng, I-Ming, and Uhlig, H. H., "Fretting Corrosion of Mild Steel in Air and in Nitrogen," *Journal of Applied Mechanics*, Vol. 21, No. 4, December 1954, pp. 395-400.

29. Bill, R. C., "Fretting of Nickel-Chromium-Aluminum Alloys at Temperatures up to 816 °C," NASA Technical Note D-7570, 1974.

30. Hurricks, P. L., "The Fretting Wear of Mild Steel from Room Temperature to 200 °C," *Wear*, 19, 1972, p. 207.

31. Fink, M., "Wear Oxidation, A New Component of Wear," *Transactions, American Society of Steel Treating*, Vol. 18, 1930, p. 1026.

32. Dies, K., "Friction Oxditation as a Chemico-Mechanical Process," *The Engineering Digest*, Vol. 2, 1945, p. 14.

33. Mason, W. P., and White, S. D., "New Techniques for Measuring Forces and Wear in Telephone Switching Apparatus," *Bell System Technical Journal*, Vol. 31, 1952, p. 469.

34. Sproles, E. S. Jr., and Duquette, D. J., "Interface Temperature Measurements in the Fretting of a Medium Carbon Steel," *Wear*, 47, 1978, pp. 387-396.

35. Gaul, D. J., and Duquette, D. J., "The Effect of Fretting and Environment on Fatigue Crack Initiation and Early Propagation in a Quenched and Tempered 4130 Steel," *Metallurgical Transactions*, Vol. 11A, September 1980, pp. 1555-1561.

36. Feng, I-Ming, and Uhilig, H. H., "Fretting Corrosion of Mild Steel in Air and in Nitrogen," *Journal of Applied Mechanics*, Vol. 21, No. 4, December 1954, pp. 395-400.

37. Bill, R. C., "Fretting Wear of Iron, Nickel and Titanium Under Varied Environmental Conditions," *NASA Technical Memorandum 78972*, April 18, 1979, pp. 1-29.

38. Quinn, T. F. J., "Role of Oxidation in Mild Wear of Steel," *British Journal of Applied Physics*, Vol. 13, 1962, pp. 33-37.

39. Bill, R. C., "Fretting of AISI 9310 Steel and Selected Fretting-Resistant Surface Treatements," *ASLE Transactions*, Vol. 21, No. 3, 1978, pp. 236-242.

40. Ohmae, N., Nakai, T., Tsukizoe, T., "Prevention of Fretting by Ion Plated Film," *Wear*, 30, 1974, pp. 299-309.

41. Chivers, T. C., and Gordelier, S. C., "Fretting Fatigue Palliatives: Some Comparative Experiments," *Wear*, 96, 1984, pp. 153-175.

42. Furey, M. J., "The Formation of Polymeric Films Directly on Rubbing Surfaces to Reduce Wear," *Wear*, 26, 1973, pp. 369-392.

43. Bill, R. C., "Selected Fretting-Wear-Resistant Coatings for Titanium-6-percent-aluminum-4-percent-vanadium Alloy," *NASA Technical Note D-8214*, 1976.

44. Liu, H. W., Corten, H. T., and Sinclair, G. M., "Fretting Fatigue Strength of Titanium Alloy RC130B," *ASTM Proceedings*, Vol. 57, 1957.

45. Higham, P. A., Stott, F. H., and Bethune, B., "The Influence of Polymer Composition on the Wear of the Metal Surface During Fretting of Steel on Polymer," *Wear*, 47, 1978, pp. 71-80.

46. Rosen, S. L., *Fundamental Principles of Polymeric Materials*, John Wiley & Sons, New york, 1983, p. 44.

47. Schawrtz S. J., and Goodman S. H., *Plastic Materials and Processes*, Van Nostrand Reinhold Company, New York, 1982, pp. 184-193.

48. Billmeyer, F. W., *Textbook of Polymer Science*, Third Edition, John Wiley & Sons, New York, 1984, pp. 383-384.

49. Houston, J. J., "Polystyrene," *Modern Plastics Encyclopedia*, 1985-1986, pp. 76-78.

50. Billmeyer, F. W., op. cit., p. 144.

51. Steijn, R. P., "Friction and Wear of Plastics," *Metals Engineering Quarterly*, Vol. 7, No. 2, May 1967, pp. 9-21.

52. Shooter, K. V., and Thomas, P. H., "Frictional Properties of Some Plastics," *Research*, Vol. 2, Suppl. 2, 1949, p. 533.

53. Pooley, C. M., and Tabor, D., "Friction and Molecular Structure: the Behavior of Some Thermoplastics," *Proceedings of the Royal Society of London*, 1972, A329, pp. 251-274.

54. Briscoe, B. J., "The Friction of Polymers: A Short Review," *Friction and Traction*, Vol. 19, 1977, pp. 81-92.

55. Archard, J. F., "Contact and Rubbing of Flat Surfaces," *Journal of Applied Physics*, Vol. 24, 1956, p. 981.

56. Lewis, R. B., "Predicting the Wear of Sliding Plastic Surfaces," *Mechanical Engineering*, Vol. 86, 1964, p. 32.

57. Lewis R. B., "Wear of Plastics-Evaluation for Engineering Application," ASME Paper No. 63-WA-325, 1963.

58. Clinton, W. C., Ku, T. C., and Schumacher, R. A., "Extension of the Engineering Model for Wear to Plastics, Sintered Metals and Platings," *Wear*, 7, 1964, p.354.

59. Bayer, R. G., Clinton, W. C., Nelson, C. W., Schumacher, "Engineering Model for Wear," *Wear*, 5, 1962, p. 378.

60. Furey, M. J., "Metallic Contact and Friction Between Sliding Surfaces," *Transactions, American Society of Lubrication Engineers*, 4, 1961, pp. 1-11.

61. Sankar, J., "Data Acquisition Systems for Three-Dimensional Representation and Analysis of Surface Topography and Surface Temperatures in Tribological Processes," Masters Thesis, Mechanical Engineering, Virginia Polytechnic Institute and State University,

62. Struik, L. C. E., "Physical Aging: Influence on the Deformation Behavior of Amorphous Polymers," *Failure of Plastics*, edited by Brostow, W., and Corneliussen, R., D., Hanser Publishers, New York, 1986, pp. 209-234.

63. Hertzberg, R. W., *Deformation and Fracture Mechanics of Engineering Materials*, Second edition, John Wiley & Sons, New York, 1983, pp. 216-222.

64. Ihara, T., Shaw, M. C., and Bhushan, B., "A Finite Element Analysis of Contact Stress and Strain in an Elastic Film on a Rigid Substrate-Part II: With Friction," *ASME Transactions*, Vol. 108, October 1986, pp. 534-539.

65. Moreno, A., Moet, A., and Baer, E., "Craze Growth Kinetics and the Mechanical Behavior of Thin Polystyrene Films," *Deformation, Yield and Fracture of Polymers*, edited by Andrews, E. H., Fifth International Conference of the Plastic and Rubber Institute, London, 1982, pp. 16.1-16.6.

66. Gent, A., "Hypothetical Mechanism of Crazing in Glassy Plastics," *Journal of Materials Science*, Vol. 5, 1970, pp. 925-950.

67. Prest, W. M., and Luca, D. J., "The Alignment of Polymers During the Solvent-Coating Process," *Journal of Applied Physics*, Vol. 51, October 1980, pp. 5170-5174.

68. Kaush, H. H., and Jud, K., "Molecular Aspects of Crack Formation and Healing in Glass Polymers," *Deformation, Yield and Fracture of Polymers*, edited by Andrews, E. H., Fifth International Conference of the Plastic and Rubber Institute, London 1982, pp. 9.1-9.6.

69. Kaush, H. H., "Intersegmental Interactions and Chain Scission," *Failure of Plastics*, edited by Brostow, W., and Corneliussen, R. D., Hanser Publishers, New York, 1986, pp. 84-97.

70. Terselius, B., Ulf, W. G., and Jansson, J. F., "Mechano-Chemical Phenomena in Polymers," *Failure of Plastics*, edited by Brostow, W., and Corneliussen, R. D., Hanser Publishers, New York, 1986, pp. 273-286.

71. Heinicke, G., *Tribochemistry*, Carl Hanser Verlag, Munchen, 1984.

72. Zakrevskii, V. A., Tomashevskii, E. E., and Baptizmanskii, V. V., "EPR Studies of Rupture Points in Mechanically Stressed Polyamide Macromolecules," *Soviet Physics-Solid State*, Vol. 9, No. 5, November 1967, pp. 1118-1122.

73. Ohara, K., "Molecular Processes During Friction of Polymer Films Observed by Thermally Stimulated Depolarization Currents," *Wear*, 73, 1981, pp. 147-155.

74. Furey, M. J., Eiss, N. S., Mabie, H. H., and Swetizer, K. A., "Effects of Thin Polymeric Surface Films on Fretting Corrosion and Wear," *Proceedings, XIth International Conference in Organic Coatings Science and Technology*,Athens, Greece, 8-12 July 1985, pp. 29-45.

75. Furey, M. J., Eiss, N. S., Mabie, H. H., and Swetizer, K. A., "The Effect of Thin Polymeric Surface Films on Fretting Corrosion and Wear," *Trybologia*, No. 3, 1986, pp. 4-7 (in Polish).

Appendix A. List of Equipment.

1. Vibration Fatigue Testing Machine

   Manufacturer: All American Tool & Mfg. Co.

   Model No.: 10-VA-T

2. Cycle Counter

   Manufacturer: Hewlett-Packard

   Model No.: 5326B

   Serial No.: 1612AO3614

3. Bridge Amplifier, A

   Manufacturer: Vishay Instruments

   Model No.: Vishay/Ellis-1

   Serial No.: 032461

4. Bridge Amplifier, B

   Manufacturer: Vishay Instruments

   Model No.: Vishay/Ellis-1

   Serial No.: 032457

5. Strip Chart Recorder, A

Manufacturer: Gould Inc.

Model No.: 15-6327-57

Serial No.: 15840

6. Strip Chart Recorder, B

Manufacturer: Gould Inc.

Model No.: 15-6327-57

Serial No.: 15846

7. Digital Hygrometer-Thermometer

Manufacturer: Fisher Scientific

Model No.: 11-661-7A

8. Photomacroscope

Manufacturer: Wild Heerbrugg Ltd.

Model No.: 420

Serial No.: 189759

9. Automatic Exposure Meter and Shutter Piece

Manufacturer: Wild Heerbrugg Ltd.

Model No.: MPS 55/512 Photo Automat

Serial No.: 112598

10. External Light Source

Manufacturer: Volpi

Model No.: Intralux 600

11. Scanning Electron Microscope

Manufacturer: JOEL

Model No.: JSM-35C

Serial No.: EP156086-79

12. Sputter Coater

Manufacturer: SPI

Model No.: 12121

Serial No.: 001126

13. Profilometer Electronic Unit

Manufacturer: Rank Precision Industries, Ltd.

Model No.: 112

Serial No.: 1000-F-3113

14. Profilometer Rectilinear Recorder

Manufacturer: Rank Precision Industries, Ltd.

Model No.: 112

Serial No.: 1005-2775

15. Coating Thickness Gauge

Manufacturer: Elektro Physik

Model No.: F102

Serial No.: 82083

16. Ultrasonic Cleaner

Manufacturer: Fisher Scientific

Model No.: B-92

Serial No.: 0131

17. Vacuum Oven

Manufacturer: Fisher Scientific

Model No.: 281

Serial No.: 3365

Appendix B. Procedures.

B.1 Disk Surface Preparation.

The disks were sand blasted to assure proper adhesion between the polymer coating and the disk. The following procedure was followed.

1. Place the ground disks in the sand blasting machine located in the shop of the Mechanical Engineering department at VPI&SU (make sure the ground side is facing upward).
2. Close the door and place oneself at the operator position.
3. Check that the pressure is between 60 and 70 psi.. Hold the spraying gun at about 5-7 cm. from the disks.
4. Spray for about 30 seconds with a smooth uniform circular motion.
5. Take the disks to cleaning.

B.2 Specimen Cleaning Procedure.

1. Place the specimen in a methanol bath by means of the special holder shown in Figure 51 and place them in the ultrasonic cleaner.
2. Turn the ultrasonic cleaner on and run for five minutes.
3. Place the clean specimen in a clean container.
4. Place 200 cc. of methanol in a clean beaker. Bring to a boil.
5. Place the specimen in a steel mesh and put it in the beaker containing the boiling methanol. The assembly is shown in Figure 52
6. Leave the specimen in the evaporating bath for 15 minutes.
7. Repeat steps 5 and 6 using 250 cc. of hexane in place of the methanol.
8. Let the specimen cool to room temperature and store in a dessicator for later use.

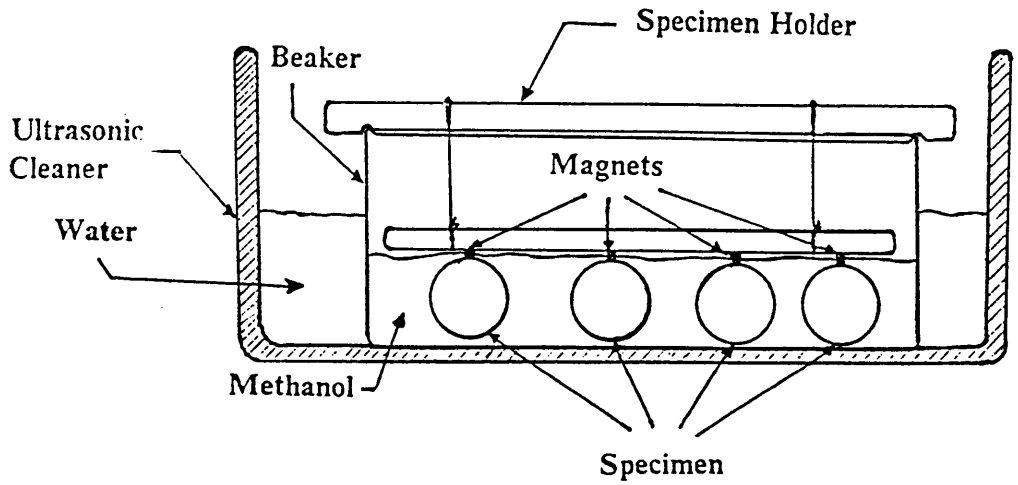

Figure 51. Ultrasonic Cleaning.

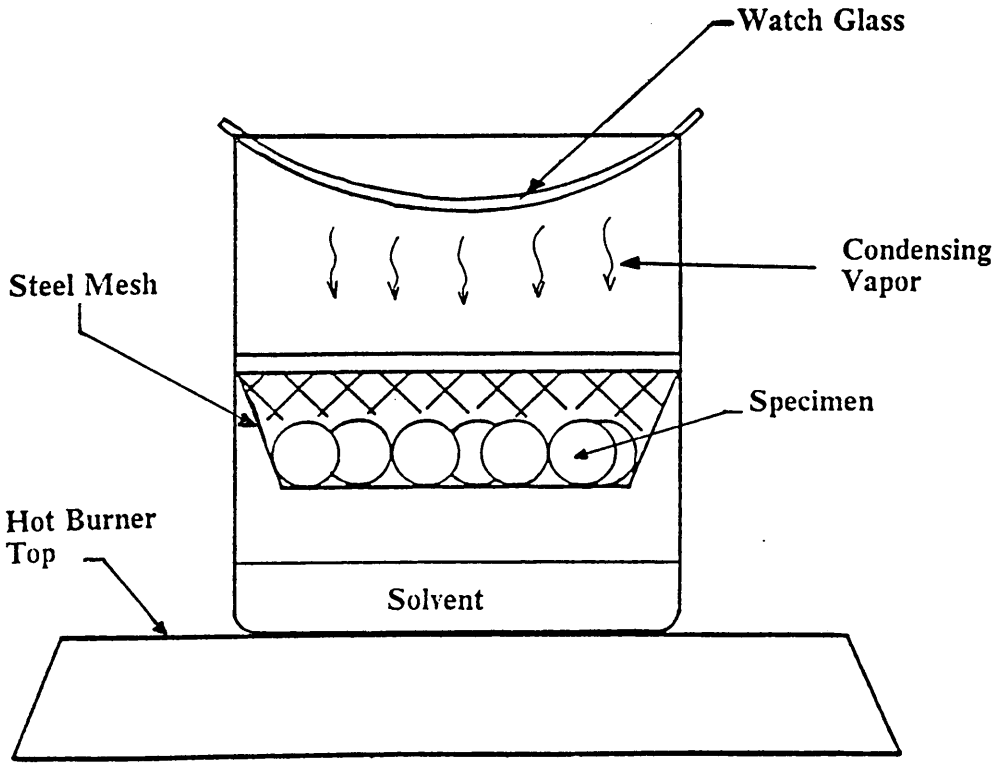

Figure 52. Vapor Cleaning.

B.3 Coating Procedure.

The procedure used in this study applies to coating disks. However the same steps can be used for coating balls.

The data given in Table 8 on page 127 apply only to disks coated with polystyrene dissolved in MEK and following exactly the procedure that follows. Any deviation will result in different thicknesses and different coating quality.

1. Place sand blasted disks on the top of the hood window as shown in Figure 53. Make sure the hood fan is off.
2. Fill a jar with the desired polymer solution (see Table 8 on page 127).

Table 8. Coatings-Thickness and Required Number of Dips and Concentrations

Average Thickness (μm)	Actual Thickness (μm)	Code Name	Number of Dips and Concentration dips,(conc.)
7.9	7.4 - 8.9	PS3	2,(100gr/l)
13	11 - 14	PS5	1,(200gr/l)
23	22 - 24	PS9	4,(100gr/l)
31	29 - 32	PS12	2,(100gr/l);1,(200gr/l)
38	37 - 39	PS15	2(150gr/l);1,(100gr/l)
46	44 - 47	PS18	1,(200gr/l);1,(150gr/l);1(100gr/l)
52	50 - 56	PS20	1,(200gr/l);1,(150gr/l);2,(100gr/l)

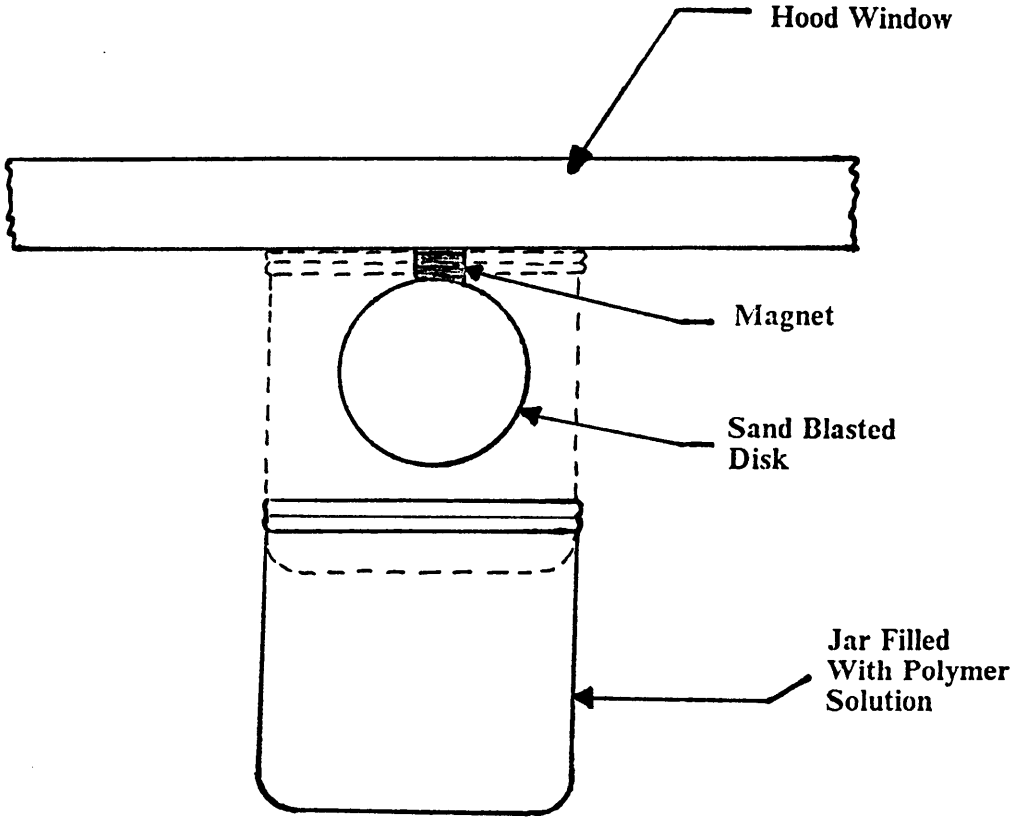

Figure 53. Film Deposition Technique.

3. Bring the jar with the solution up to the disk until fully covered (see Figure 53 on page 127).
4. Leave the jar in position for a count of three.
5. Take the jar away. Try to keep as smooth a motion as possible.
6. Let dry for 15 minutes.
7. Repeat as many times as necessary (see Table 8).
8. After the last coating has been applied let the disk dry for 15 minutes. Then place the disk on the oven tray (face up) and let dry for two hours.
9. Turn the oven on and set it to a temperature of 75 ^{0}C (2.6 on the oven dial). Leave the disk in the oven for 24 hours.
10. After the 24 hours have passed raise the temperature to 120 ^{0}C (4.4 on the oven dial). Pull a full vacuum. Leave the disk in the oven for 2 hours.
11. Turn the oven off and release the vacuum. Let the disk cool to room temperature.
12. Measure film thickness with the thickness gage. Store the disk in a desiccator for later use.

B.4 Force calibration.

1. Turn on equipment. Be sure all recording equipment is on before turning on the post amplifier.
2. Assemble calibration set-up as shown in Figure 54
3. Set equipment.

    Left (A) bridge amplifier:

        Span: 95%

Balancing Resistance: ≅112

Right (B) bridge amplifier:

Span: 95%

Balancing Resistance: ≅245

Chart Recorders:

Sensitivity: 20 mV/div. (knob at X1 position)

Speed: 1 mm/sec.

4. Set recorder pen at zero position by moving the position adjustment knob.
5. Check for null balance. If needed balance by moving the balancing resistance knob on the bridge amplifier (Be sure to check with the chart recorder. The pen must not change position when everything is connected.)
6. Apply one pound calibration weight and adjust sensitivity so that the recorder pen deflects half a scale division.
7. Unload and adjust again zero position. It may be necessary to check for null balance again.
8. Repeat steps 6 and 7 as many times as necessary.
9. Increase load and repeat steps 6 through 8 until the full scale is covered.

B.5 Contact Calibration.

1. Set chart recorder sensitivity at 2 mV/div.
2. Isolate yoke and plate holder.
3. Set recorder pen at zero position.
4. Cause contact.

5. Adjust sensitivity so that pen recorder deflects to full scale position.

6. Repeat steps 3 through 5 as needed.

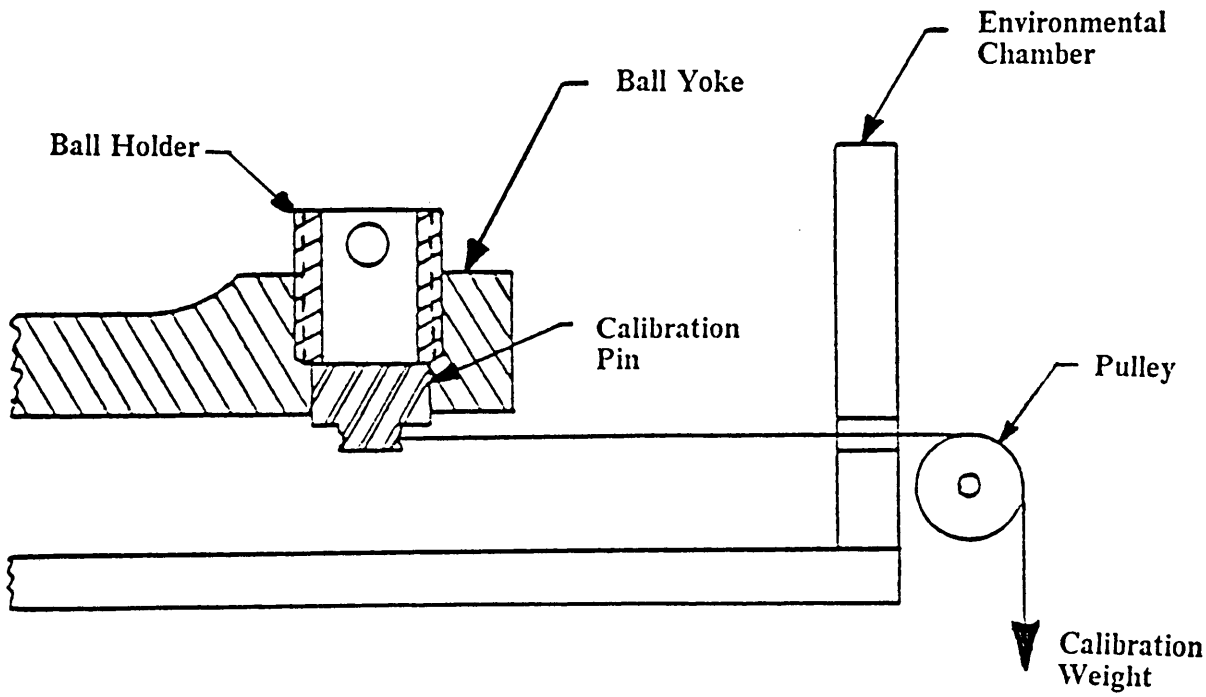

Figure 54. Force Calibration.

B.6 Wear Scar Three Dimensional Mapping.

1. Secure the disk on the x-y table under the profilometer stylus by using double-stick tape . Position the disk so that the profile will be taken in the direction of sliding.
2. Tape the 2.5 μm steel sheet on the edge of the disk away from the wear scar. Adjust the disk position so that the profilometer stylus is resting on the disk surface, away from the wear scar, while its skid is on the steel sheet. Use the x-y table for this purpose. Make sure the first trace is outside the wear scar. Also try to position the steel sheet perpendicular to the stylus.
3. Turn on the Talysurf electronic unit.
4. Set magnification dial in position 1 (500); select AV as the travelling speed; select L as the travelling distance.
5. Lower the gear box so that the recorder needle deflects on the positive side (left) up to the paper limit. Do not move the gear box during the measurement of one wear scar.
6. Connect the Talysurf to the IBM PC by means of the proper cable. Connect for external triggering.
7. Load the SCOPE program on the IBM PC.
8. The program will ask for several options. Match the Taly-surf parameters with the one described in point 4. Next the program will allow for setting the sampling rate by asking the number of sampling points per trace and the interval between them (in milliseconds). The only limit is that the total number of points, that is the number of points per trace times the number of traces. must not exceed 5000. Also make sure the time interval is long enough to cover the full scar length. This can be estimated by using the stylus speed and the wear scar length as measured from

photographs or other methods. For this particular study 300 points with an interval of 20 ms were chosen. Sampling rate must not be changed from trace to trace if within the same wear scar. If two different wear scar are to be compared the same sampling rate for both of them should be used. Last, select the external triggering option.

9. Start the Talysurf. View the trace on the screen; if satisfactory store on a diskette. Name the file with a suffix followed by the trace number.
10. Use the x-y table to move the disk to the next trace position. Repeat the measurement.
11. Continue until the wear scar has been completely covered. Make sure that the distance between traces is always the same.
12. To create the three dimensional map and estimate the debris and the wear volumes log on the TRIBOL account on VM3 and run AUTOMAP2 (press F6 key). This is an interactive program in EXEC2 which will generate the data file with the map and calculate the debris and wear volumes.
13. Use MOVIE.BYU to view the three dimensional map.

Appendix C. Measurements.

For both film thicknes and film roughness four measurements were done for each disk.

C.1 Film Thickness.

Table 9. Film Thickness Measurements for Disk Set 1.

Code Name	Meas. # 1 (μm)	Meas. # 2 (μm)	Meas. # 3 (μm)	Meas. # 4 (μm)
PS3	7.4	7.6	7.5	8.9
PS5	11	14	11	11
PS9	23	22	23	22
PS12	29	30	29	30
PS15	37	37	38	38
PS18	46	44	46	47
PS20	50	51	53	55

Table 10. Film Thickness Measurements for Disk Set 2.

Code Name	Meas. # 1 (μm)	Meas. # 2 (μm)	Meas. # 3 (μm)	Meas. # 4 (μm)
PS3	7.5	7.6	7.6	7.6
PS5	13	13	11	14
PS9	24	23	24	22
PS12	32	31	31	31
PS15	37	37	39	38
PS18	47	46	46	44
PS20	50	53	50	53

Table 11. Film Thickness Measurements for Disk Set 3.

Code Name	Meas. # 1 (μm)	Meas. # 2 (μm)	Meas. # 3 (μm)	Meas. # 4 (μm)
PS3	7.5	8.9	8.9	7.5
PS5	14	14	11	13
PS9	24	22	23	23
PS12	32	31	31	31
PS15	38	38	39	37
PS18	46	46	44	47
PS20	51	56	50	50

Table 12. Summary of Film Thickness Measurements.

Code Name	Average Thickness (μm)	Standard Deviation (μm)	Range (min-max) (μm)
PS3	7.9	0.61	7.4 - 8.9
PS5	13	1.14	11 - 14
PS9	23	1.02	22 - 24
PS12	31	0.76	29 - 32
PS15	38	0.97	37 - 39
PS18	46	0.94	44 - 47
PS20	52	2.24	50 - 56

C.2 Film Roughness, R_a.

Table 13. Film Roughness Measurements for Disk Set 1.

Code Name	Meas. # 1 (μm)	Meas. # 2 (μm)	Meas. # 3 (μm)	Meas. # 4 (μm)
PS3	1.1	1.2	1.0	1.0
PS5	1.1	1.2	1.4	1.0
PS9	0.9	0.8	0.7	1.0
PS12	1.1	0.9	0.8	0.6
PS15	0.9	1.0	0.5	0.7
PS18	0.5	0.5	0.4	0.4
PS20	0.5	0.45	0.6	0.5

Table 14. Film Roughness Measurements for Disk Set 2.

Code Name	Meas. # 1 (μm)	Meas. # 2 (μm)	Meas. # 3 (μm)	Meas. # 4 (μm)
PS3	1.3	1.2	1.1	1.0
PS5	1.1	1.2	1.0	0.9
PS9	0.9	1.0	1.0	0.9
PS12	0.6	0.9	0.9	0.6
PS15	0.9	0.6	0.6	0.5
PS18	0.5	0.7	0.5	0.5
PS20	0.4	0.5	0.6	0.4

Table 15. Film Roughness Measurements for Disk Set 3.

Code Name	Meas. # 1 (μm)	Meas. # 2 (μm)	Meas. # 3 (μm)	Meas. # 4 (μm)
PS3	1.3	1.4	1.1	1.1
PS5	1.1	1.2	1.1	1.3
PS9	1.2	0.9	1.0	0.6
PS12	0.9	0.7	1.1	0.6
PS15	0.7	0.5	0.7	0.8
PS18	0.4	0.6	0.3	0.7
PS20	0.5	0.4	0.5	0.5

Table 16. Summary of Film Roughness Measurements.

Code Name	Average Roughness (μm)	Standard Deviation (μm)	Range (min-max) (μm)
PS3	1.2	0.13	1.0 - 1.4
PS5	1.1	0.14	0.9 - 1.4
PS9	0.9	0.12	0.6 - 1.2
PS12	0.8	0.19	0.6 - 1.1
PS15	0.7	0.17	0.5 - 1.0
PS18	0.5	0.12	0.3 - 0.7
PS20	0.5	0.07	0.4 - 0.6

Appendix D. Experimental Data.

D.1 Life-Thickness Experiments.

D.1.1 Film Life Data.

Table 17. Film Life Data for Disk Set 1.

Code Name	Test # 1 (sec)	Test # 2 (sec)	Test # 3 (sec)	Test # 4 (sec)
PS3	0	90	20	15
PS5	75	190	135	80
PS9	135	230	265	130
PS12	325	395	294	460
PS15	1000	900	700	310
PS18	3450	1394	1760	1200
PS20	6473	10804	8253	4788

Table 18. Film Life Data for Disk Set 2.

Code Name	Test # 1 (sec)	Test # 2 (sec)	Test # 3 (sec)	Test # 4 (sec)
PS3	33	100	90	58
PS5	105	12	95	140
PS9	197	213	271	230
PS12	350	540	500	310
PS15	310	530	720	420
PS18	1985	2760	3600	1400
PS20	9245	9560	10920	9175

Table 19. Film Life Data for Disk Set 3.

Code Name	Test # 1 (sec)	Test # 2 (sec)	Test # 3 (sec)	Test # 4 (sec)
PS3	3	11	3	13
PS5	16	17	12	32
PS9	283	230	222	163
PS12	239	528	356	290
PS15	418	390	707	457
PS18	771	1416	1107	700
PS20	4800	8997	6035	8817

Table 20. Summary of Film Life Data.

Code Name	Average Life (sec)	Standard Deviation (sec)	Range (min-max) (sec)
PS3	36	37.8	0 - 100
PS5	76	59.5	12 - 190
PS9	214	50.1	130 - 283
PS12	382	101.5	239 - 540
PS15	572	229.5	310 - 1000
PS18	1795	977.1	700 - 3600
PS20	8156	2130.7	4788 - 10920

D.1.2 Friction Data.

Table 21. Initial Coefficient of Friction for Disk Set 1.

Code Name	Test # 1	Test # 2	Test # 3	Test # 4
PS3	0.60	0.60	0.58	0.62
PS5	0.61	0.62	0.60	0.58
PS9	0.62	0.64	0.66	0.64
PS12	0.69	0.72	0.70	0.69
PS15	0.73	0.74	0.75	0.74
PS18	0.79	0.83	0.77	0.81
PS20	0.80	0.83	0.82	0.81

Table 22. Initial Coefficient of Friction for Disk Set 2.

Code Name	Test # 1	Test # 2	Test # 3	Test # 4
PS3	0.60	0.63	0.59	0.58
PS5	0.60	0.59	0.61	0.60
PS9	0.64	0.65	0.64	0.64
PS12	0.70	0.70	0.70	0.70
PS15	0.74	0.75	0.76	0.72
PS18	0.82	0.80	0.80	0.78
PS20	0.82	0.83	0.85	0.79

Table 23. Initial Coefficient of Friction for Disk Set 3.

Code Name	Test # 1	Test # 2	Test # 3	Test # 4
PS3	0.59	0.60	0.60	0.62
PS5	0.60	0.60	0.59	0.60
PS9	0.64	0.65	0.63	0.63
PS12	0.69	0.68	0.70	0.70
PS15	0.75	0.74	0.74	0.76
PS18	0.81	0.80	0.80	0.80
PS20	0.82	0.83	0.79	0.81

Table 24. Summary of Initial Coefficient of Friction Data.

Code Name	Average Friction μ_i	Standard Deviation	Range (min-max)
PS3	0.60	0.015	0.58 - 0.63
PS5	0.60	0.008	0.58 - 0.62
PS9	0.64	0.010	0.62 - 0.66
PS12	0.70	0.010	0.69 - 0.72
PS15	0.74	0.011	0.72 - 0.76
PS18	0.80	0.014	0.78 - 0.83
PS20	0.82	0.018	0.79 - 0.85

Table 25. Final Coefficient of Friction for Disk Set 1.

Code Name	Test # 1	Test # 2	Test # 3	Test # 4
PS3	0.80	0.81	0.78	0.80
PS5	0.82	0.83	0.82	0.82
PS9	0.91	0.89	0.92	0.89
PS12	0.93	0.92	0.93	0.90
PS15	0.95	0.95	0.95	0.96
PS18	0.97	0.98	0.99	0.98
PS20	0.99	1.00	1.05	0.99

Table 26. Final Coefficient of Friction for Disk Set 2.

Code Name	Test # 1	Test # 2	Test # 3	Test # 4
PS3	0.79	0.80	0.80	0.80
PS5	0.81	0.82	0.82	0.82
PS9	0.89	0.89	0.90	0.90
PS12	0.91	0.92	0.92	0.92
PS15	0.95	0.94	0.96	0.95
PS18	0.98	0.98	0.98	0.97
PS20	1.05	0.99	1.00	1.00

Table 27. Final Coefficient of Friction for Disk Set 3.

Code Name	Test # 1	Test # 2	Test # 3	Test # 4
PS3	0.80	0.80	0.79	0.80
PS5	0.81	0.82	0.80	0.83
PS9	0.90	0.90	0.90	0.90
PS12	0.92	0.91	0.92	0.93
PS15	0.94	0.94	0.96	0.95
PS18	0.98	0.98	0.97	0.99
PS20	1.00	1.05	0.95	0.97

Table 28. Summary of Final Coefficient of Friction Data.

Code Name	Average Friction μ_f	Standard Deviation	Range (min-max)
PS3	0.80	0.008	0.78 - 0.81
PS5	0.82	0.008	0.80 - 0.83
PS9	0.90	0.009	0.89 - 0.92
PS12	0.92	0.009	0.90 - 0.93
PS15	0.95	0.007	0.94 - 0.96
PS18	0.98	0.007	0.97 - 0.99
PS20	1.00	0.010	0.99 - 1.05

D.1.3 Wear Scar Dimensions.

Table 29. Wear Scar Dimensions.

Code Name	a (μm)	b (μm)	R = a/b	D = b-a (μm)
PS3	733	1378	0.53	644
PS5	855	1411	0.61	556
PS9	1111	1867	0.59	755
PS12	1444	1889	0.76	444
PS15	1467	1889	0.77	422
PS18	1489	1933	0.77	444
PS20	1822	2177	0.86	289

D.2 Wear-Time Experiments

Table 30. Experimental Results and Mapping Datas for the 38 μm Film.

Time (sec)	Friction μ_i	Friction μ_f	Total Traces	Surface Traces
30	0.70	0.93	6	1 & 5
60	0.70	0.95	9	1,2 & 8,9
90	0.70	0.95	8	1,2 & 7,8
120	0.78	0.95	9	1,3 & 8,9
150	0.78	0.95	7	1,2 & 6,7
180	0.75	0.96	6	1 & 5,6
210	0.70	0.95	8	1,2 & 7,8
240	0.75	0.96	8	1,2 & 7,8
300	0.75	0.93	8	1,2 & 7,8
330	0.70	0.96	10	1,2 & 10
360	0.70	0.94	11	1,2 & 10,11

Table 31. Wear Scar Dimensions for the 38 μm Film.

Time (sec)	a (μm)	b (μm)	R = a/b	D = b-a (μm)
30	778	1167	0.67	389
60	911	1244	0.73	333
90	1056	1333	0.80	277
120	1156	1356	0.85	200
150	1156	1600	0.72	444
180	1156	1227	0.95	72
210	1156	1800	0.64	64
240	1000	1222	0.82	222
300	1156	1844	0.63	689
330	1267	1667	0.76	399
360	1333	2000	0.67	667

Table 32. Experimental Results and Mapping Datas for the 52 μm Film.

Time (sec)	Friction μ_i	Friction μ_f	Total Traces	Surface Traces
30	0.80	1.00	6	1 & 5,6
60	0.81	0.98	9	1,3 & 8,9
90	0.82	1.00	8	1,3 & 8
120	0.80	1.00	6	1 & 6
150	0.81	1.00	7	1,2 & 6,7
300	0.82	1.00	7	1,2 & 6,7
600	0.81	1.00	7	1,2 & 6,7
900	0.82	1.00	7	1,2 & 6,7
1200	0.82	0.95	8	1,2 & 7,8
1800	0.83	1.00	12	1,3 & 11,12
2400	0.82	1.00	11	1,3 & 10,11
3000	0.81	0.98	11	1,2 & 10,11
3600	0.81	0.98	11	1,2 & 10,11
4200	0.83	0.98	9	1,3 & 8,9
4800	0.83	0.98	10	1,2 & 9,10
5400	0.82	1.00	9	1 & 8,9

Table 33. Wear Scar Dimensions for the 52 μm Film.

Time (sec)	a (μm)	b (μm)	R = a/b	D = b-a (μm)
30	844	1011	0.93	167
60	1022	1277	0.80	255
90	1045	1211	0.87	166
120	1022	1289	0.79	267
150	1022	1267	0.81	244
300	1022	1289	0.79	267
600	1067	1333	0.80	267
900	1289	1356	0.95	67
1200	1444	1556	0.93	111
1800	1333	1800	0.74	467
2400	1356	1889	0.72	533
3000	1444	2067	0.70	622
3600	1622	1956	0.83	333
4200	1556	2000	0.78	444
4800	1711	2000	0.86	289
5400	1689	2067	0.82	378

Appendix E. Computer Programs.

E.1 AUTOMAP2 Program.

```
&TRACE OFF
REL G
EXEC TDISK 20 G
CLEAR
&BEGTYPE 17

**********************************************************************
**********************************************************************
**                                                                  **
**          AUTOMATIC MAPPING OF ROUGH SURFACES                     **
**                                                                  **
**********************************************************************
********************     JAYARAM SANKAR     ************************
********************     UPDATED NOV 24,1986  **********************
**********************************************************************

        VIRGINIA POLYTECHNIC INSTITUTE AND STATE UNIVERSITY
            MECHANICAL ENGINEERING DEPARTMENT
              BLACKSBURG,  VIRGINIA 24061

WAIT.....
```

```
CP SLEEP 4 SEC
CLEAR
&LOOP 1 5
&TYPE
&BEGTYPE 15
*************************************************************************
*                                                                       *
*    THIS SYSTEM GENERATES 3-D MAPS OF SURFACES FROM PARALLEL           *
*    TALYSURF TRACES. THE FILES ARE LOADED FROM THE FLOPPY DISC         *
*    OF THE IBMPC AND THE DATA IS THEN TREATED TO GENERATE 3 - D        *
*    MAPS OF THE SURFACE WHICH CAN BE DISPLAYED USING MOVIE.BYU.        *
*                                                                       *
*    THIS PROGRAM RELEASES THE 'G' DISK. SO IF YOU HAVE ANYTHING        *
*    IMPORTANT IN YOUR G DISK PLEASE USE THE 'ACCESS' COMMAND TO        *
*    ATTACH THE G DISK AGAIN ( AFTER THIS PROGRAM IS EXECUTED).         *
*                                                                       *
*************************************************************************


    PRESS <RETURN> TO CONTINUE

CP SLEEP
CLEAR
-100
&BEGTYPE 17


        FOR GENERATING THE FILE CONTAINING THE INFORMATION
        REGARDING THE 3-D GEOMETRY OF THE SURFACE, YOU
        SHOULD HAVE FILES CONTAINING THE DATA FROM THE
        TALYSURF, AS GENERATED BY THE PROGRAM "SCOPE"
        ON THE DATA ACQUISITION SYSTEM. EACH TALYSURF
        TRACE SHOULD BE IN A SEPARATE FILE .



        YOU CAN HAVE UP TO 27 FILES FOR EACH MAP.

        DO YOU HAVE THE NECESSARY FILES ? (Y/N)

&READ VARS &YES3
&IF .&YES3 NE .N &SKIP 10
CLEAR
&BEGTYPE 7


          SORRY!! YOU CANNOT GENERATE A SURFACE MAP USING THIS
          PROGRAM IF YOU DO NOT HAVE THE DATA IN THE PROPER
```

```
                FORMAT.

&GOTO -450
&IF .&YES3 NE .Y &GOTO -100
CLEAR
&BEGTYPE 7

            GIVE THE NAME OF THE FILE IN WHICH YOU WANT
            TO STORE THE 3-D GEOMETRY INFORMATION
                ( ONLY FILENAME)

&READ VARS &FIL3
FILEDEF 15 DISK F15 DATA G
FILEDEF 18 DISK F18 DATA G
FILEDEF 9 DISK UPP EXEC G
FILEDEF 7 DISK OUT OUT G
FILEDEF 8 DISK FILE &FIL3 G
CLEAR
&BEGTYPE 11


            GIVE THE NAME OF THE FILE IN WHICH YOU WANT
            TO STORE THE INFORMATION FOR THE CONTOUR LINES
                ( ONLY FILENAME)


&READ VARS &FIL4
LOADMOD INPUT
START
CLEAR
&BEGTYPE 5

        DO YOU WANT TO CALCULATE THE WEAR AND DEBRIS VOLUMES?


&READ VARS &WEARQ
&IF .&WEARQ EQ .N &SKIP 1
EXEC WEARTR

FILEDEF 7 DISK OUT OUT G
```

```
-500
CLEAR
&BEGTYPE 15

*************************************************************************
*                                                                       *
*       THE GEOMETRY FILE WILL BE CREATED ON A TEMPORARY DISK.          *
*                                                                       *
*        DO YOU WANT IT COPIED ON TO YOUR "A" DISK ? (A)                *
*                                                                       *
*                        OR                                             *
*                                                                       *
*        DO YOU WANT IT SENT TO SOME OTHER USERID  ? (S)                *
*                                                                       *
*            TYPE "A" OR "S" OR TYPE "Q" TO QUIT                        *
*                                                                       *
*************************************************************************

&READ VARS &YES4
&IF .&YES4 EQ .A &SKIP 3
&IF .&YES4 EQ .S &SKIP 2
&IF .&YES4 EQ .Q &GOTO -450
&GOTO -500
&IF .&YES4 NE .S &SKIP 10
CLEAR
&BEGTYPE 7

*************************************************************************
*                                                                       *
*          GIVE THE USERID AND NODE OF THE RECIPIENT                    *
*                                                                       *
*************************************************************************

&READ VARS &YES5 &YES6
-600
CLEAR
&BEGTYPE 7

*************************************************************************
*                                                                       *
*        DO YOU WANT TO BE LOGGED OFF WHEN IT IS ALL OVER ? (Y/N)       *
*                                                                       *
*************************************************************************

&READ VARS &YES7
&IF .&YES7 EQ .Y &SKIP 2
&IF .&YES7 EQ .N &SKIP 1
&GOTO -600
CLEAR
&BEGTYPE 20
```

```
**************************************************************************
**************************************************************************
**                                                                      **
**              I WILL TAKE CARE OF THE REST                            **
**                                                                      **
**                  HAVE A GOOD DAY !                                   **
**                                                                      **
**************************************************************************
*******************      JAYARAM  SANKAR     ***************************
**************************************************************************

        VIRGINIA POLYTECHNIC INSTITUTE AND STATE UNIVERSITY
             MECHANICAL ENGINEERING DEPARTMENT
               BLACKSBURG,  VIRGINIA 24061


CP SLEEP 4 SEC
CLEAR
EXEC UPP
CLEAR
&BEGTYPE 18




**************************************************************************
**************************************************************************
**                                                                      **
**              PLEASE DO NOT USE THIS TERMINAL                         **
**                                                                      **
**************************************************************************
*******************      JAYARAM  SANKAR     ***************************
**************************************************************************

        VIRGINIA POLYTECHNIC INSTITUTE AND STATE UNIVERSITY
             MECHANICAL ENGINEERING DEPARTMENT
               BLACKSBURG,  VIRGINIA 24061
                  FEBRUARY 04, 1986

FILEDEF 9 DISK FILE &FIL4 G
LOADMOD AUTAPP
START
LOADMOD MPAUT
START
&IF .&WEARQ EQ .N &SKIP 1
EXEC WEAR &FIL3
&IF .&YES4 NE .A &SKIP 3
```

```
COPY FILE &FIL3 G = = A
COPY FILE &FIL4 G = = A
COPY WEAR &FIL3 G = = A
&IF .&YES4 NE .S &SKIP 3
EXEC SENDFILE FILE &FIL3 G TO &YES5 AT &YES6
EXEC SENDFILE FILE &FIL4 G TO &YES5 AT &YES6
EXEC SENDFILE WEAR &FIL3 G TO &YES5 AT &YES6
&IF .&YES7 NE .Y &SKIP 1
EXEC LOGOFF
-450
&EXIT
```

E.2 WEARTR Program.

```
C*************************************************************************
C
C                WEARTR PROGRAM
C
C  This program reads and creates a file with the traces needed for
C  fitting the plane and the magnification value.  The created file
C  will be used as input for the WEAR program.
C
C*************************************************************************
C
C  The traces before the wear scar are read in.
      WRITE(7,*)'WHICH TRACES DO YOU WANT TO USE FOR FITTING '
      WRITE(7,*)'THE PLANE? THEY MUST BE BOTH BEFORE AND AFTER'
      WRITE(7,*)'THE TRACES DESCRIBING THE WEAR SCAR.'
      WRITE(7,*)'INPUT TRACE RANGE BEFORE WEAR SCAR. IF ONLY'
      WRITE(7,*)'ONE TRACE IS USED TYPE TRACE NUMBER AND THEN'
      WRITE(7,*)'A ZERO (0).'
      READ(7,*)NII,NIF
C  The traces after the wear scar are read in.
      WRITE(7,*)'INPUT TRACE RANGE AFTER WEAR SCAR. IF ONLY'
      WRITE(7,*)'ONE TRACE IS USED TYPE TRACE NUMBER AND THEN'
      WRITE(7,*)'A ZERO (0).'
      READ(7,*)NFI,NFF
      WRITE(45,*)NII,NIF,NFI,NFF
C  The magnification is read in.
      WRITE(7,*)'GIVE THE MAGNIFICATION VALUE'
      READ(7,*)AMAG
      WRITE(45,*)AMAG
      STOP
      END
```

E.3 WEAR Program.

```
C*****************************************************************
C
C                    WEAR PROGRAM
C
C  This program estimates wear and debris volumes of a wear scar
C  generated on a flat surface. The program uses the same data
C  file created for generating the three dimensional maps. The
C  map needs to have been generated with at least one trace outside
C  the wear scar on both sides. This program will use those traces
C  to fit a plane which will represent the untouched surface. The
C  plane is modeled according to the following:
C
C              AX + BY + CXY + D = Z,
C
C  where X, Y, and Z are as defined in the mapping program. The datas
C  from the outside traces are used to create a [F] matrix with X, Y,
C  XY, AND 1 as its entries. The following system is hence created:
C
C              [F] [FT] {C} = [FT] {Y}
C
C  where [FT] is the transpose of [F], and {C} contains the unknowns
C  a, b, c, and d. The system is then solved for {C} and the equation
C  for the plane is found.
C  Next the program compares all the datas from the map to the
C  fitted plane. The data points are separeted into above or below
C  the plane. The so separated data represent the wear and the
C  debris. The wear and debris volumes are calculated by first
C  estimating the respective area for each trace. and then summing
C  them up and multiply them by the total number of traces used
C  and the distance between the traces.
C
C*****************************************************************
C
C
C
      DIMENSION X(5000),Y(5000),Z(5000),ZP(400),ZN(500)
      DIMENSION F(5000,4),FT(4,5000),A(4,4),B(4,1),MPL(2,5000)
      DIMENSION C(4,1),XP(500),XN(500),WK(9),ZPL(500,1)
C   Read values in.
      READ (5,120) NP,NJ,NPT,NCON,NTEST
      READ(5,120) ((MPL(I,J),I = 1,2),J = 1,NP)
      NT = NP+1
      NP = (MPL(2,1)-MPL(1,1)+2)
      NTOT=NT*NP
      READ (5,130) (X(I),Y(I),Z(I),I = 1,NTOT)
 130   FORMAT (6E12.5)
 120   FORMAT (16I5)
C  The traces needed for fitting the plane are read in.
```

```
      READ(45,*)NII,NIF,NFI,NFF
      READ(45,*) AMAG
C _The Z values are scaled down.
      DO 1 I = 1,NTOT
      Z(I) = Z(I)/AMAG
1     CONTINUE
C  The distance between traces is calculated.
      D = Y(NP+1) - Y(1)
      YT=(NT-1)*D
C  The loops are set up.
      NST1=NP*NII+1
      IF(NII.EQ.1)NST1=1
      NF1=NP*NIF
      IF(NIF.EQ.0)NF1=NII*NP
      NST2=(NFI-1)*NP+1
      NF2=NP*NFF
      IF(NFF.EQ.0)NF2=NFI*NP
C  The F matrix is generated.
      N1=NIF-NII
      N2=NFF-NFI
      IF(NIF.EQ.O)N1=1
      IF(NII.EQ.0)N2=1
      NPL=(N1+N2)*NP
      DO 11 I=1,NPL
      DO 11 J=1,4
      F(I,J)=0.0
      ZPL(I,1)=0.0
11    CONTINUE
      IC=1
      DO 20 II=NST1,NF1
      F(IC,1)=X(II)
      F(IC,2)=Y(II)
      F(IC,3)=X(II)*Y(II)
      F(IC,4)=1.
      ZPL(IC,1)=Z(II)
      IC=IC+1
20    CONTINUE
      DO 19 II=NST2,NF2
      F(IC,1)=X(II)
      F(IC,2)=Y(II)
      F(IC,3)=X(II)*Y(II)
      F(IC,4)=1.
      ZPL(IC,1)=Z(II)
      IC=IC+1
19    CONTINUE
      IC=IC-1
C  The transpose of F is created.
      DO 33 I=1,4
      DO 33 J=1,IC
33    FT(I,J)=0.0
      DO 2 J=1,4
```

```
      DO 2 I=1,IC
 2     FT(J,I)=F(I,J)
C  The B matrix is created.
      DO 3 I=1,4
      B(I,1)=0.0
      C(I,1)=0.0
 3     CONTINUE
      CALL MULT(FT,ZPL,4,400,4,IC,1,B,4)
C  The A matrix is created.
      DO 12 I=1,4
      DO 12 J=1,4
 12    A(I,J)=0.0
      CALL MULT(FT,F,4,5000,4,IC,4,A,4)
C   The values of a,b,c, and d are found.
      CALL GAUSS(A,B,4,1,4,C)
C  The values above or below the fitted plane are separated.
      AWEAR=0.0
      ADEBRI=0.0
      ZMIN=0.0
      ZMAX=0.0
      ZF=0.0
      NI=1
      DO 6 J=1,NT
      NPS=0
      NNG=0
      DO 77 I=1,IC
      ZN(I)=0.0
      ZP(I)=0.0
      XN(I)=0.0
 77    CONTINUE
      DO 7 I=NI,NP*J
      ZF=C(1,1)*X(I)+C(2,1)*Y(I)+C(3,1)*X(I)*Y(I)+C(4,1)
      ZC=Z(I)-ZF
C  Values below the plane.
      IF(ZC.LT.0)THEN
      NNG=NNG+1
      ZN(NNG)=ABS(ZC)
C  The lowest point is found.
      IF(ZN(NNG).GT.ZMIN)ZMIN=ZN(NNG)
      XN(NNG)=X(I)
C  Values above the plane.
      ELSEIF(ZC.GT.0)THEN
      NPS=NPS+1
      ZP(NPS)=ZC
C  The highest point is found.
      IF(ZP(NPS).GT.ZMAX)ZMAX=ZP(NPS)
      XP(NPS)=X(I)
      ENDIF
 7    CONTINUE
      NI=I+1
C  The areas are estimated.
```

```
      IF(NNG.NE.0)THEN
      CALL AREA(XN(1),XN(NNG),NNG,ZN,ARNGT)
      AWEAR=AWEAR+ARNGT
      ENDIF
      IF(NPS.NE.0)THEN
      CALL AREA(XP(1),XP(NPS),NPS,ZP,ARPST)
      ADEBRI=ADEBRI+ARPST
      ENDIF
 6    CONTINUE
C  The volumes are calculated.
      VWEAR=YT*AWEAR
      VDEBRI=YT*ADEBRI
      VDIFF=VWEAR-VDEBRI
C  The results are written out.
      ZMIN=ZMIN*1000.0
      ZMAX=ZMAX*1000.0
      WRITE(7,10)VWEAR,VDEBRI,VDIFF
 10    FORMAT(////,7X,'THE WEAR VOLUME IS : ',2X,F16.5,' MM**3',//,7X,
     1'THE DEBRIS VOLUME IS ; ',F16.5,' MM**
     2'THE DIFFERENCE IS : ',3X,F16.5,' MM**3')
      WRITE(7,100)ZMIN,ZMAX
 100   FORMAT(///,4X,'MAXIMUM DEPTH OF PENETRATION = ',F16.5,' MICRONS'
     1,//,4X,'HIGHEST POINT ABOVE SURFACE  = ',F16.5,' MICRONS')
      WRITE(6,10)VWEAR,VDEBRI,VDIFF
      WRITE(6,100)ZMIN,ZMAX
      STOP
      END

**********************************************************************
C
C  THIS SUBROUTINE ESTIMATE THE AREA UNDER A CURVE BY USING
C  SIMPSON'S APPROXIMATION.
C
C
C  The Variables are:
C
C              Y  =  Points under which area is to be estimated
C              A  =  Initial point from which area is to be estimated
C              B  =  Final point to which area is to be estimated
C              N  =  Total number of points
C              ARA  =  Resulting area
C
C
C
      SUBROUTINE AREA(A,B,N,Y,ARA)
      DIMENSION Y(400)
      AP=0.0
      AP=Y(1)+Y(N)+4.*Y(N-1)
      DO 1 I=1,N-4,2
 1    AP=AP+Y(I+1)*4.+Y(I+2)*2.
      ARA=((B-A)/(3.*N))*AP
```

```
      RETURN
      END
C
C
C*********************************************************************
C
C
C THIS SUBROUTINE CALCULATES THE PRODUCT OF TWO MATRICES.
C
C  The Variables are:
C
C              X,Y = Matrices to be multiplied
C              MX,MY = Respective row dimensions in main program
C              M = Rows of X
C              K = Rows of Y
C              N = Columns of X
C              XM = Resulting multiplied matrix
C              MS = Row dimension of XM in main program
C
C
      SUBROUTINE MULT(X,Y,MX,MY,M,K,N,XM,MS)
      DIMENSION X(MX,K),Y(MY,N),XM(MS,N)
      DO 2 I = 1,M
      DO 2 J = 1,N
      XM(I,J) = 0.0
      DO 2 L = 1,K
      XM(I,J) = X(I,L)*Y(L,J)+XM(I,J)
 2    CONTINUE
      RETURN
      END
C
C
C*********************************************************************
C  GAUSS SOLUTION OF A SYSTEM OF N EQUATIONS
C
C  This subroutine solves a set of n equations and n unknowns by
C  using Gauss elimination. This is done by using two other
C  subroutines FACTOR, and SOLVE.
C  Both the coefficient and constants matrices are destroyed.
C
C
C  The variables are:
C
C              A=Coefficient Matrix
C              B=Constants Matrix
C              IN=Number of Equations and Unknowns
C              K=Columns of B
C              MROW=Rows As In Dimension Statemant
C              X=Solution Matrix
C
C
```

```
      SUBROUTINE GAUSS (A,B,IN,K,MROW,X)
      DIMENSION A(MROW,MROW),B(MROW,K),X(MROW,K),D(120),IPV(120)
      N=IN
      CALL FACTOR(A,IPV,N,MROW,D,IERROR)
      IF(IERROR.EQ.2)WRITE(6,10)
 10   FORMAT(5X,//,'The coefficient matrix may be singular',///)
      CALL SOLVE(A,B,IPV,N,K,MROW,X)
      RETURN
      END
C
C
C
C  This subroutine creates A" (the transformed matrix). The system uses
C  implicit scaling and checks for singularity.


      SUBROUTINE FACTOR(AP,IPV,N,MROW,D,IERROR)
      DIMENSION AP(MROW,MROW),IPV(120),D(120)
      DO 100 L=1,N-1
      DO 7 I=1,N
 7    D(I)=0.0
      DO 10 I=L,N
      DO 10 J=L,N
      DUMMY=ABS(AP(I,J))
      IF(D(I).LT.DUMMY) D(I)=DUMMY
 10   CONTINUE
C Search for maximum pivot
      XMAXP=0.
      DO 20 I=L,N
      DUMMY=ABS(AP(I,L)/D(I))
      IF(DUMMY.GT.XMAXP) THEN
      XMAXP=DUMMY
      IPV(L)=I
C  Check for singularity
      IF(IPV(L).EQ.0) GO TO 17
      ENDIF
 20   CONTINUE
C Interchange rows if necessary
      IF(L.NE.IPV(L)) THEN
        DO 35 I=L,N
        AIJ=AP(L,I)
        AP(L,I)=AP(IPV(L),I)
        AP(IPV(L),I)=AIJ
 35     CONTINUE
      ENDIF
C  Do the column elimination
      DO 40 I=L+1,N
      AP(I,L)=-AP(I,L)/AP(L,L)
      DO 40 J=L+1,N
      AP(I,J)=AP(I,J)+AP(I,L)*AP(L,J)
 40   CONTINUE
```

```
 100  CONTINUE
C
C Set IERROR=1 or abnormal return
      IERROR=1
      RETURN
 17   IERROR=2
      RETURN
      END


C  This subroutine creates b" and solve the system of equations by
C  back substitution.


      SUBROUTINE SOLVE(AP,B,IPV,N,K,MROW,X)
      DIMENSION B(MROW,K),AP(MROW,MROW),IPV(120),X(MROW,K)
C  b" is formed.
      BL = 0.0
      DO 1 ICK=1,K
      DO 10 L=1,N-1
      IF(IPV(L).NE.L) THEN
      BL=B(L,K)
      B(L,K)=B(IPV(L),K)
      B(IPV(L),K)=BL
      ENDIF
      DO 10 J=L+1,N
      B(J,K)=B(J,K)+B(L,K)*AP(J,L)
 10   CONTINUE
C  Backsolve to obtain a solution to Ax=b.
      DO 7 I = 1,N
 7    X(I,K) = 0.0
      X(N,K)=B(N,K)/AP(N,N)
      DO 20 I=N-1,1,-1
      SUM=0.
      DO 20 J=I+1,N
      SUM=AP(I,J)*X(J,K)+SUM
      X(I,K)=(B(I,K)-SUM)/AP(I,I)
 20   CONTINUE
 1    CONTINUE
      RETURN
      END
```

The vita has been removed from the scanned document